Continuum Dynamics of Solid-Solid Phase Transitions

Thesis by

Xiaoguang Zhong

In Partial Fulfillment of the Requirements

for the Degree of

Doctor of Philosophy

California Institute of Technology

Pasadena, California

1995

(Submitted May 19, 1995)

Acknowledgements

I am grateful to Professor James K. Knowles, my research advisor, for his insightful guidance, encouragement, patience and interest in my work. He has helped me in many other ways. I am also indebted to Professor Thomas Y. Hou. The many stimulating discussions I had with him led to the development of the numerical method presented in this thesis.

I am pleased to acknowledge Professor Kaushik Bhattacharya for his many suggestions and helps.

My four years at Caltech have been wonderful, especially, as I fell in love with Lily. Special thanks are due to her for her understanding, friendship and love. I dedicate this thesis to my dear wife, Lily.

Abstract

This work focuses on the applications in dynamics of recently developed continuum-mechanical models of solid-solid phase transitions. The dynamical problems considered here involve only one space coordinate, and attention is limited to hyperelastic materials that involve two phases. This investigation has two purposes. The first is to determine the predictions of the models in complicated situations. Secondly, the present study attempts to develop analytical and numerical approaches to problems that may be relevant to the interpretation and understanding of experiments involving phase transitions under dynamical conditions.

The first problem studied involves the study of a semi-infinite bar initially in an equilibrium state that involves two material phases separated by a phase boundary at a given location. The end of the bar is suddenly subject to a constant impact velocity that persists for a finite time and is then removed. Interaction between the phase boundary and the elastic waves generated by the impact and subsequent reflections are studied in detail, and the trajectory of the phase boundary is determined exactly. The second task addressed involves the development of a Riemann solver to be applied to the numerical solution of Riemann problems for two-phase elastic materials. Riemann problems for such materials involve complications not present in the corresponding problems that arise, for example, in classical gas dynamics. Finally, a finite-difference method of Godunov type is developed for the numerical treatment of boundary-initial-value problems arising in the model of Abeyaratne and Knowles. The method is applied to specific problems.

Contents

List of Figures

Chapter 1 Introduction

There are three levels of understanding phase transformations in solids: the microscopic level, the mesoscopic level and the macroscopic level. The macroscopic level deals with bulk averages across microstructures and is the domain of continuum mechanics and thermodynamics. Here we are concerned about models at the macroscopic level, i.e. continuum models.

Continuum modeling of phase transformations has been a very active research area recently. This has much to do with some remarkable properties of materials capable of phase transformations, such as the shape memory effect, that can be exploited for engineering applications. For example, shape memory alloys exhibit the capacity to hysteretically recover significant deformation, absorbing large amounts of energy in the process. They can therefore serve as energy absorbers or damping devices in active control systems [82]. In addition, mechanical properties of a material can sometimes be improved by phase transformations, such as in the toughening of certain ceramics by stress-induced martensitic transformation of embedded particles [28]. In the design of a mechanical device, or in the analysis of the toughness of materials, it is the macroscopic behavior that is of primary interest.

The goal of continuum modeling of phase transformations in solids is to predict patterns of microstructures, to understand why certain materials exhibit certain patterns and to explain the macroscopic properties of the materials. The ultimate goal will be to provide new perspectives on the development of materials whose behavior is specified by engineering applications. Though there has been some progress in such modeling, there is still a long way to go.

1.1 Martensitic transformation

Most current continuum models for solid-solid phase transformations are concerned with martensitic transformations or use martensitic transformations as a prototype. In the following, a summary of the characteristics of martensitic transformation is given ([17, 20, 26], and [66]). The emphasis is on phenomenological observations.

The martensitic transformation is a diffusionless, solid-to-solid phase transformation in crystalline solids. The composition of the product phase is the same as that of the original phase. The change during the transformation occurs in the crystal structure, such as cubic to tetragonal, cubic to orthorhombic. Geometrically, the transformation is characterized by a first- order change in crystal lattices. The phases involved in the transformation are austenite and martensite. Austenite, which is the stable phase at high temperature, has greater symmetry than martensite, which is the stable phase at low temperature. This change of symmetry gives rise to variants of martensite – identical crystal lattices of martensite which are oriented differently with respect to the austenite lattice. During the austenite-to-martensite transformation, volume changes are often small, and in some cases are zero within the limit of experimental error. The martensite crystals are usually flat plates, which thin towards their extremities and so have a lenticular cross section. The plane of the lattice on which martensite is formed is called the habit plane.

A martensitic transformation can be induced by changes of temperature as well as by the application of stress. In a sense, the effects of temperature and stress are interchangeable. In general the transformation should be considered as a thermal-mechanical process.

We say a transformation is a thermoelastic martensitic transformation if martensite forms and grows continuously as the temperature is lowered, and shrinks and vanishes as the temperature is raised. The thermoelastic transformation either on cooling or on heating in the absence of external stress causes no macroscopic mechanical effects. There are several critical temperatures for the transformation, denoted by M_s, M_f, A_s, A_f, T_0. The martensitic transformation begins spontaneously at the

martensite start temperature M_s, and as the temperature is lowered, more and more material transforms until the temperature M_f is reached, at which the martensitic transformation stops. Similarly, for the martensite-to-austenite transformation, as the temperature is raised to A_s, the reverse transformation begins, and martensite is totally transformed back to austenite at A_f. T_0 is the transformation temperature, at which martensite and austenite are equally stable in the absence of stress. In the language of thermodynamics, at T_0, both martensite and austenite phases minimize the free energy density.

A mechanical analogue to the thermoelastic martensitic transformation is the notion of pseudoelastic behavior. Pseudoelasticity refers to the hysteretic loading-unloading characteristic observed in the stress-induced martensitic transformation. In this case, the transformation proceeds continuously with increasing applied stress and is reversed continuously as the stress is decreased. When single crystals are used, the direction of applied stress is very important, and some reactions maybe inhibited or aided by a suitably oriented stress. Above M_s, deformation may also result in a martensitic transformation, even though the temperature is too high for a spontaneous reaction, the highest temperature at which martensite maybe formed under stress is called M_d. In general, the martensite-austenite transformation can be aided in the same way.

There are many alloys that are capable of martensitic transformations; examples are NiTi, FeNiC, CuZnAl. A list of such alloys maybe found in table 1 of [26]. In addition, ceramic materials such as Zirconia also exhibit this type of phase transformation.

1.2 Continuum models for phase transformations in solids

To construct a continuum model for phase transformations in solids, one must characterize the material by appropriate constitutive relations, and transformation con-

ditions (nucleation criterion and kinetic relations). There are many studies in this respect, for example, those in [12], [16] and [54] for shape memory alloys and those in [83, 84] for transformation plasticity. However there is as yet no well accepted constitutive theory. For transformation conditions, one can refer to the review [29] by Fisher et al. Another important issue is how to model the deformations associated with phase transformations. Two phases can be separated by a phase boundary where certain quantities are discontinuous, as in models by Ball & James [14] and Abeyaratne and Knowles[2, 5] , or the phases may be separated by a transition zone, where certain quantities change rapidly but are still continuous such as in regularized theory, for example [75, 85], or an order parameter approach may be used[31].

In the continuum mechanical theories of phase transformations, there are several widely used approaches for continuum modeling, such as the linear elastic model [49], models based on the Eshelby inclusion theorem and numerical simulations. The Eshelby model is mainly used in the transformation plasticity analysis; it is for irreversible phase transitions. Linear elastic models are for thermoelastic phase transformations, especially thermoelastic martensitic transformations. In the linear elastic model, one computes the elastic energy of a particle with known transformation strain as a function of its moduli, shape and habit plane. One then uses it to measure the energetic stability of the preferred habit, and one can sum up the elastic energy and surface energy to predict the preferred shape plane, habit plane and composite state as a function of volume. There are some limitations on the linear elastic model [18], [90]. It linearizes the transformation strain, which is appreciable; it ignores the rotational component of the finite strain which alters the crystallographic habit and it produces a spurious degeneracy in the preferred habit plane that is not present in crystallographic theory. Due to the limitations of the linear elastic model, it can miss important details of microstructure of phase transformations [18].

Recently, there has been significant progress in the modeling of thermoelastic martensitic transformations that make use of nonlinear thermoelastic theory. The main approaches in this category include the minimization of energy upon which some microstructures are successfully predicted by Ball & James [14] and Bhattacharya [17],

the Abeyaratne-Knowles model (cited hereafter as the A-K model) which qualitatively predicts hysteresis [2], the shape memory effect [10] in martensitic transformations and is consistent with viscosity regularized theory. Each of these approaches has its advantages and disadvantages. The different approaches originated from different techniques used to attack the nonuniqueness problem in the modelling of phase transformation by finite elasticity. The nonuniqueness is due to the nonconvexity of the strain energy or free energy function.

1.3 Finite elasticity theory for reversible phase transformations

Ericksen [27] pioneered the research on the use of finite thermoelasticity theory to model phase transformations in solids by considering the equilibrium of a bar of material that can change phase. Now it is well established that a nonlinear elastic material capable of phase transformation has a nonconvex free energy function, Abeyaratne [1], Rosakis [73]. The nonconvexity, or more generally the loss of strong ellipticity, of the free energy function, leads to the nonuniqueness of the solutions to boundary value problems or initial-boundary value problems in finite elasticity even though entropy conditions are imposed [2, 5].

In the setting of continuum mechanics, the nonuniqueness of solutions is due to the lack of constitutive information about the phase transformation process. In order to get a unique solution to a boundary value problem or initial-boundary value problem, various constitutive postulates are made, such as a maximum energy dissipation criterion by Dafermos [25], absolute minimization of energy by Ericksen [27], Ball & James [14], viscosity regularization [44, 75, 85] and postulates of a constitutive nature at a phase boundary by Abeyaratne & Knowles [2, 3].

The above approaches are basically bulk theories with surface effects ignored. For models that consider surface effects, one may refer to [37, 51, 59]. Though the surface effect may be very important in some cases [22], in the following only the three widely

used bulk theories and associated computation methods are briefly discussed.

Minimization of free energy

Absolute minimization of energy assumes that a material is conservative at every particle including those on the phase boundaries, so that the material prefers the equilibrium state which renders the appropriate energy functional an absolute minimum. In the models of this kind, there is no dissipation on a phase boundary in a quasi-static process.

As the constitutive postulate implies, this approach can only be applied to the investigation of the stable equilibrium state of a material. This work is a direct generalization of Roitburd's linear elastic model [72]. If finite elasticity theory is adapted, the approach merges the advantages of the linear elastic model and the phenomenological crystallographic theory. Many interesting results have been obtained, especially for martensitic phase transformations. Ball and James [14] predicted observed fine phase mixtures, Bhattacharya [17] predicted the wedge-like microstructure in martensite and more recently James and Kinderlehrer [46] applied the approach to meagnetostriction. Kohn and Muller [51], by including a surface effect, predicted twin branching in martensite.

Though minimization of energy in finite elasticity has successfully predicted microstructures in martensite and other materials, the limitation of the approach is obvious. It cannot be applied to the situations involving metastablity and dynamical processes. For a comprehensive review of the approach one can refer to [18, 64]

Viscoelasticity

From a different perspective, one may take the view that the lack of uniqueness of solutions is due to the elasticity model itself, and thus that a regularization of the elastic theory by viscosity will remove the nonuniqueness: one can use viscoelasticity theory as a criterion to select a solution from many solutions in the elastic theory.

According to this philosophy a weak solution of an elastic theory is admissible only if it can be obtained as the limit of a solution of a broader theory – viscoelasticity in the limit of vanishing viscosity (and possibly other higher order quantities, such as capillarity). With linear viscosity regularization, the existence and uniqueness of a strong solution are guaranteed [75]. This approach has been applied to phase transition problems in one dimension [69], in two dimensions [85] and three dimensions [50].

However as shown by Abeyaratne & Knowles [6], regularized theory may be viewed as a continuum model with a special kinetic relation at phase boundaries.

The A-K Model

Borrowing from another viewpoint widely used in materials science, Abeyaratne & Knowles postulated two additional constitutive relations on a phase boundary. One is the nucleation criterion, which determines when and where a new phase will initiate from a parent phase, and the other is a kinetic relation which determines the rate of phase transformation, or in other words the propagation speed of phase boundaries. The postulate has its counter part in materials science. In the model, the phase boundary is a mechanism for dissipation.

Abeyaratne & Knowles showed that for a finite bar with a nonmonotonic stress-strain relation, the boundary-value problem associated with a quasi-static process has an infinite number of solutions [2]. In order to select a unique solution they postulated a kinetic relation and a nucleation criterion on a phase boundary. Thus they selected a unique solution which predicts material response that is qualitatively in agreement with experimental observation in uni-axial tension tests. Later they extended the idea to a fully dynamical mechanical theory, again selecting a unique solution from many possible solutions [5]. This approach has also been applied to the thermomechanical theory for a quasi-static process [7, 47]. For a dynamical phase transformation, thermal effects cannot be realistically omitted. Recently Abeyaratne and Knowles [8, 9] extended their approach to dynamical processes with heat con-

duction or to adiabatic dynamical processes. In this theoretical development, they considered only one-dimensional initial value problems. Jiang [48] has generalized the A-K model to electrical-thermo-mechanical processes.

Pence [70] considered initial-boundary value problems for a semi-infinite bar, accounting for the interaction of a single phase boundary with an acoustic wave. Lin and Pence [55], [56] considered the large time behavior of a phase boundary in a finite bar. For the example of multiple phase boundaries situations one can refer to [10].

Though there are many difficulties, the A-K approach has been applied to two-dimensional problems. Fried [30] showed that materials with nonconvex free energy can sustain smooth curved phase boundaries in antiplane shear equilibrium states, and he also investigated the stability of a phase boundary in anti-plane shear. Rosakis [74] shows that an inclusion of martensite in a austenite matrix must have cusps in its boundary in a two-dimensional anti-plane shear problem. Rosakis and Tsai [87] extended the result to a steady-state propagation of a twin in a infinite domain.

Now the main challenges for the A-K model are: (1) How to analyze one-dimensional general initial-boundary value problems, so that one can compare predictions of the model to more complicated experimental observations; (2) How to generalize the model to higher dimensions: Construction or derivation of appropriate free energy functions and kinetic relations, as well as appropriate nucleation criteria.

Computational methods

Due to the strong nonlinearity associated with the initial-boundary value problems arising in the modeling of phase transformations, it is usually impossible to get explicit analytical solutions for the ordinary initial-boundary value problems.

Various numerical methods have been applied to phase transformation problems. The finite element method based upon a linear elastic model is widely used in the simulation of martensitic transformation [90] and in the transformation plasticity [32, 83]. Collins and Luskin [24], and Nicolaides and Walkington [65] investigated solid-solid phase transformation problems numerically by the minimization of energy.

Slemrod [83] applied a Lax-Friedrichs scheme to a system of conservation laws of mixed type. This basically changed the original system of conservation laws into a system with viscosity-capillarity regularization. Silling [78] used a dynamic relaxation technique to model quasi-static phase transformation processes, and later he extended his modelling to the dynamic growth of martensitic plates in an elastic material [79]. Swart and Holmes [85], Affouf and Caflisch [11] and Kloueck & Luskin [50] applied numerical methods directly to the regularized theory. There is no uniqueness problem, but the applicability of the regularized theory is limited. More recently Mamiya and Simo applied the finite element method to the Abyaratne-Knowles model for the quasi-static case [60].

1.4 Scope of this work

This work focuses on a one-dimensional dynamic mechanical model of phase transformation proposed by Abeyaratne & Knowles [5]. Only two-phase hyperelastic materials are considered. The purpose of this investigation is two fold. First, to investigate the analytical predictions of the model in some complicated situations, such as the interaction of a phase boundary and a shock wave or the determination of the large time dynamical behavior of a phase boundary in a domain with a boundary. Secondly, we analyze general initial-boundary value problems so that one can compare the predictions of the model to experimental observations.

The main results obtained are:

- An approximate Riemann solver is developed for two-phase elastic materials. Riemann problems for such materials involve complications not present in the corresponding problems that arise, for example, in classical gas dynamics.

- An exact solution is obtained for the dynamical behavior of a phase boundary in a semi-infinite bar. A thorough analysis of the solution reveals many interesting phenomena. The solution can be used to illustrate that a phase boundary can reach an equilibrium state at large time after the application of a disturbance

of finite duration.

- A finite difference method of Godunov type is developed for the model. The method is proved to deliver correct solutions. Through a numerical experiment, it is shown that a dynamic solution converges to the static solution in large time. With this method, it is possible to analyze any initial-boundary value problem for the A-K model.

Chapter 2 Preliminaries

The materials in the Abeyaratne-Knowles model are characterized by nonconvex strain energy functions. These materials can describe stable deformations as well as metastable deformations. In this model, phases correspond to disjoint deformation domains of a strain energy function. In the domains, a deformation is stable, metastable or unstable. Based on the fact that an unstable deformation is not observable in solid-solid phase transformations, it is assumed that a deformation will jump from one stable or metastable phase to another when certain critical conditions are satisfied. This leads to the formation of a phase boundary.

The basic assumptions are:

(1) The deformation is C^2 away from shock fronts or phase boundaries; deformation gradients are discontinuous across shock fronts or phase boundaries, but the deformation is continuous.

(2)Two supplementary constitutive relations are postulated: a kinetic relation at a phase boundary and a nucleation criterion.

The assumptions imply that the deformation at a phase boundary is coherent and phase boundaries are kinetically driven. Unlike the situation in conventional shock wave theories, a phase boundary is not the result of the overlapping of characteristics. In the following, only the one-dimensional version of the model is presented.

2.1 Governing equations

Consider a one-dimensional bar with uniform cross section A that occupies the interval [0,L] in an unstressed reference configuration. In a longitudinal motion of the bar, the particle at x is carried to the point $x + u(x,t)$ at time t, where the displacement u is required to be continuous with piecewise first and second order derivatives on

$[0, L]$ for $t > 0$. Let

$$\gamma = u_x, v = u_t \tag{2.1}$$

denote strain and particle velocity respectively. It is assumed that $\gamma(x,t) > -1$ so that the mapping $x \to x + u(x,t)$ is invertible at each time t.

The equation of motion and the compatibility equation are

$$\sigma'(\gamma)\gamma_x - \rho v_t = 0, \tag{2.2}$$

$$v_x - \gamma_t = 0. \tag{2.3}$$

The characteristics for this system are:

$$\frac{dx}{dt} = \pm c(\gamma),$$

where $c = \sqrt{\frac{\sigma'(\gamma)}{\rho}}$. The corresponding Riemann invariants along each characteristics are:

$$v - \int c d\gamma = constant,$$

along $dx/dt = c(\gamma)$;

$$v + \int c d\gamma = constant,$$

along $dx/dt = -c(\gamma)$.

If there is a strain discontinuity at $x = s(t)$, jump conditions must hold

$$\dot{s}(\gamma_+ - \gamma_-) = -(v_+ - v_-), \tag{2.4}$$

$$\sigma(\gamma_+) - \sigma(\gamma_-) = -\rho\dot{s}(v_+ - v_-), \tag{2.5}$$

where $()_+$, $()_-$ denote quantities right in front of the discontinuity and behind it.

Let

$$W(\gamma) = \int_0^\gamma \sigma(\gamma')d\gamma' \tag{2.6}$$

be the strain energy per unit volume for the material. Consider the restriction of

the motion to the time $[t_1, t_2]$ and to the piece of the bar that occupies the interval $[x_1, x_2]$ in the reference state. Suppose that γ and v are smooth on $[x_1, x_2]$ in the time interval $[t_1, t_2]$ except at the moving discontinuity $x = s(t)$. Let E(t) be the total mechanical energy at time t for the piece of the bar under consideration:

$$E(t) = \int_{x_1}^{x_2} [W(\gamma(x,t)) + \frac{1}{2}\rho v^2(x,t)]dx. \tag{2.7}$$

A direct calculation establishes the the following work-energy identity:

$$\sigma(x_2)v(x_2,t) - \sigma(x_1)v(x_1,t) - \dot{E}(t) = f(t)\dot{s}(t)A, \tag{2.8}$$

where the *driving traction* f(t) is defined by

$$f = \hat{f}(\gamma_-, \gamma_+) = \int_{\gamma_-}^{\gamma_+} \sigma(\gamma)d\gamma - \frac{1}{2}[\sigma(\gamma_+) + \sigma(\gamma_-)](\gamma_+ - \gamma_-). \tag{2.9}$$

The admissibility condition imposed on the phase boundary is

$$f(t)\dot{s}(t) \geq 0. \tag{2.10}$$

Under isothermal conditions the admissibility condition is a consequence of the second law of thermodynamics, see [52].

2.2 Supplementary constitutive relations

Besides the equations of motion, the stress-strain relation, jump conditions and the admissibility condition, two supplementary constitutive relations must be specified in order to uniquely determine a solution of the system. The two supplementary constitutive relations are the kinetic relation and the nucleation criterion. The kinetic relation relates the phase boundary propagation speed $\dot{s}$ to the driving traction $f(t)$ acting on the phase boundary. The nucleation criterion determines when a new phase will be nucleated from the parent phase. These two relations are material-dependent

only. In this work, we use the following kinetic relation and nucleation criterion:

1. Kinetic relation:

$$f = \phi(\dot{s}), \tag{2.11}$$

where $\phi(\dot{s})$ is a monotonically increasing function that *may* be discontinuous at $\dot{s} = 0$.

2. Nucleation criterion:

Assume that there is a two-phase material, with low-strain phase A, high-strain phase B, then for this material we have

$$f \leq f_{cr} \leq 0 \tag{2.12}$$

for a phase A-to-phase B transformation;

$$f \geq f_{cr}^{*} \geq 0 \tag{2.13}$$

for a phase B-to-phase A transformation; f_{cr}^{*}, f_{cr} are critical driving tractions.

2.3 Trilinear materials

The simplest elastic material capable of phase transformation is the so called *trilinear material.* The trilinear stress-strain relation can be expressed as:

$$\sigma(\gamma) = \begin{cases} \mu_1 \gamma, & -1 < \gamma < \gamma_m, \\ \frac{\sigma_m - \sigma_M}{\gamma_m - \gamma_M}(\gamma - \gamma_M) + \sigma_M, & \gamma_m < \gamma < \gamma_M, \\ \mu_2(\gamma - \gamma_t), & \gamma_M < \gamma < \infty \end{cases} \tag{2.14}$$

where $\sigma_m = \mu\gamma_m$, $\sigma_M = \mu(\gamma_M - \gamma_T)$.

We call $-1 < \gamma < \gamma_m$ phase 1 or low-strain phase, $\gamma_m < \gamma < \gamma_M$ phase 2 or unstable phase and $\gamma_M < \gamma$ phase 3 or high-strain phase. The low-strain phase and the high-strain phase are metastable phases, the third phase is the unstable phase.

If we consider the martensitic transformation as our prototype, we can identify the low-strain phase as austenite and the high-strain phase as martensite. Let $c_i = \sqrt{\frac{\mu_i}{\rho}}$, $i = 1, 2$ be the sound speeds in the low- strain phase and the high-strain phase.

It is easy to see that

$$\mu_1 > 0, \mu_2 > 0, \gamma_m < \gamma_M.$$

To guarantee the noconvexity of the corresponding strain energy function, we require that

$$\mu_1 \gamma_m > \mu_2(\gamma_M - \gamma_t),$$

see Figure 2.1.

For this material the driving traction on a high-strain-low-strain phase boundary is

$$f(\gamma_-, \gamma_+) = \frac{(\mu_1 - \mu_2)}{2}(\gamma_+\gamma_- - \gamma_M\gamma_m) + \frac{\mu_2\gamma_t}{2}(\gamma_+ + \gamma_- - \gamma_M - \gamma_m), \tag{2.15}$$

for a low-strain-high-strain phase boundary $\hat{f}(\gamma_-, \gamma_+) = -f(\gamma_-, \gamma_+)$.

In an equilibrium state we can write the driving traction in terms of stress σ:

$$f(\sigma) = \frac{\mu_1 - \mu_2}{2\mu_1\mu_2}\sigma^2 + \gamma_t\sigma - \frac{\mu_1 - \mu_2}{2}\gamma_m\gamma_M - \frac{\mu_2\gamma_t}{2}(\gamma_m + \gamma_M - \gamma_t). \tag{2.16}$$

The Maxwell stress σ_0 of the material is the unique stress for which $f(\sigma) = 0$. It is easy to show that $f(\sigma)$ is monotonically increasing, and $f(\sigma_m) < 0, f(\sigma_M) > 0$.

If we let $\mu_1 = \mu_2 = \mu$ then the Maxwell stress is

$$\sigma_0 = \frac{1}{2}(\sigma_m + \sigma_M). \tag{2.17}$$

The strains corresponding to the Maxwell stress in the low-strain phase and high-strain phase are

$$\gamma_0^l = \frac{1}{2}(\gamma_m + \gamma_M - \gamma_T), \tag{2.18}$$

$$\gamma_0^h = \frac{1}{2}(\gamma_m + \gamma_M + \gamma_T). \tag{2.19}$$

The jump conditions become

$$c^2(\gamma_+ - \gamma_-) + \dot{s}(v_+ - v_-) = c^2\gamma_T, \tag{2.20}$$

$$(v_+ - v_-) + \dot{s}(\gamma_+ - \gamma_-) = 0. \tag{2.21}$$

The Riemann invariants are

$$v \pm c\gamma = constant. \tag{2.22}$$

The jump conditions and the stress-strain relation imply that

$$|\dot{s}| < c \tag{2.23}$$

for a phase boundary propagation speed.

In the following chapters, the special trilinear material with $\mu_1 = \mu_2$ is used unless an otherwise specification is assumed. For this material, we can reformulate the nucleation criterion in terms of strains for convenience.

- An alternative version of nucleation criterion

  Assume that there is a two-phase material, with low-strain phase A, high-strain phase B; for this material we have

  $$\gamma \geq \gamma_{cr} \geq \gamma_0^1 \tag{2.24}$$

  for phase A-to-phase B transformation;

  $$\gamma \leq \gamma_{cr}^* \leq \gamma_0^3 \tag{2.25}$$

  for phase B-to-phase A transformation. $\gamma_{cr}^*, \gamma_{cr}$ are critical strains.

2.4 A more general material

The dynamics of a more general constitutive law for an elastic material capable of undergoing a phase transition has been considered by Lin [57].

For this material, $\sigma(\gamma)$ is assumed to be a twice continuously differentiable function that first increases with γ, then decreases and finally increases again as shown in Figure 2.2. More precisely, it is assumed that there are three numbers γ_M, γ_m and γ_{in} with $0 < \gamma_m < \gamma_{in} < \gamma_M$ such that

$$\sigma'(\gamma)\begin{cases} > 0, -1 < \gamma < \gamma_m, \\ = 0, \gamma = \gamma_m, \\ < 0, \gamma_m < \gamma < \gamma_M, \\ = 0, \gamma = \gamma_M, \\ > 0, \gamma > \gamma_M, \end{cases} \tag{2.26}$$

and

$$\sigma''(\gamma)\begin{cases} < 0, -1 < \gamma < \gamma_{in}, \\ = 0, \gamma = \gamma_{in}, \\ > 0, \gamma > \gamma_{in}. \end{cases} \tag{2.27}$$

Further, it is supposed that $\sigma(0) = 0$ and that $\sigma(\gamma) \to -\infty$, $\sigma'(\gamma) \to \infty$ as $\gamma \to -1$; $\sigma(\gamma) = \mu_\infty \gamma + \sigma_T + O(1)$ as $\gamma \to \infty$, where μ_∞ and σ_T are constants. The stress-strain curve therefore consists of three branches, two of which are rising, while the other is declining; it has a single inflection point at the strain $\gamma = \gamma_{in}$ and is asymptotic, at large tensile strains, to the straight line $\sigma(\gamma) = \mu_\infty \gamma + \sigma_T + O(1)$. As in the trilinear material, $(-1, \gamma_m]$, (γ_m, γ_M), $[\gamma_M, \infty)$ are identified as the low-strain phase, unstable phase and high-strain phase. The low-strain phase and high-strain phase are metastable.

This material can sustain rarefaction waves (fans) and shock waves, and the shocks are dissipative. Trilinear materials cannot sustain fans and the shock waves in trilinear materials are dissipation free.

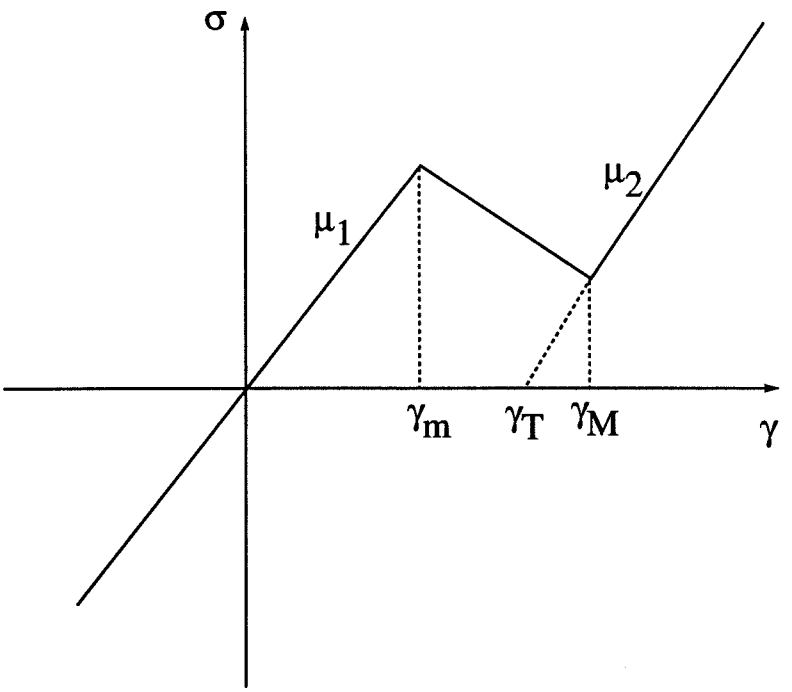

Figure 2.1: A trilinear material

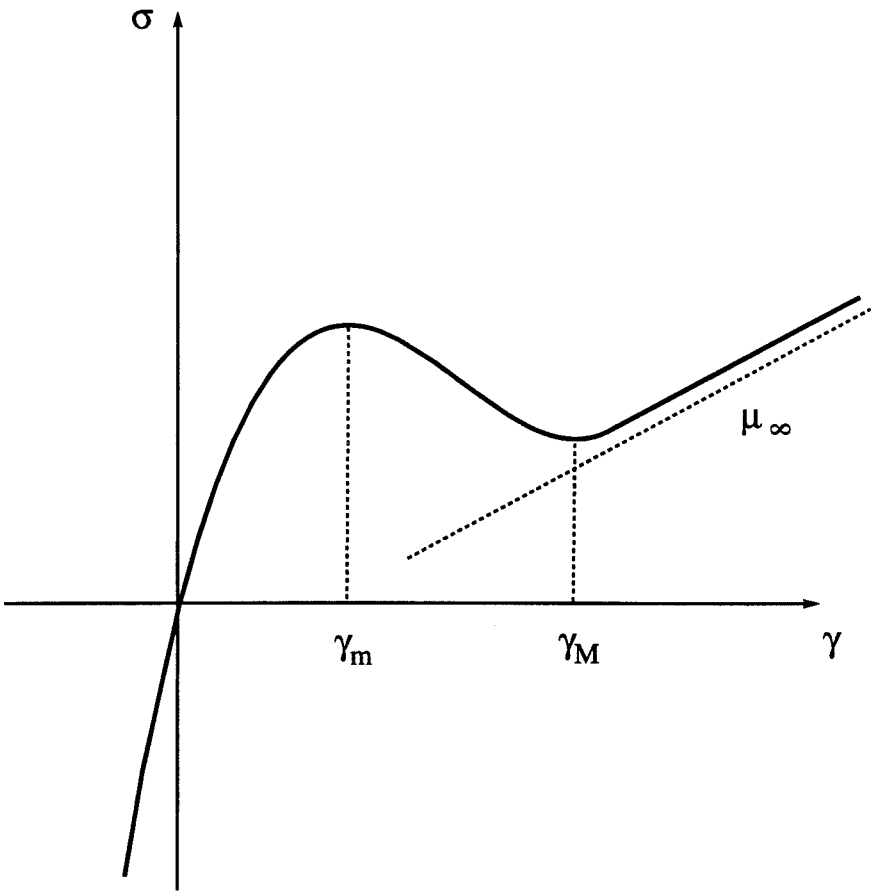

Figure 2.2: A more general material

Chapter 3 Riemann problems

The study of a Riemann problem provides powerful tools towards the understanding of the wave structures of the solution of hyperbolic systems and systems of mixed type. As a matter of fact, the model considered here is developed through the investigation of various Riemann problems. Besides the theoretical significance of the Riemann problems, their solutions can be used as building blocks for some computational algorithms for discontinuous solutions, as in the methods of Godunov type and particularly the method developed in Chapter 6.

It is easy to check that there exist self-similar solutions for the governing equations (2.2), (2.3). When we solve the governing equations for self-similar solutions, we can reduce them and the related jump conditions to a group of algebraic equations. For trilinear materials, the algebraic equations are quite easy to solve. But for a nontrilinear two-phase material , it is not so easy to solve the algebraic equations. Recently Lin [57] considered such a nontrilinear material and solved a Riemann problem with special initial data.

In the following, a summary of solutions to Riemann problems for trilinear materials is given in Section 3.1. These solutions are to be used later in Chapter 6. In Section 3.2, we first discuss some general features of solution to Riemann problem for general two-phase elastic materials, then we propose an approximate Riemann solver. Some remarks are made in Section 3.3 on trilinear materials and general two-phase elastic materials.

3.1 Solutions to Riemann problems: trilinear materials

Following the procedure described in [5], by using the entropy inequality and the jump conditions, it is easy to show that Riemann problems for arbitrary trilinear materials have the following features:

1. If there is no initial data in the unstable phase, then the unstable phase will not appear later.

2. There cannot be two phase boundaries propagating in the same direction.

3. There are at most two phase boundaries in any solution of a Riemann problem; if there are two phase boundaries, they propagate in opposite directions.

4. If $c_1 \neq c_2$ we call a phase boundary supersonic if $\dot{s} > min(c_1, c_2)$, subsonic if $\dot{s} < min(c_1, c_2)$. When a phase boundary propagates into the phase with larger sound speed, then $\dot{s} < min(c_1, c_2)$. We always have $\dot{s} < max(c_1, c_2)$.

With these features, it is easy to solve the following Riemann problems.

Suppose we have a Riemann problem with initial data:

$$v(x,0), \gamma(x,0) = \begin{cases} v_L, \gamma_L, & -\infty < x < 0, \\ v_R, \gamma_R, & 0 < x < \infty, \end{cases} \tag{3.1}$$

for the governing equations (2.2), (2.3), using the special trilinear material given in Section 2.3. Here we only seek self-similar solutions. The solutions to the Riemann problem are given below for two cases.

Case 1. Initial strains γ_L, γ_R are in the low-strain phase.

Let

$$v(x,t) = \hat{v}(\frac{x}{t}), \tag{3.2}$$

$$\gamma(x,t) = \hat{\gamma}(\frac{x}{t}) \tag{3.3}$$

and

$$\lambda = \frac{x}{t}. \tag{3.4}$$

Substitute (3.2)-(3.4) into (2.2) and (2.3), we have

$$\begin{pmatrix} c^2 & \lambda \\ \lambda & 1 \end{pmatrix} \begin{Bmatrix} \hat{\gamma}' \\ \hat{v}' \end{Bmatrix} = 0. \tag{3.5}$$

In order to have a solution to (3.5), we have either

$$\begin{Bmatrix} \hat{\gamma}' \\ \hat{v}' \end{Bmatrix} = 0 \tag{3.6}$$

or

$$\det \begin{pmatrix} c^2 & \lambda \\ \lambda & 1 \end{pmatrix} = 0. \tag{3.7}$$

i.e.

$$\hat{v}(\frac{x}{t}) = constant, \tag{3.8}$$

$$\hat{\gamma}(\frac{x}{t}) = constant \tag{3.9}$$

or

$$\lambda = \pm c. \tag{3.10}$$

So we have piecewise constant solutions with possible discontinuities at $\frac{x}{t} = \pm c$. By the alternative nucleation criterion, if $\frac{1}{2c}(v_R - v_L + c(\gamma_R + \gamma_L)) \leq \gamma_{cr}$, then there will be no new phase initiated and the solutions are in the form:

$$v(x,t), \gamma(x,t) = \begin{cases} v_L, \gamma_L, & -\infty < x < -ct, \\ v_0, \gamma_0, & -ct < x < ct, \\ v_R, \gamma_R, & ct < x < \infty. \end{cases} \tag{3.11}$$

We can determine (v_0, γ_0) by the jump conditions at the positions of shock waves, $x = \pm ct$:

$$v_L - v_0 - c(\gamma_L - \gamma_0) = 0, \tag{3.12}$$

$$v_R - v_0 + c(\gamma_R - \gamma_0) = 0, \tag{3.13}$$

which give

$$\gamma_0 = \frac{1}{2c}(v_R - v_L + c(\gamma_R + \gamma_L)), \tag{3.14}$$

$$v_0 = v_L + c(\gamma_0 - \gamma_L). \tag{3.15}$$

(see Figure 3.1a)

By the nucleation criterion, if $\frac{1}{2c}(v_R - v_L + c(\gamma_R + \gamma_L)) > \gamma_{cr}$, then the above solution is invalid. There is a new phase initiated at the origin. According to the general features of Riemann problems, there are two phase boundaries propagating in the opposite directions. In a procedure similar to that lead to (3.5), we can show that the solution has the following structure (see Figure 3.1b):

$$v(x,t), \gamma(x,t) = \begin{cases} v_L, \gamma_L, & -\infty < x < -ct, \\ v_1, \gamma_1, & -ct < x < -\dot{s}t, \\ v_2, \gamma_2, & -\dot{s}t < x < \dot{s}t, \\ v_3, \gamma_3, & \dot{s}t < x < ct, \\ v_R, \gamma_R, & ct < x < \infty \end{cases} \tag{3.16}$$

where

$$\gamma_1 = h - \frac{c\dot{s}\gamma_T}{c^2 - \dot{s}^2},$$

$$\gamma_2 = h + \frac{c\gamma_T}{c + \dot{s}},$$

$$\gamma_3 = h - \frac{c\dot{s}\gamma_T}{c^2 - \dot{s}^2},$$

$$v_1 = v_L - c\gamma_L + ch - \frac{c^2\dot{s}\gamma_T}{c^2 - \dot{s}^2},$$

$$v_2 = v_L - c\gamma_L + ch,$$

$$v_3 = v_R + c\gamma_R - ch + \frac{c^2\dot{s}\gamma_T}{c^2 - \dot{s}^2},$$

$$h = \frac{1}{2c}(v_R - v_L + c(\gamma_R + \gamma_L)).$$

The phase boundary speed $\dot{s}$ is determined by the kinetic relation,

$$\frac{\mu\gamma_T}{2}(\gamma_m + \gamma_M - \gamma_1 - \gamma_2) = \phi_{13}(-\dot{s}). \tag{3.17}$$

Case 2. The initial strains γ_L, γ_R are in the high-strain phase and low-strain phase respectively.

There is only one phase boundary in the solution; see Figure 3.2 . The solutions are:

$$v(x,t), \gamma(x,t) = \begin{cases} v_L, \gamma_L, & -\infty < x < -ct, \\ v_-, \gamma_-, & -ct < x < \dot{s}t, \\ v_+, \gamma_+, & \dot{s} < x < ct, \\ v_R, \gamma_R, & ct < x < \infty. \end{cases} \tag{3.18}$$

where

$$\gamma_- = h - \frac{c\gamma_T}{2(c + \dot{s})},$$

$$v_- = v_L + c(\gamma_- - \gamma_L),$$

$$\gamma_+ = h + \frac{c\gamma_T}{2(c - \dot{s})},$$

$$v_+ = v_R - c(\gamma_+ - \gamma_R),$$

$$h = \frac{1}{2c}(v_R - v_L + c(\gamma_R + \gamma_L)).$$

The phase boundary speed $\dot{s}$ is determined by the kinetic relation,

$$\frac{\mu\gamma_T}{2}(\gamma_m + \gamma_M - \gamma_- - \gamma_+) = \phi_{13}(\dot{s}). \tag{3.19}$$

Riemann problems with other initial data can be solved similarly.

For completeness, a special initial-boundary value problem corresponding to impact is considered. The problem is defined in $(0, \infty)$, with the following initial conditions :

$$v(x,0) = v_0, 0 < x < \infty, \tag{3.20}$$

$$\gamma(x,0) = \gamma_0, 0 < x < \infty \tag{3.21}$$

and a velocity boundary condition at $x = 0$:

$$v(0,t) = v_b, 0 < t < \infty, \tag{3.22}$$

where v_b is a constant.

Case 1: The material is initially in the low-strain phase, i.e. $\gamma_0 < \gamma_{cr}$.

If $v_b > v_0 + c(\gamma_0 - \gamma_{cr})$, then the solution is: (Figure 3.3a)

$$v(x,t), \gamma(x,t) = \begin{cases} v_b, \frac{v_0 - v_b}{c} + \gamma_0, & 0 < x < ct, \\ v_0, \gamma_0, & ct < x < \infty; \end{cases} \tag{3.23}$$

If $v_b < v_0 + c(\gamma_0 - \gamma_{cr})$, then the solution is: (Figure 3.3b)

$$v(x,t), \gamma(x,t) = \begin{cases} v_b, \gamma_b, & 0 < x < \dot{s}t, \\ v_p, \gamma_p, & \dot{s}t < x < ct, \\ v_0, \gamma_0, & ct < x < \infty, \end{cases} \tag{3.24}$$

where

$$\gamma_b = \frac{v_0 + c\gamma_0}{c} - \frac{v_b}{c} + \frac{c\gamma_T}{c + \dot{s}},$$

$$v_p = v_b + \frac{c^2 \dot{s} \gamma_T}{c^2 - \dot{s}^2},$$

$$\gamma_p = \frac{v_0 + c\gamma_0}{c} - \frac{v_b}{c} - \frac{c\dot{s}\gamma_T}{c^2 - \dot{s}^2}.$$

The phase boundary speed $\dot{s}$ is determined by the kinetic relation:

$$\frac{\mu \gamma_T}{2}(\gamma_p + \gamma_b - \gamma_m - \gamma_M) = \phi_{31}(\dot{s}).$$

Case 2. The material is initially in the high-strain phase, i.e. $\gamma_0 > \gamma_{cr}^*$.

If $v_b < v_0 + c(\gamma_0 - \gamma_{cr}^*)$, then the solution is the same as (3.23)(Figure 3.3a).

If $v_b > v_0 + c(\gamma_0 - \gamma_{cr}^*)$, then the solution is the same as (3.24)(Figure 3.3b). But $\dot{s}$ is determined by the kinetic relation:

$$\frac{\mu\gamma_T}{2}(\gamma_m + \gamma_M - \gamma_p - \gamma_b) = \phi_{13}(\dot{s}). \tag{3.25}$$

3.2 Solutions to Riemann problems: general two-phase elastic materials

By general two-phase elastic materials, we mean a material that can be characterized by a strain energy function $W(\gamma)$ such that

- $W(\gamma) > 0$,
- $\sigma(\gamma) = W'(\gamma)$, $\sigma(0) = 0, \sigma'(0) > 0$,
- $\sigma'(\gamma) > 0, -1 < \gamma < \gamma_m$,
  $\sigma'(\gamma) < 0, \gamma_m < \gamma < \gamma_M$,
  $\sigma'(\gamma) > 0, \gamma > \gamma_M$.

We call $-1 < \gamma < \gamma_m$ low-strain phase, $\gamma_m < \gamma < \gamma_M$ unstable phase and $\gamma > \gamma_M$ high-strain phase.

3.2.1 General features of solutions to Riemann problems

As in the case of trilinear materials, one can use the entropy inequality and the jump conditions to demonstrate the following features of the Riemann problem:

1. Two fans cannot propagate in the same direction, neither can two shock waves.
2. Two phase boundaries cannot propagate in the same direction.
3. A fan and a shock wave cannot propagate in the same direction.

4. When a phase boundary and a fan or a shock propagate in the same direction, the phase boundary cannot travel faster than the fan or the shock.

With these features in mind, one can easily determine all the possible solution structures for any initial data for a Riemann problem. However it is not easy to determine which solution structure is the right one for specific initial data. Lin [58] proposed a nontrilinear two-phase elastic material, and he solved a Riemann problem with special initial data and demonstrated that one can uniquely determine a solution through the kinetic relation and the nucleation criterion.

3.2.2 An approximate Riemann solver

It is not easy to obtain explicit analytical Riemann solutions for a general two-phase elastic material capable of phase transition. To solve the Riemann problem numerically requires the iteration of highly nonlinear equations. In practice, it is time consuming, and the convergence of the iteration cannot be guaranteed. Motivated by Roe's scheme [71] for the computation of shock waves, an approximate Riemann solver is proposed. The idea is to determine Riemann solutions by solving a constant coefficient linear system of conservation laws instead of the original nonlinear system. For conservation laws (2.2), (2.3), we approximate

$$f(U)_x = \begin{pmatrix} 0 & -\frac{\sigma'(\gamma)}{\rho} \\ -1 & 0 \end{pmatrix} \begin{Bmatrix} v_x \\ \gamma_x \end{Bmatrix} \approx \begin{pmatrix} 0 & -c^2 \\ -1 & 0 \end{pmatrix} \begin{Bmatrix} v_x \\ \gamma_x \end{Bmatrix} = AU_x. \tag{3.26}$$

Here c is a constant.

We consider a Riemann problem with initial data in different phases only, which means $U_l = (v_l, \gamma_l)$, $U_r = (v_r, \gamma_r)$ with γ_l, γ_r in the high-strain phase and the low-strain phase respectively. The algorithm for the approximate Riemann solver reads as:

1. Let $c_l = (\frac{\sigma'(\gamma_l)}{\rho})^{1/2}$, $c_r = (\frac{\sigma'(\gamma_r)}{\rho})^{1/2}$. Then we approximate the general stress-

strain relationship $\sigma(\gamma)$ by the following trilinear stress-strain relation:

$$\hat{\sigma}(\gamma) = \begin{cases} \rho c_r^2(\gamma - \gamma_r) + \sigma(\gamma_r), & -1 < \gamma < \gamma_m, \\ \frac{\hat{\sigma}_m - \hat{\sigma}_M}{\gamma_m - \gamma_M}(\gamma - \gamma_M) + \hat{\sigma}_M, & \gamma_m < \gamma < \gamma_M, \\ \rho c_l^2(\gamma - \gamma_l) + \sigma(\gamma_l) & \gamma_M < \gamma < \infty \end{cases} \tag{3.27}$$

where $\hat{\sigma}_m = \rho c_r^2(\gamma_m - \gamma_r) + \sigma(\gamma_r), \hat{\sigma}_M = \rho c_l^2(\gamma_M - \gamma_l) + \sigma(\gamma_l)$.

Solve the conservation laws for the trilinear material for the U_-^1, U_+^1, which are U right behind and in front of the phase boundary. The phase boundary propagation speed $\dot{s}_1$ is determined by the kinetic relation.

2. From the conservation requirement in hyperbolic regions, we improve the linear coefficient matrix A in the following way:

$$f(U_l) - f(U_-^n) = \hat{A}_l(U_l - U_-^n), \tag{3.28}$$

$$f(U_r) - f(U_+^n) = \hat{A}_r(U_r - U_+^n). \tag{3.29}$$

From which we have

$$c_l = (\frac{\sigma(\gamma_l) - \sigma(\gamma_-^n)}{\rho(\gamma_l - \gamma_-^n)})^{1/2}, \tag{3.30}$$

$$c_r = (\frac{\sigma(\gamma_r - \sigma(\gamma_+^n)}{\rho(\gamma_l - \gamma_+^n)})^{1/2}. \tag{3.31}$$

Then we can approximate the general stress-strain relationship $\sigma(\gamma)$ by an improved trilinear stress-strain relation which has a form the same as that in step 1. We solve the new approximate conservation laws for the new trilinear stress-strain relation for the U_-^{n+1}, U_+^{n+1} which are U behind and in front of the phase boundary. The phase boundary propagation speed $\dot{s}_n$ is determined by kinetic relation.

3. If $|\dot{s}_n - \dot{s}_{n-1}| < \epsilon$, then we have the following approximate solutions: $\dot{s} = \dot{s}_n$, $U_- = U_-^n$, $U_+ = U_+^n$.

4. If $\sigma'(\gamma_l) > \sigma'(\gamma_-)$, then we replace the left shock by a rarefaction wave in

$-(\frac{\sigma'(\gamma_l)}{\rho})^{1/2} < \frac{x}{t} < -(\frac{\sigma'(\gamma_-)}{\rho})^{1/2}$. If $\sigma'(\gamma_r) > \sigma'(\gamma_+)$, we replace the right shock by a rarefaction wave in $(\frac{\sigma'(\gamma_+)}{\rho})^{1/2} < \frac{x}{t} < (\frac{\sigma'(\gamma_r)}{\rho})^{1/2}$.

It can be easily checked that the above algorithm satisfies the three conditions suggested by Roe [71] in hyperbolic regions. As the phase boundary is not known priori, the above "linearized" conservation laws are still in fact nonlinear.

We apply the approximate Riemann solver to two Riemann problems for a hypothetical nontrilinear stress-strain relation:

$$\sigma(\gamma) = \begin{cases} -\frac{0.0071}{1+\gamma} + 14.64\gamma - 0.953, -1 < \gamma < -0.9, \\ \gamma(\gamma^2 - 4.4\gamma + 5), -0.9 \leq \gamma < 4, \\ \frac{950}{1+\gamma} + 55.8\gamma - 399.8, 4 \leq \gamma < \infty \end{cases} \tag{3.32}$$

with $\gamma_m = 0.770646, \gamma_M = 2.1629$. This stress-strain relation is that for a material model proposed by Lin [57].

Test 1. 1-shock, 1-subsonic phase boundary, 1-shock

initial condition: $(v_l, g_l, v_r, g_r) = (0, 2.5, -0.5, 0.5)$, $\rho = 1$ and $\omega = 0.5$.

methods	Approximate Riemann solver	Exact Riemann solver
$\dot{s}$	-0.14070	-0.15547
v_+	-0.10279	-0.11767
γ_+	0.23198	0.24046
v_-	0.23859	0.26024
γ_-	2.65840	2.67122

Test 2. 1-shock, 1-subsonic phase boundary, 1-rarefaction wave

initial conditions: $(v_l, g_l, v_r, g_r) = (-1.6, 2.7, 0.1, 0.1)$, $\rho = 1$ and $\omega = 0.5$.

methods	Approximate Riemann solver	Exact Riemann solver
$\dot{s}$	0.49437	0.51091
v_+	−0.10773	−0.06913
γ_+	0.20767	0.18677
v_-	−1.39407	−1.40610
γ_-	2.80966	2.80359

For "exact Riemann solver," we mean a procedure to obtain Riemann solutions from original nonlinear equations by numerical iteration. An algorithm proposed by Shacham [76] for the numerical solution of constrained nonlinear algebraic equations is used here. From the two tests, we see that the approximate Riemann solver works resonably well, with an error for phase boundary propagation speed is less than 7%.

There are several advantages of the approximate Riemann solver over the "exact Riemann solver." When using the "exact Riemann solver," we have to make an initial guess of the solutions, we may encounter degenerate situations with Jacobian determinant zero, and we cannot always guarantee that the numerical solutions satisfy the entropy inequality. There are no such troubles for the approximate Riemann solver.

3.3 Remarks

The motion described by trilinear materials is much simpler than that described by general two-phase elastic materials. Trilinear materials can describe phase boundaries, but it cannot describe rarefaction fans. However, from the general features of Riemann problems for trilinear materials and for general two-phase elastic materials, we see that the behavior of phase boundaries described by trilinear materials is qualitatively the same as that described by general two-phase elastic materials. So the trilinear material model is a good approximation as far as phase boundary behavior is concerned.

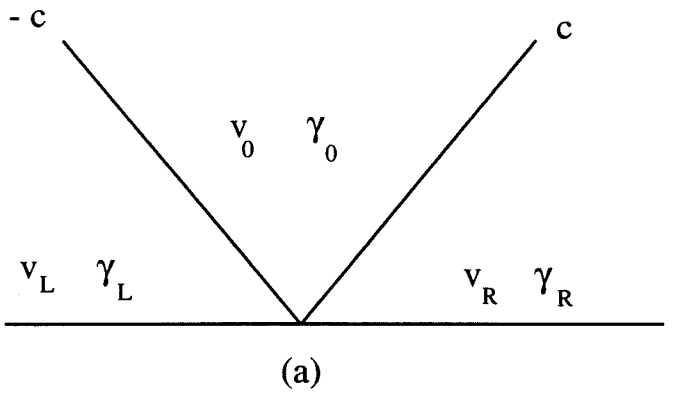

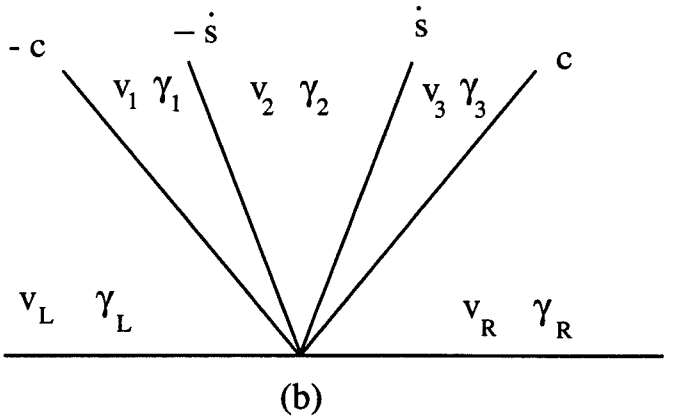

Figure 3.1: Form of solution to Riemann problem with initial data in the low-strain phase

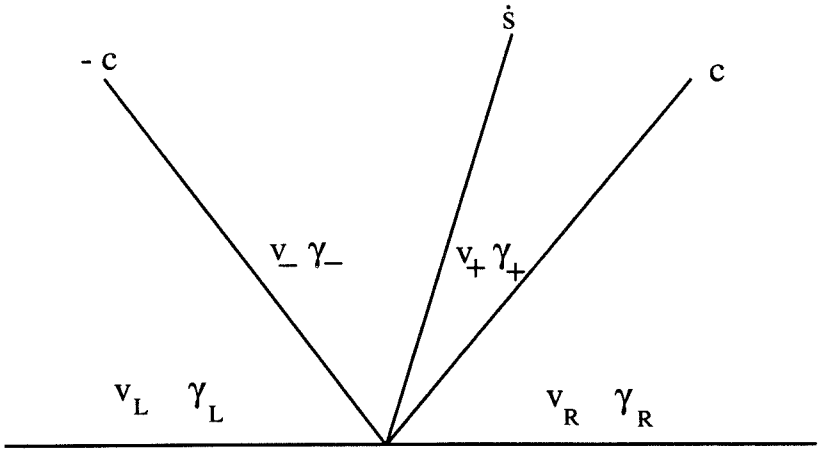

Figure 3.2: Form of solution to Riemann problem with initial data in the low-strain phase and high-strain phase

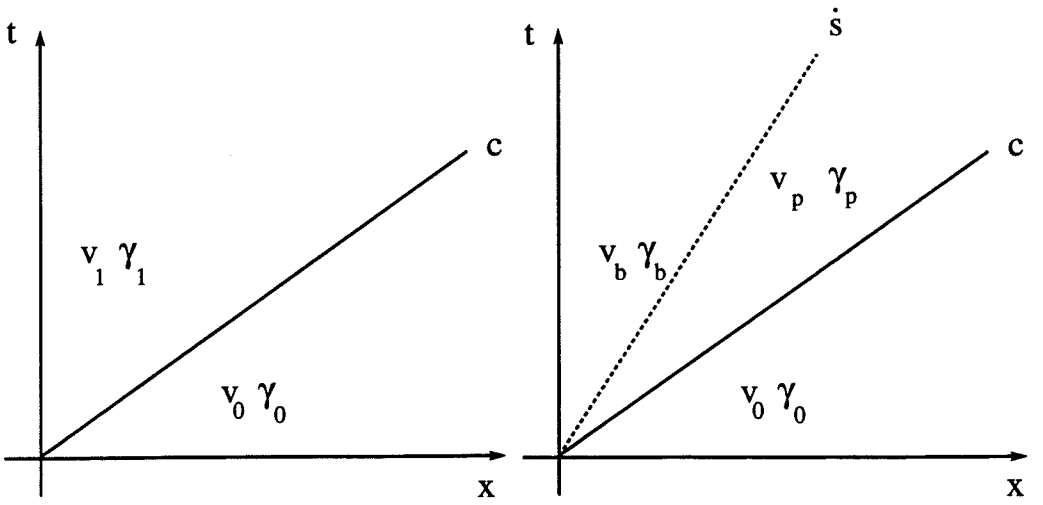

Figure 3.3: Form of solution to a special initial-boundary value problem

Chapter 4 Modeling of Martensitic transformation induced by a tensile pulse

Under circumstances that lead to quasi-static thermomechanical responses of phase transforming materials, the predictions of the models of the kind developed by Abeyaratne & Knowles have been extensively and favorably compared qualitatively with corresponding experimental observations, e.g. see [2], [47] and [10]. There are situations where inertial effects cannot be ignored, e.g. phase transforming materials subjected to dynamic loadings. Here we apply the model presented in Chapter 2 to describe the dynamics of martensitic transformations induced by tensile stress pulses in impact experiments.

From an impact experiment, Meyers & Guimaraes [61] found that a tensile pulse produced by the reflection of shock waves at a free boundary generated martensitic transformation in a Fe-Ni-C alloy, while compressive waves only produced dislocations. Snell et al. [81] also observed martensitic phase transformation in a disc-shaped Fe-Ni-C alloy in an impact experiment. The transformed region was formed near the free surface of the disc, rather than the impact surface. Later, Meyers [61] showed that the distribution of the martensites in Snell et al.'s experiment was due to a tensile pulse. In 1986, Thadhani & Meyers [86] investigated the kinetics of martensitic transformation induced by a tensile pulse in a delicately designed one-dimensional experiment. Meyers [62] and Thadhani & Meyers [86] analyzed the martensitic transformation induced by a tensile pulse. This martensitic transformation, observed in Fe-Ni-C alloys, provides us a prototype for one-dimensional continuum modeling of phase transformations in a dynamical process.

Here we formulate a mathematical problem corresponding to the Thadani & Meyer experiment. The problem to be solved in the modeling is more complicated than common initial-boundary value problems because there are interactions between the

impactor and the specimen.

4.1 Formulation of the problem

The main concern here is to use a model of the kind developed by Abeyaratne & Knowles to describe the dynamics of martensitic transformations induced by a tensile pulse in impact experiments. For a particular experimental set up one can refer to [86] of Thadani & Meyers .

In an impact experiment, we have an impactor and a specimen. Assume the impactor is a single-phase material bar with length l, while the specimen is a two-phase material bar of length L. The impactor moves at a constant speed v_0 prior to impact, while the specimen is stationary. At time t=0, the impactor hits the specimen. It is assumed that at $t = 0$, the impactor occupies the interval $[-l, 0)$, while the specimen occupies the interval $(0, L]$.

In the modeling, we take the undeformed impactor and the specimen in $[-l, L]$as the reference configuration. We assume the material of the impactor is an elastic material which is characterized by the stress-strain relation $\sigma = \mu'\gamma$. The material of the specimen is assumed to be the special trilinear material defined in Section 2.2. Here we can interpret the high-strain phase of the material as martensite, while the low-strain phase is austenite. Denote by ρ, ρ' the densities of the two materials respectively. Further, let $c = \sqrt{\frac{\mu}{\rho}}, c' = \sqrt{\frac{\mu'}{\rho'}}$ be the the speeds of the sound waves in the two materials.

As initial conditions, we take

$$v(x,0) = \begin{cases} v_0, & -l < x < 0, \\ 0, & 0 < x \leq L \end{cases} \tag{4.1}$$

and

$$\gamma(x,0) = \begin{cases} 0, & -l < x < 0, \\ 0, & 0 < x \leq L. \end{cases} \tag{4.2}$$

The boundary conditions are:

$$\sigma(-l,t) = 0, \qquad \sigma(L,t) = 0. \tag{4.3}$$

In an impact experiment, the impactor and the specimen are in contact for a time t^* after the impact; subsequently the two are separated. Thus we have the following interface conditions:

$$\sigma(0+,t) = \sigma(0-,t) \tag{4.4}$$

$$v(0+,t) = v(0-,t) \tag{4.5}$$

when t is in $(0,t^*)$;

$$\sigma(0+,t) = 0, \qquad \sigma(0-,t) = 0, \tag{4.6}$$

$$v(0+,t) > v(0-,t) \tag{4.7}$$

when t is in (t^*,∞).

It should be noted that t^* is not known in advance, but rather is determined as part of the solution of the problem. This makes the impact problem more complicated than a standard initial-boundary value problem.

4.2 Analytical solution of the problem for short time

We further assume that a low-strain-phase to high-strain-phase transformation can happen only under tension. It is also assumed that $L > \frac{c}{c}l$ for simplicity of analysis.

For the problem formulated in Section 4.1, we have piecewise constant initial data and constant boundary values. We can construct a solution to the problem by using the solutions of Riemann problem. In a procedure similar to the one used in Chapter 3, we show that the problem has a solution that can be illustrated by Figure 4.1 at the initial stage.

This is a piecewise constant solution. In this case, the governing equations reduce

to a group of algebraic equations. From jump conditions at $x = ct$ and $x = -c't$ and continuity conditions at $x = 0$, we have

$$v_- - v_0 - c'(\gamma_- - 0) = 0, \tag{4.8}$$

$$v_+ + c\gamma_+ = 0, \tag{4.9}$$

$$v_- = v_+, \tag{4.10}$$

$$\mu'\gamma_- = \mu\gamma_+. \tag{4.11}$$

It follows that,

$$v_+ = v_- = \frac{v_0}{(1 + \frac{c'\mu}{\mu' c})} \tag{4.12}$$

$$\gamma_+ = -\frac{v_0}{c(1 + \frac{c'\mu}{\mu' c})} \tag{4.13}$$

$$\gamma_- = -\frac{v_0}{c'(1 + \frac{c\mu'}{\mu c'})}. \tag{4.14}$$

As $L > \frac{c}{c'}l$, the reflected shock wave from $x = -l$ will reach the interface $x = 0$ earlier than the reflected shock wave from $x = L$, as shown in Figure 4.1. Denote by t^* the time the reflected shock wave in the impactor reaches $x = 0$. Right before t^*, the particle velocity in the impactor is:

$$v = v_- + c'\gamma_- < v_+. \tag{4.15}$$

Thus we have $v(0-, t^*) < v(0+, t^*)$, which means the impactor and the specimen are separated at time $t^* = \frac{2l}{c'}$. This suggests that we can ignore the impactor after t^*.

For $0 < t < t^*$, we have

$$v_1 = v(0, t) = \frac{v_0}{1 + \frac{c'}{\mu'}\frac{\mu}{c}} \tag{4.16}$$

and

$$\gamma_1 = \gamma(0,t) = -\frac{v_0}{c(1+\frac{c'}{\mu'}\frac{\mu}{c})} \tag{4.17}$$

in the specimen.

For $t > t^*$,

$$\sigma(0,t) = 0. \tag{4.18}$$

We can view the impact on the specimen as an incident wave with finite duration, see Figure 4.1. When the front of the incident wave $x = ct$ reaches the free end, it is reflected. In region II, the reflected wave and the incident wave cancel each other,

$$v_1 - v_2 - c(\gamma_1 - \gamma_2) = 0, \tag{4.19}$$

$$\gamma_2 = 0, \tag{4.20}$$

that is

$$v_2 = 2v_1 > 0, \tag{4.21}$$

and

$$\gamma_2 = 0. \tag{4.22}$$

Here the fact that $\gamma_2 = 0$ is due to the boundary condition at $x = L$. When the reflected wave front encounters the rear of the incident wave, a tensile pulse emerges, which can be found by solving a suitable Riemann problem. Two situations have to be taken into account, depending on whether a phase transition occurs.

Case 1: No phase transition occurs. When the magnitude of v_0 is small enough, there is no new phase initiated. At the point in space where the reflected wave front collides with the rear of the incident wave, we have a Riemann problem with initial data $v_L = v_4 = 0$, $\gamma_L = \gamma_4 = 0$, $v_R = v_2 = 2v_1$, $\gamma_R = \gamma_2 = 0$. We can obtain v_3 and γ_3 by solving it:

$$\gamma_3 = \frac{v_1}{c} = -\gamma_1 > 0, \tag{4.23}$$

$$v_3 = c\gamma_3 = v_1 > 0. \tag{4.24}$$

The necessary condition for the solution to be valid is that, $\gamma_3 < \gamma_{cr}$, where γ_{cr} is the critical strain for nucleation of a low-strain phase to high-strain phase transformation. The necessary condition can be written in term of v_0:

$$v_0 < c(1 + \frac{c'\mu}{\mu' c})\gamma_{cr}. \tag{4.25}$$

Under this condition, there will be no additional phase transformation later. It is easy to show that the bar will be in tension and compression alternatively as time goes on, see Figure 4.2.

Case 2: A phase transition occurs. When $v_0 > c(1 + \frac{c'\mu}{\mu' c})\gamma_{cr}$, a new phase is initiated due to the generated tensile pulse. We can determine the deformation state at this time by solving a Riemann problem with initial data $v_L = v_4 = 0$, $\gamma_L = \gamma_4 = 0$, $v_R = v_2 = 2v_1$, $\gamma_R = \gamma_2 = 0$. As demonstrated in Chapter 3, there are two and only two phase boundaries at the nucleation point, see Figure 4.3. By the jump conditions at shock waves and phase boundaries, we have

$$\begin{aligned}
v_{11} - v_L - c(\gamma_{11} - \gamma_L) &= 0, && (4.26)\\
v_{13} - v_R + c(\gamma_{13} - \gamma_R) &= 0, && (4.27)\\
\mu(\gamma_{12} - \gamma_T) - \mu\gamma_{11} - \rho\dot{s}(v_{12} - v_{11}) &= 0, && (4.28)\\
v_{112} - v_{11} - \dot{s}(\gamma_{12} - \gamma_{11}) &= 0 && (4.29)\\
\mu(\gamma_{12} - \gamma_T) - \mu\gamma_{13} + \rho\dot{s}(v_{12} - v_{13}) &= 0, && (4.30)\\
v_{12} - v_{13} + \dot{s}(\gamma_{12} - \gamma_{13}) &= 0. && (4.31)
\end{aligned}$$

The deformation state in the bar right after the initiation of the new phase is given by

$$\begin{aligned}
\gamma_{11} &= -\gamma_1 - \frac{c\dot{s}\gamma_T}{c^2 - \dot{s}^2}, && (4.32)\\
\gamma_{12} &= -\gamma_1 + \frac{c\gamma_T}{c + \dot{s}}, && (4.33)\\
\gamma_{13} &= -\gamma_1 - \frac{c\dot{s}\gamma_T}{c^2 - \dot{s}^2}, && (4.34)
\end{aligned}$$

$$v_{11} = -c\gamma_1 - \frac{c^2\dot{s}\gamma_T}{c^2 - \dot{s}^2}, \tag{4.35}$$

$$v_{12} = -c\gamma_1, \tag{4.36}$$

$$v_{13} = -c\gamma_1 + \frac{c^2\dot{s}\gamma_T}{c^2 - \dot{s}^2}. \tag{4.37}$$

The solutions (4.32) - (4.37) are expressed in terms of $\dot{s}$, where $\dot{s}$ is determined by kinetic relation $f = \phi(\dot{s})$. Thus the state of the bar is totally determined. We can now determine when and where the phase transition occurs.

When

$$L > \frac{c}{c'}l \tag{4.38}$$

and

$$v_0 > c(1 + \frac{c'\mu}{\mu' c})\gamma_{cr} \tag{4.39}$$

a new phase will be nucleated at time t_n:

$$t_n = \frac{l}{c'} + \frac{L}{c}. \tag{4.40}$$

The position of the nucleation point is

$$x_n = L - \frac{lc}{c'}. \tag{4.41}$$

Prior to interaction of the shock waves and the phase boundaries, the new phase will grow. When interaction of the phase boundaries and shock waves occurs, the phase boundary speeds of the two phase boundaries will change. We can determine each interaction between a phase boundary and a shock wave by solving a suitable Riemann problem. The situation gets quite complicated as time goes on and it is impossible to describe all interactions for large time. There are at least two possible cases for the interaction of shock waves and phase boundaries; see Figure 4.4.

The time and location of nucleation depend on the geometry and the material properties of the impactor and specimen, but they do not depend on the magnitude of v_0 directly. On the other hand, whether there are disconnected high-strain phase

regions or not depends on the magnitude of v_0, among other factors. From the solutions, we see that the transformed region or regions are away from either ends of the specimen. This analytical prediction is in qualitative agreement with experimental observations [81, 86]. But we cannot determine the ultimate equilibrium positions of the phase boundaries because we only have short time solutions at the current stage. We have to use a numerical method to obtain information for the long-time evolution of phase boundaries and the final equilibrium state of the bar. This will not be done here.

4.3 Comments

As shown in Section 4.2, the approach of Abeyaratne and Knowles can be applied to martensitic transformations that arise in impact experiments. Compared with the analysis of Meyers [62] and Thadhani & Meyers [86], this approach has the following advantages: It can predict the critical v_0 for the initiation of martensitic transformation, it can predict possible reverse transformations (high-strain phase to low-strain phase), as in Figure 4.4, and it can also predict the martensitic transformations by a successive tensile stress. Furthermore the approach of Abeyaratne and Knowles can describe the long-time behavior of phase boundaries, including the final equilibrium state of the specimen. Because the model is a one-dimensional continuum model, it is unable to give any information about the microstructural changes during the transformation or the morphological features of martensites.

Within the one-dimensional continuum mechanical frame work, the modeling can be improved in several ways. For example, an adiabatic assumption may be used instead of the isothermal model used here. This is because the isothermal assumption does not strictly hold at a phase boundary in a dynamical process associated with the martensitic transformation.

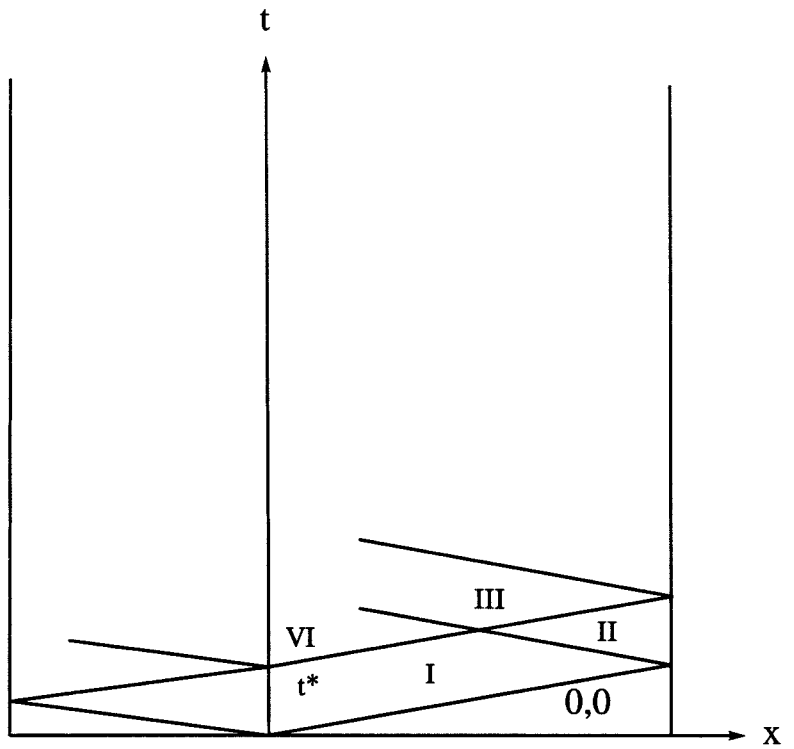

Figure 4.1: Schematic diagram for the impact problem

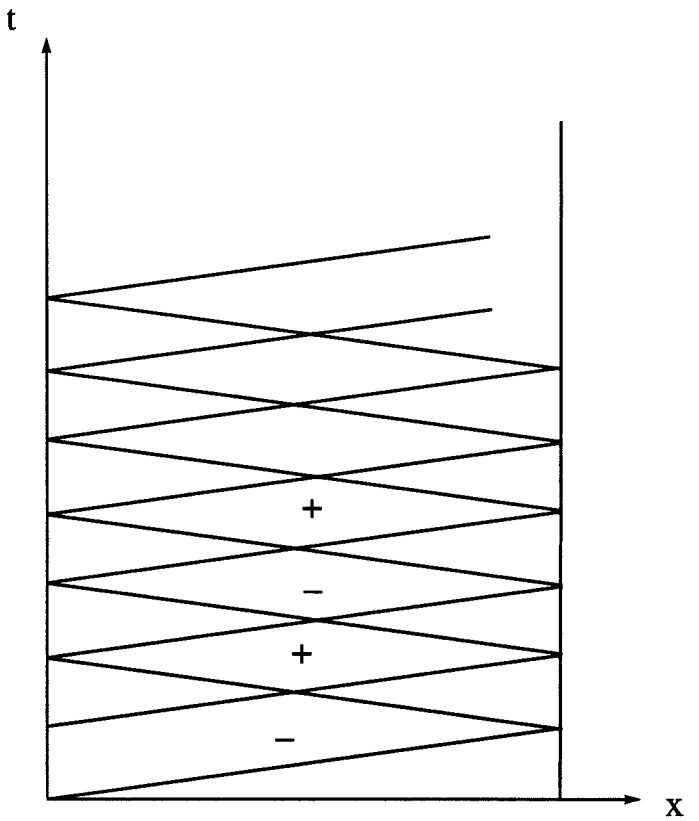

Figure 4.2: Form of solution to case 1: alternation of a tensile and a compressive wave

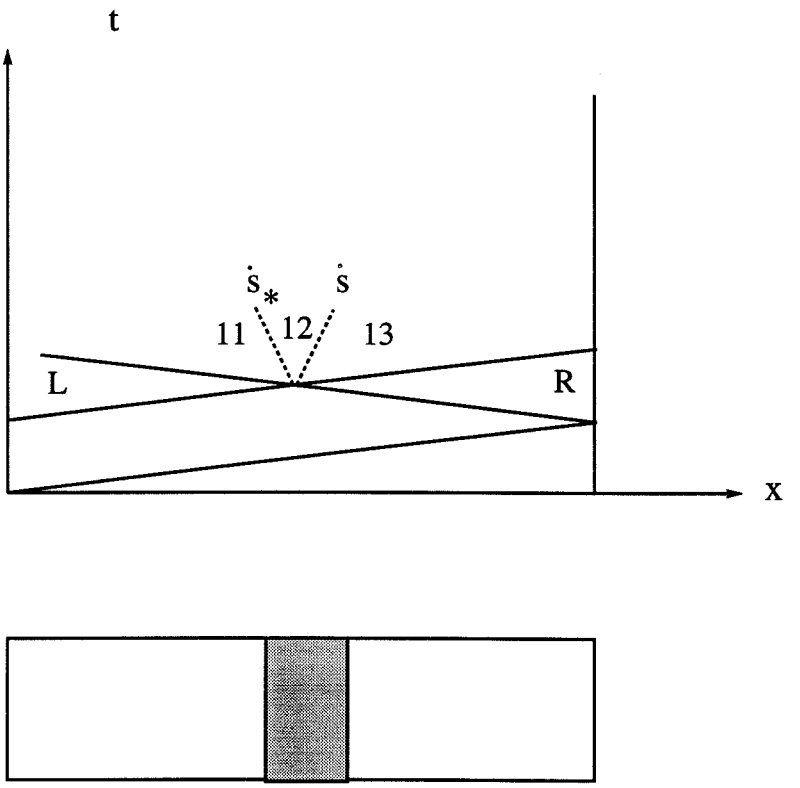

Figure 4.3: Form of solution that involves nucleation of a new phase: a)nucleation of high-strain phase; b)The transformed region in the bar: the shaded region corresponds to high-strain phase

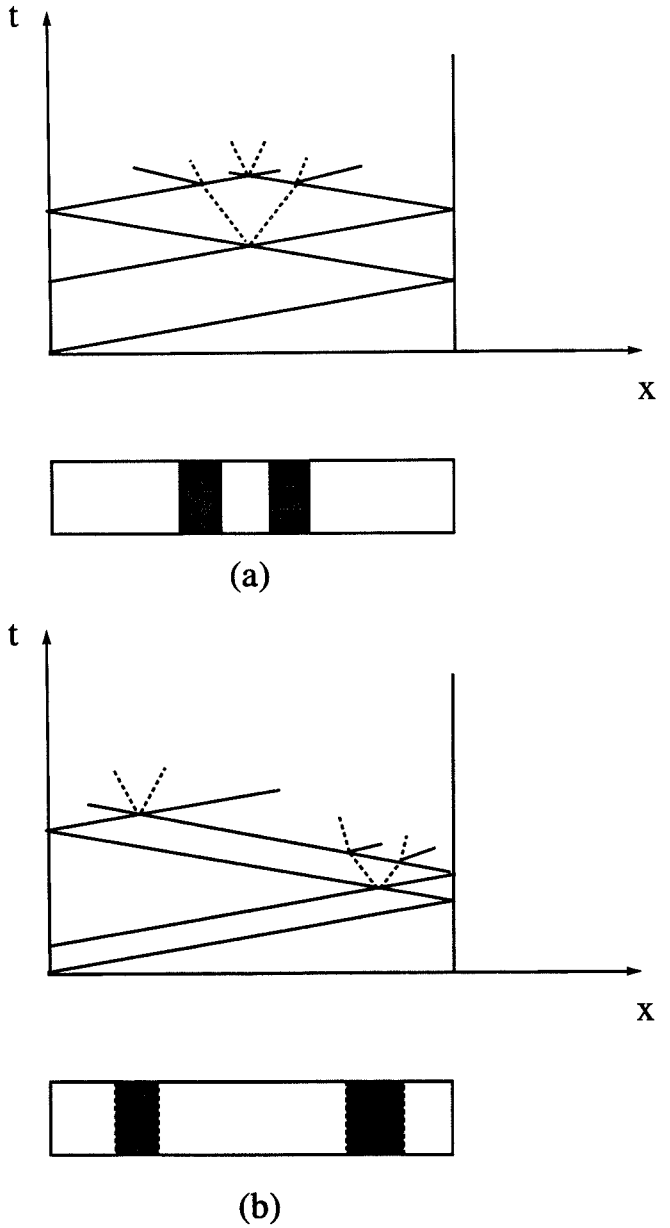

Figure 4.4: Form of solution: a) low-strain phase is initiated from high-strain phase; b)a tensile pulse induces high-strain phase

Chapter 5 Large time dynamical behavior of a phase boundary: an exact solution

It has been shown by Abeyaratne & Knowles [5] and James [44] that the motion of a phase boundary is dissipative in a nonlinear elastodynamic theory for solid-solid phase transformations. Thus one expects that the dynamical system associated with phase transformations may reach an equilibrium state at large time, or from an energy perspective, the dynamical system will eventually reach a minimum energy state.

Recently, Lin & Pence [55], [56] made an effort to solve this problem in a one-dimensional setting. Due to the formidable analytical difficulties in solving a fully dynamic problem and then identifying the large time equilibrium state, they attacked the problem by an approximate energy approach. They showed that total energy dissipated is the energy necessary to settle the dynamical system into a new minimum energy state.

Here an attempt is made to obtain an analytical solution for the large time dynamical behavior of a phase boundary in the frame work of Abeyaratne & Knowles [2, 5]. In order to obtain an analytical solution for the phase boundary motion at large time, we choose the simplest possible problem. A semi-infinite bar intially possessing a single phase boundary is considered. The material of the bar is assumed to be trilinear, with common elastic moduli in the two metastable phases. We make no approximations in obtaining our analytical solution.

Unfortunately the approach to get the exact solution to this problem cannot be used to solve the problem of finite bar considered by Lin & Pence [55], [56]. A numerical approach is inevitable for the finite bar problem.

The initial-boundary value problem to be solved is formulated in Section 5.1. In the problem we assume that the material is the special trilinear material defined in Section 2.3. The kinetic relation is assumed to be the simplest one, $f = \omega \dot{s}$,

where ω is a constant. There is a preexisting phase boundary. In Section 5.2, we analyze the short time behavior of the phase boundary due to an external disturbance. We determine restrictions on the external disturbance and material parameters that prevent the initiation of new phase boundaries. We solve the problem for *large* time in Section 5.3, relying on the assumption that there is only one phase boundary at any time. Simple nonlinear recursive formulae are obtained for the motion of the phase boundary and the deformation in the bar. In Section 5.4 we consider the problem formulated in Section 5.1 for general monotonically increasing kinetic function $\phi(\dot{s})$. Numerical calculations that support our analytical results are carried out in Section 5.5.

5.1 Formulation of an initial-boundary value problem

A semi-infinite bar is under consideration. The material of the bar is assumed to be the special trilinear material defined in Section 2.3. The motion of a phase boundary is governed by kinetic relation $f = \phi(\dot{s})$, with $\phi(\dot{s}) = \omega\dot{s}$. As defined in Chapter 2, f is the dynamical driving traction on a phase boundary, and $\dot{s}$ is the phase boundary propagation speed. The nucleation criterion is the one given in Section 2.2.

Initially, the bar is in the low-strain phase for $0 \leq x < s_0$, and in the high-strain phase for $s_0 < x < \infty$. The bar is in equilibrium state. Thus the phase boundary at s_0 is initially stationary. From the kinetic relation, $f = \omega\dot{s}$, we conclude that $f = 0$, so that the bar is initially in Maxwell state:

$$v(x,0) = v_0^- = 0, \tag{5.1}$$

$$\gamma(x,0) = \gamma_0^- = \frac{1}{2}(\gamma_m + \gamma_M - \gamma_T) \tag{5.2}$$

for $0 \leq x < s_0$;

$$v(x,0) = v_0^+ = 0, \tag{5.3}$$

$$\gamma(x,0) = \gamma_0^+ = \frac{1}{2}(\gamma_m + \gamma_M + \gamma_T) \tag{5.4}$$

for $s_0 < x < \infty$.

At $t = 0$, the end of the bar is suddenly subjected to a velocity v_0 which is maintained constant until time t^* and then reduced instantly to zero. The boundary conditions can be described as:

$$v(0,t) = v_0, \quad 0 \leq t < t^*, \tag{5.5}$$

$$v(0,t) = 0, \quad t > t^*. \tag{5.6}$$

This boundary condition is equivalent to the following displacement boundary condition:

$$u(0,t) = v_0 t + u_0 \quad , 0 \leq t \leq t^*, \tag{5.7}$$

$$u(0,t) = v_0 t^* + u_0, \quad t > t^*, \tag{5.8}$$

where u_0 is the initial displacement of the particle at $x = 0$ with respect to a reference configuration.

5.2 A short time analysis

In this section we will solve the problem formulated in Section 5.1 for short time. We assume that there are no new phase boundaries nucleated due to the interaction of the original phase boundary and the incident wave or due to the boundary condition. We will determine restrictions on the v_0 and the kinetic relation that assure that this assumption is valid.

As we have piecewise constant initial data and boundary values, we can solve the problem by dealing with suitable Riemann problems. It is easy to show that the solution is piecewise constant; see Figure 5.3. The governing equations are then reduced to jump conditions on shock waves and jump conditions and the kinetic

relation on the phase boundary.

At first the incident compressive wave propagates toward the stationary phase boundary. The strain γ_0 (Figure 5.3) can be determined by the jump condition on shock AB:

$$v_0 - v_0^- + c(\gamma_0 - \gamma_0^-) = 0, \tag{5.9}$$

so

$$\gamma_0 = -\frac{v_0}{c} + \gamma_0^- < \gamma_0^-. \tag{5.10}$$

On shock CD, the jump condition is,

$$\bar{v} - v_0 + c(\bar{\gamma} - \gamma_0) = 0. \tag{5.11}$$

Due to boundary condition, we have

$$\bar{\gamma} = \gamma_0^-, \tag{5.12}$$

$$\bar{v} = 0. \tag{5.13}$$

When the leading edge of the incident wave reaches the phase boundary, the incident wave is both reflected by the phase boundary and transmitted through it. The jump conditions on the phase boundary and shock waves are:

$$(v_1^+ - v_0^+) + c(\gamma_1^+ - \gamma_0^+) = 0, \tag{5.14}$$

$$\mu(\gamma_1^+ - \gamma_T) - \mu\gamma_1^- + \rho\dot{s}_1(v_1^+ - v_1^-) = 0, \tag{5.15}$$

$$(v_1^+ - v_1^-) + \dot{s}_1(\gamma_1^+ - \gamma_1^-) = 0, \tag{5.16}$$

$$(v_1^- - v_0) - c(\gamma_1^- - \gamma_0) = 0. \tag{5.17}$$

Solving (5.14)-(5.17), we find that

$$v_1^- = v_0 + \frac{c\dot{s}_1\gamma_T}{2(c + \dot{s}_1)}, \tag{5.18}$$

$$\gamma_1^- = -\frac{v_0}{c} + \gamma_0^- + \frac{\dot{s}_1\gamma_T}{2(c + \dot{s}_1)}, \tag{5.19}$$

$$v_1^+ = v_0 - \frac{c\dot{s}_1\gamma_T}{2(c-\dot{s}_1)}, \tag{5.20}$$

$$\gamma_1^+ = -\frac{v_0}{c} + \gamma_0^+ + \frac{\dot{s}_1\gamma_T}{2(c-\dot{s}_1)}. \tag{5.21}$$

Here $\dot{s}_1$ is determined by the kinetic relation, $f = \omega\dot{s}$, i.e.,

$$\frac{\mu\gamma_T}{2}(\gamma_M + \gamma_m - \gamma_1^+ - \gamma_1^-) = \omega\dot{s}_1. \tag{5.22}$$

The velocity v and strain γ are determined from jump conditions on the shocks FD and DE,

$$v - v_1^- + c(\gamma - \gamma_1^-) = 0, \tag{5.23}$$

$$v - \bar{v} - c(\gamma - \bar{\gamma}) = 0. \tag{5.24}$$

Thus

$$v = \frac{c\dot{s}_1\gamma_T}{2(c+\dot{s}_1)}, \tag{5.25}$$

$$\gamma = \frac{\gamma_m + \gamma_M}{2} - \frac{c\gamma_T}{2(c+\dot{s}_1)}. \tag{5.26}$$

We determine v_1 and γ_1 from a jump condition

$$v - v_1 + c(\gamma - \gamma_1) = 0 \tag{5.27}$$

and boundary condition. We find that

$$v_1 = 0, \tag{5.28}$$

$$\gamma_1 = \frac{\gamma_m + \gamma_M}{2} - \frac{(c-\dot{s}_1)\gamma_T}{2(c+\dot{s}_1)}. \tag{5.29}$$

Now we determine $v_2^\pm, \gamma_2^\pm$ formally. The corresponding jump conditions are

$$\mu(\gamma_2^+ - \gamma_T) - \mu\gamma_2^-) + \dot{s}_2(v_2^+ - v_2^-) = 0, \tag{5.30}$$

$$(v_2^+ - v_2^-) + \dot{s}_2(\gamma_2^+ - \gamma_2^-) = 0, \tag{5.31}$$

$$v_2^- - v - c(\gamma_2^- - \gamma) = 0, \tag{5.32}$$

$$v_2^+ - v_1 + + c(\gamma_2^+ - \gamma_1^+) = 0. \tag{5.33}$$

From equations (5.30)-(5.33),

$$\gamma_2^- = \frac{1}{2}(\gamma_m + \gamma_M) - \frac{c\gamma_T}{2(c + \dot{s}_2)}, \tag{5.34}$$

$$\gamma_2^+ = \frac{1}{2}(\gamma_m + \gamma_M) + \frac{c\gamma_T}{2(c - \dot{s}_2)}. \tag{5.35}$$

Therefore, the driving traction f on phase boundary $\dot{s}_2$ can be expressed as

$$\begin{aligned} f &= \frac{\mu\gamma_T}{2}(\gamma_M + \gamma_m - \gamma_2^- - \gamma_2^+) \\ &= -\frac{\mu\gamma_T^2 c\dot{s}_2}{2(c^2 - \dot{s}^2)}. \end{aligned} \tag{5.36}$$

It is easy to show that f is monotonically decreasing with respect to $\dot{s}_2$. From the kinetic condition $f = \omega\dot{s}$, we have,

$$-\frac{\mu\gamma_T^2 c\dot{s}_2}{2(c^2 - \dot{s}^2)} = \omega\dot{s}_2. \tag{5.37}$$

There is only one solution of (5.37), namely

$$\dot{s}_2 = 0. \tag{5.38}$$

Thus we have

$$v_2^- = 0, \tag{5.39}$$

$$\gamma_2^- = \gamma_0^-, \tag{5.40}$$

$$v_2^+ = 0, \tag{5.41}$$

$$\gamma_2^+ = \gamma_0^+. \tag{5.42}$$

Therefore, after the passage of the incident wave, the phase boundary will be stationary for while.

Certain restrictions must now be imposed to assure that there is no new phase boundary nucleated.

Restrictions on the short time analysis

First we require that

$$\frac{2s_0}{c} > t^*. \tag{5.43}$$

This is because that it is assumed in the above analysis that the shock wave reflected by the phase boundary will reach $x = 0$ at time $t > t^*$.

Secondly, we require that $\gamma_1^{\pm}$ belong to appropriate phases. To check this, it is necessary to check whether a Riemann problem with initial data γ_L and γ_R in the low-strain and high-strain phases respectively has a solution that satisfies phase segregation conditions. For the Riemann problem with initial data (v_L, γ_L) and (v_R, γ_R), where γ_L belongs to the low-strain phase and γ_R belongs to the high-strain phase (Figure 5.4) we have

$$\gamma^+ = h + \frac{c\gamma_T}{2(c - \dot{s})}, \tag{5.44}$$

$$\gamma^- = h - \frac{c\gamma_T}{2(c + \dot{s})}, \tag{5.45}$$

where

$$h = \frac{1}{2c}(v_R + c\gamma_R - v_L + c\gamma_L). \tag{5.46}$$

By the phase segregation condition, we require that $\gamma^+ > \gamma_M$ and $\gamma^- < \gamma_m$. Then we have

$$\gamma_M - \frac{c\gamma_T}{2(c - \dot{s})} < h < \gamma_m + \frac{c\gamma_T}{2(c + \dot{s})}. \tag{5.47}$$

The expression (5.47) can be expressed in term of the driving traction f. From Chapter 2, we have

$$f = \frac{\mu\gamma_T}{2}(\gamma_M + \gamma_m - \gamma^- - \gamma^+) \tag{5.48}$$

So

$$\frac{\mu\gamma_T}{2}(\gamma_M - \gamma_m - \frac{c^2\gamma_T}{c^2 - \dot{s}^2}) < f < \frac{\mu\gamma_T}{2}(\gamma_m - \gamma_M + \frac{c^2\gamma_T}{c^2 - \dot{s}^2}). \tag{5.49}$$

Inequality (5.49) can be illustrated in the $f - \dot{s}$ plane as in Figure 5.5. The shaded region in Figure 5.5 is the place where (5.49) is satisfied.

In order to have a solution which satisfies phase segregation conditions, the curve corresponding to kinetic relation $f = \omega\dot{s}$ must lie in the shaded region in Figure 5.5. So we further require that

$$0 < \omega < \omega_0. \tag{5.50}$$

We can determine an upper bound ω_0 for ω by determining the slope of the line which is tangent to the curve $f = \frac{\mu\gamma_T}{2}(\gamma_m - \gamma_M + \frac{c^2\gamma_T}{c^2 - \dot{s}^2})$ and passes through the origin. This gives

$$\omega_0 = \frac{\mu\gamma_T^2}{c} y^2 \sqrt{\frac{y-1}{y}}, \tag{5.51}$$

where y satisfies

$$y^2 - \frac{3}{2}y + \frac{\gamma_M - \gamma_m}{2\gamma_T} = 0. \tag{5.52}$$

Thirdly, we require that γ, γ_1 are in the low-strain phase. It can be shown that this requirement is equivalent to the inequality

$$\frac{\gamma_M + \gamma_m}{2} - \frac{c - \dot{s}}{2(c + \dot{s})}\gamma_T < \gamma_m \tag{5.53}$$

where $\dot{s}$ is determined by (5.22). The equation (5.22) can be rewritten as

$$\frac{2v_0}{c\gamma_T} = (\frac{c}{c^2 - \dot{s}^2} + \frac{2\omega}{\mu\gamma_T^2})\dot{s}.$$

The inequality (5.53) can be simplified as

$$\dot{s} < c\frac{1 - c_\gamma}{1 + c_\gamma},$$

thus the restriction on v_0 is

$$0 < v_0 < \frac{c\gamma_T}{2}\left(\frac{c}{c^2 - \dot{s}_0^2} + \frac{2\omega}{\mu\gamma_T^2}\right)\dot{s}_0 \tag{5.54}$$

where $\dot{s}_0 = c \ \frac{1-c_\gamma}{1+c_\gamma}$ and $c_\gamma = \frac{\gamma_M - \gamma_m}{\gamma_T}$.

When the three conditions (5.43), (5.50) and (5.54) are satisfied, there is no new phase boundary nucleated, and after the initial interaction between the phase boundary and the incident wave, the phase boundary will remain stationary for a while.

If $\omega > \omega_0$, we cannot find solutions of Riemann problems that satisfy the phase segregation condition. If v_0 is too large, then (5.54) will be violated and new phase boundaries will be nucleated.

The result that the phase boundary will remain stationary for a while obtained here was first postulated by Pence [70]. By using the approach of Abeyaratne & Knowles, we obtain the result rigorously and impose appropriate explicit restrictions on initial data, boundary data and material parameters. This result can be generalized to situations, with "square incident wave" replaced with "arbitrary pulse," the kinetic relation replaced with $f = \phi(\dot{s})$, and the material can be an arbitrary trilinear material.

5.3 Large time phase boundary behavior: motion of the phase boundary

Recursive formulae for (v, γ)

From the assumption that no new phase boundary is nucleated, the solution to be found can be illustrated by the $x-t$ plot shown in Figure 5.6. As in Section 5.2, we can show that the solution is piecewise constant. Thus the phase boundary propagation speed $\dot{s}(t)$ is piecewise constant in time as well. The part of the trajectory of the phase boundary that separates regions $\pm k$ (see Figure 5.6) corresponds to phase boundary propagation speed $\dot{s}_k$. The part of the trajectory that separates regions

$\pm\bar{k}$ corresponds to the phase boundary propagation speed $\dot{\bar{s}}_k$. We denote particle velocities and strains in regions $\pm k$ by $v_k^{\pm}$ and $\gamma_k^{\pm}$, in regions $\pm\bar{k}$ by $\bar{v}_k^{\pm}$ and $\bar{\gamma}_k^{\pm}$, and so on.

From boundary conditions,we have $v_i = 0$ and $\bar{v}_i = 0$. From results obtained in Section 5.2, we know that

$$\dot{\bar{s}}_1 = 0, \tag{5.55}$$

$$\bar{v}_1^- = 0, \tag{5.56}$$

$$\bar{\gamma}_1^- = \gamma_0^-, \tag{5.57}$$

$$\bar{v}_1^+ = 0, \tag{5.58}$$

$$\bar{\gamma}_1^+ = \gamma_0^+. \tag{5.59}$$

Now we will show by induction that

$$\dot{\bar{s}}_i = 0, \tag{5.60}$$

$$\bar{v}_i^- = 0, \tag{5.61}$$

$$\bar{\gamma}_i^- = \gamma_0^-, \tag{5.62}$$

$$\bar{v}_i^+ = 0, \tag{5.63}$$

$$\bar{\gamma}_i^+ = \gamma_0^+, \tag{5.64}$$

$$\bar{\gamma}_i = \gamma_0^-, \tag{5.65}$$

for all i.

Assume that

$$\dot{\bar{s}}_k = 0, \tag{5.66}$$

$$\bar{v}_k^- = 0, \tag{5.67}$$

$$\bar{\gamma}_k^- = \gamma_0^-, \tag{5.68}$$

$$\bar{v}_k^+ = 0, \tag{5.69}$$

$$\bar{\gamma}_k^+ = \gamma_0^+, \tag{5.70}$$

$$\bar{\gamma}_k = \gamma_0^-, \tag{5.71}$$

in regions $\pm\bar{k}$. Then in regions $\pm\overline{k+1}$, from jump conditions on the phase boundary and shock waves, we have

$$\begin{aligned}
\bar{v}_{k+1}^+ - \bar{v}_{k+1}^- + \dot{\bar{s}}_{k+1}(\bar{\gamma}_{k+1}^+ - \bar{\gamma}_{k+1}^-) &= 0, && (5.72)\\
\mu(\bar{\gamma}_{k+1}^+ - \gamma_T) - \mu\bar{\gamma}_{k+1}^- + \rho\dot{\bar{s}}_{k+1}(\bar{v}_{k+1}^+ - \bar{v}_{k+1}^-) &= 0, && (5.73)\\
\bar{v}_{k+1}^+ - v_0^+ + c(\bar{\gamma}_{k+1}^+ - \gamma_0^+) &= 0, && (5.74)\\
\bar{v}_{k+1}^- - \bar{v}_{k+1} - c(\bar{\gamma}_{k+1}^- - \bar{\gamma}_{k+1}) &= 0, && (5.75)\\
\bar{v}_{k+1} - \bar{v}_k^- - c(\bar{\gamma}_{k+1} - \bar{\gamma}_k^-) &= 0. && (5.76)
\end{aligned}$$

From (5.72)-(5.76), we find that

$$\begin{aligned}
\bar{\gamma}_{k+1} &= \bar{\gamma}_k^- = \gamma_0^-, && (5.77)\\
\bar{\gamma}_{k+1}^- &= \frac{\gamma_m + \gamma_M}{2} - \frac{c\gamma_T}{2(c + \dot{\bar{s}}_{k+1})}, && (5.78)\\
\bar{\gamma}_{k+1}^+ &= \frac{\gamma_m + \gamma_M}{2} + \frac{c\gamma_T}{2(c - \dot{\bar{s}}_{k+1})}. && (5.79)
\end{aligned}$$

The driving traction f on the phase boundary ($\dot{\bar{s}}_{k+1}$) is

$$\begin{aligned}
f &= \frac{\mu\gamma_T}{2}(\gamma_M + \gamma_m - \bar{\gamma}_{k+1}^- - \bar{\gamma}_{k+1}^+)\\
&= -\frac{\mu\gamma_T^2 c\dot{\bar{s}}_{k+1}}{2(c^2 - \dot{\bar{s}}_{k+1}^2)}. && (5.80)
\end{aligned}$$

From kinetic relation $f = \omega\dot{\bar{s}}_{k+1}$, we obtain $\dot{\bar{s}}_{k+1} = 0$. From (5.72)-(5.76), we find

$$\begin{aligned}
\dot{\bar{s}}_{k+1} &= 0, && (5.81)\\
\bar{v}_{k+1}^- &= 0, && (5.82)\\
\bar{\gamma}_{k+1}^- &= \gamma_0^-, && (5.83)\\
\bar{v}_{k+1}^+ &= 0, && (5.84)\\
\bar{\gamma}_{k+1}^+ &= \gamma_0^+, && (5.85)
\end{aligned}$$

$$\bar{\gamma}_{k+1} = \gamma_0^-. \tag{5.86}$$

So (5.60)-(5.65) hold for all i.

Now we solve for velocities and strains in regions $\pm k$ and k. From results obtained in Section 5.2, we know v_1, γ_1, v_1^-, γ_1^-, v_1^+ and γ_1^+. Assume v_i, γ_i, v_i^-, γ_i^-, v_i^+ and γ_i^+ are known, and consider regions $\pm(i+1)$. From jump conditions on the phase boundary and shock waves,

$$\mu(\gamma_{i+1}^+ - \gamma_T) - \mu\gamma_{i+1}^-) + \rho\dot{s}_{i+1}(v_{i+1}^+ - v_{i+1}^-) = 0, \tag{5.87}$$

$$(v_{i+1}^+ - v_{i+1}^-) + \dot{s}_{i+1}(\gamma_{i+1}^+ - \gamma_{i+1}^-) = 0, \tag{5.88}$$

$$v_{i+1}^- - v_i - c(\gamma_{i+1}^- - \gamma_i) = 0, \tag{5.89}$$

$$v_i - v_i^- + c(\gamma_i - \gamma_i^-) = 0, \tag{5.90}$$

$$v_{i+1}^+ - v_0^+ + c(\gamma_{i+1}^+ - \gamma_0^+ = 0. \tag{5.91}$$

Solving (5.87)-(5.91) for the γ's and v's yields

$$v_{i+1}^- = \frac{1}{2}(-\frac{c^2\gamma_T}{c+\dot{s}_{i+1}} + c\gamma_0^+ - (v_i^- + c\gamma_i^-)), \tag{5.92}$$

$$\gamma_{i+1}^- = \frac{1}{2}(-\frac{c\gamma_T}{c+\dot{s}_{i+1}} + \gamma_0^+ + \frac{v_i^- + c\gamma_i^-}{c}), \tag{5.93}$$

$$v_{i+1}^+ = \frac{1}{2}(-\frac{c^2\gamma_T}{c-\dot{s}_{i+1}} + c\gamma_0^+ - (v_i^- + c\gamma_i^-)), \tag{5.94}$$

$$\gamma_{i+1}^+ = \frac{1}{2}(-\frac{c\gamma_T}{c-\dot{s}_{i+1}} + \gamma_0^+ + \frac{v_i^- + c\gamma_i^-}{c}). \tag{5.95}$$

From these results, we infer the following simple formula:

$$v_i^- + c\gamma_i^- = -\frac{c^2\gamma_T}{c+\dot{s}_i} + c\gamma_0^+. \tag{5.96}$$

From the derivation we see that (5.96) holds for $i \geq 2$, but it is easy to show that it also holds for $i = 1$. So we have the following formulae for v, γ for all regions $\pm k$;

setting $x_i = \frac{\dot{s}_i}{c}$, then

$$v_{i+1}^- = \frac{c\gamma_T}{2}(-\frac{1}{1+x_{i+1}} + \frac{1}{1+x_i}), \tag{5.97}$$

$$\gamma_{i+1}^- = \frac{1}{2}(-\frac{\gamma_T}{1+x_{i+1}} - \frac{\gamma_T}{1+x_i} + 2\gamma_0^+), \tag{5.98}$$

$$v_{i+1}^+ = \frac{c\gamma_T}{2}(-\frac{1}{1-x_{i+1}} + \frac{1}{1+x_i}), \tag{5.99}$$

$$\gamma_{i+1}^+ = \frac{1}{2}(\frac{\gamma_T}{1-x_{i+1}} - \frac{\gamma_T}{1+x_i} + 2\gamma_0^+). \tag{5.100}$$

Here x_i is determined by the kinetic relation through recursion

$$-\frac{x_i}{1+x_i} = (\frac{1}{1-x_{i+1}^2} + a)x_{i+1} \quad i = 1, 2, 3... \tag{5.101}$$

and

$$\frac{2v_0}{c\gamma_T} = (\frac{1}{1-x_1^2} + a)x_1, \tag{5.102}$$

where

$$a = \frac{2\omega c}{\mu\gamma_T^2} > 0. \tag{5.103}$$

Now we have all the formulas required to determine the motion of the phase boundary and the deformation in the bar at any point in space-time.

Analysis of recursive formulae

Lemma 1: $|x_i| < 1, i = 1, 2, 3, 4.....$ and there is one and only one x_i that satisfies (5.101) or (5.102).

Proof: Let

$$f(x) = (\frac{1}{1-x^2} + a)x \tag{5.104}$$

then

$$f'(x) = \frac{1}{1-x^2} + a + \frac{2x^2}{(1-x^2)^2}. \tag{5.105}$$

By the entropy inequality (2.10), it can be shown that, $|\dot{s}_i| < c$, i.e. $|x_i| < 1$. So

$f'(x) > 0$ and $f(x)$ is monotonically increasing in the $(-1, 1)$. It is easy to see that $f(x) \to +\infty$ as x approaches 1 from below, and $f(x) \to -\infty$ as x approaches -1 from above. Thus there is only one x_1 that satisfies (5.102). Similarly for any given i, there is one and only one x_{i+1} that satisfies (5.101). This completes the proof.

Lemma 2: $x_1 > 0, x_{2k-1} > 0, x_{2k} < 0$ and $x_{2k-1} > -(1+a)x_{2k}$ for $k = 1, 2, 3.....$

Proof: Using the notation in Lemma 1, we have

$$f(0) = 0, \tag{5.106}$$

$$f(x_1) = \frac{2v_0}{c\gamma_T} > 0 \tag{5.107}$$

so $x_1 > 0$.

Now we prove $x_{2k-1} > 0, x_{2k} < 0$ by induction. For $k = 1$,

$$x_{2k-1} = x_1 > 0, \tag{5.108}$$

$$0 > -\frac{x_1}{1+x_1} = (\frac{1}{1-x_2^2} + a)x_2. \tag{5.109}$$

Notice that

$$(\frac{1}{1-x_2^2} + a) > 0, \tag{5.110}$$

so that

$$x_{2k} = x_2 < 0. \tag{5.111}$$

Assume $k = i, x_{2k-1} > 0, x_{2k} < 0$; then

$$0 < -\frac{x_{2i}}{1+x_{2i}} = (\frac{1}{1-x_{2i+1}^2} + a)x_{2i+1}, \tag{5.112}$$

$$0 > -\frac{x_{2i+1}}{1+x_{2i+1}} = (\frac{1}{1-x_{2i+2}^2} + a)x_{2i+2}, \tag{5.113}$$

so that

$$x_{2i+1} > 0, x_{2i+2} < 0. \tag{5.114}$$

Thus $k = i+1, x_{2k-1} > 0, x_{2k} < 0$. So $x_{2k-1} > 0, x_{2k} < 0$ for all k.

From

$$-\frac{x_{2k-1}}{1+x_{2k-1}} = (\frac{1}{1-x_{2k}^2} + a)x_{2k},$$

as $x_{2k-1} > 0, x_{2k} < 0$, we have:

$$x_{2k-1} > \frac{x_{2k-1}}{1+x_{2k-1}} = (\frac{1}{1-x_{2k}^2} + a)(-x_{2k}) > (1+a)(-x_{2k}),$$

i.e.

$$\frac{x_{2k-1}}{1+a} > -x_{2k} > 0. \tag{5.115}$$

This completes the proof.

Theorem 1: When $t \to \infty$, $\dot{s} \to 0$.

Proof: From (5.101), we have:

$$\begin{aligned} -\frac{x_{2k-1}}{1+x_{2k-1}} &= (\frac{1}{1-x_{2k}^2} + a)x_{2k}, \\ -\frac{x_{2k}}{1+x_{2k}} &= (\frac{1}{1-x_{2k+1}^2} + a)x_{2k+1}, \end{aligned}$$

so

$$\frac{x_{2k-1}}{1+x_{2k-1}}\frac{x_{2k}}{1+x_{2k}} = (\frac{1}{1-x_{2k}^2} + a)x_{2k}(\frac{1}{1-x_{2k+1}^2} + a)x_{2k+1}.$$

It follows that

$$\begin{aligned} x_{2k-1} &> (1+x_{2k-1})\frac{1}{1-x_{2k}}(1+a)x_{2k+1} \\ &> (1+a)x_{2k+1}, \end{aligned}$$

i.e.

$$0 < x_{2k+1} < \frac{x_1}{(1+a)^k}. \tag{5.116}$$

This leads to

$$\lim_{k\to\infty} x_{2k+1} = 0.$$

By (5.115)

$$\lim_{k\to\infty} x_{2k} = 0,$$

so that

$$\lim_{k\to\infty} x_k = 0,$$

which shows that

$$\dot{s} \to 0 \quad \text{as} \quad t \to \infty.$$

To prove the next theorem, a known result about the convergence of infinite products is cited below as Lemma 3 without proof.

Lemma 3: Assume $q_n = 1 + a_n \quad (n = 1, 2, 3, ...)$. For large enough n, if $a_n > 0$ (or $a_n < 0$), the necessary and sufficient condition for $\sqcap_{n=1}^{\infty} q_n$ to converge is that $\sum_{n=1}^{\infty} a_n$ converges.

Lemma 4: $\sum_{n=1}^{\infty} \frac{x_{2k-1}}{1-x_{2k-1}}$ and $\sum_{n=1}^{\infty} \frac{x_{2k}}{1-x_{2k}}$ converge.

Proof: By (5.116), it can be shown that

$$\frac{x_{2k+1}}{1 - x_{2k+1}} < \frac{x_1}{(1+a)^{k+1} - 1}.$$

As

$$\lim_{k\to\infty} \frac{\frac{x_1}{(1+a)^{k+1}-1}}{\frac{x_1}{(1+a)^k-1}} = \frac{1}{1+a} < 1 \tag{5.117}$$

$\sum_{k=1}^{\infty} \frac{x_1}{(1+a)^{k+1}-1}$ converges, so does $\sum_{n=1}^{\infty} \frac{x_{2k-1}}{1-x_{2k-1}}$.

By (5.115) and $x_{2k} < 0$,

$$-\frac{x_{2k}}{1 - x_{2k}} < -x_{2k} < \frac{x_1}{(1+a)^k}.$$

As $\sum_{k=1}^{\infty} \frac{x_1}{(1+a)^k}$ converges, so does $\sum_{n=1}^{\infty} \frac{x_{2k}}{1-x_{2k}}$.

Theorem 2: $s_k > s_0$, and $\lim_{k\to\infty} s_k < \bar{M}\dot{s}_1(1 + \frac{1}{a})$, where $\bar{M}$ is some finite number.

Proof: Denote the period of time that $\dot{s} = \dot{s}_k$ by t_k , the phase boundary position at the beginning of $\dot{s}_k$ by s_k, the k-th incident wave's time interval by $\bar{t}_k$, see Figure 5.7.

From the definition, we have $\bar{t}_1 = t^*, s_1 = s_0$,

$$\begin{aligned} t_k &= \frac{s_k + (\bar{t}_k - \frac{s_k}{c})\dot{s}_k}{c - \dot{s}_k} + \bar{t}_k - \frac{s_k}{c} \\ &= \frac{c\bar{t}_k}{c - \dot{s}_k}, \end{aligned}$$

i.e.,

$$t_k = \frac{\bar{t}_k}{1 - x_k}. \tag{5.118}$$

$$\bar{t}_{k+1} = \bar{t}_k + 2(t_k - \bar{t}_k) = \frac{c + \dot{s}_k}{c - \dot{s}_k}\bar{t}_k,$$

i.e.,

$$\bar{t}_{k+1} = \frac{1 + x_k}{1 - x_k}\bar{t}_k, \tag{5.119}$$

and

$$s_{k+1} = s_k + \dot{s}_k t_k = s_k + \frac{\bar{t}_k x_k}{1 - x_k}. \tag{5.120}$$

From (5.118)

$$\begin{aligned} \bar{t}_\infty &= \Pi_{k=1}^{\infty} \frac{1 + x_k}{1 - x_k}\bar{t}_1 \\ &= t^* \Pi_{k=1}^{\infty} (1 + \frac{2x_{2k}}{1 - x_{2k}}) \Pi_{k=1}^{\infty} (1 + \frac{2x_{2k-1}}{1 - x_{2k-1}}). \end{aligned}$$

By Lemma 3 and Lemma 4, there exists M (fixed) such that

$$\Pi_{k=1}^{\infty}(1 + \frac{2x_{2k-1}}{1 - x_{2k-1}}) < M, \quad \Pi_{k=1}^{\infty}(1 + \frac{2x_{2k}}{1 - x_{2k}}) < M,$$

and hence

$$\bar{t}_\infty < M^2 t^* < \infty.$$

Since

$$1 + \frac{2x_{2k-1}}{1 - x_{2k-1}} > 1,$$

we have

$$M > \sqcap_{k=1}^{\infty}(1 + \frac{2x_{2k-1}}{1 - x_{2k-1}}) > \sqcap_{k=1}^{n}(1 + \frac{2x_{2k-1}}{1 - x_{2k-1}}).$$

On the other hand, since

$$1 + \frac{2x_{2k}}{1 - x_{2k}} < 1,$$

we have

$$\bar{t}_k = t^* \sqcap_{i=1}^{k} (1 + \frac{2x_i}{1 - x_i}) < t^*(1 + \frac{2x_1}{1 - x_1}).$$

Therefore, there exists M_1 such that for all k

$$\bar{t}_k < M_1.$$

By (5.118) and the fact that x_k decays exponentially with k, there exists $\bar{M}$ such that

$$t_k < \bar{M}, \text{for all } k.$$

Now let us find s_∞. We have

$$s_{k+1} = s_1 + \dot{s}_1 t_1 + \dot{s}_2 t_2 + ... + \dot{s}_k t_k.$$

But

$$\sum_{k=1}^{\infty} \dot{s}_{2k-1} t_{2k-1} < \bar{M} c \sum_{k=1}^{\infty} x_{2k-1} < \bar{M} \dot{s}_1 (1 + \frac{1}{a}) < \infty,$$

so that

$$\sum_{k=1}^{\infty} -\dot{s}_{2k} t_{2k} < \bar{M} c \sum_{k=1}^{\infty} x_{2k} < \bar{M} \dot{s}_1 \frac{1}{a} < \infty,$$

so $\sum_{k=1}^{\infty} -\dot{s}_{2k} t_{2k}$ converges. Thus

$$s_\infty < \bar{M} \dot{s}_1 (1 + \frac{1}{a}) < \infty. \tag{5.121}$$

Now we verify that $s_k > s_0$.

$$\begin{aligned} s_{2k+1} &= s_{2k} + \frac{x_{2k}\bar{t}_{2k}}{1-x_{2k}} \\ &= s_1 + ((\frac{x_1\bar{t}_1}{1-x_1} + \frac{x_2\bar{t}_2}{1-x_2}) + ... + (\frac{x_{2k-1}\bar{t}_{2k-1}}{1-x_{2k-1}} + \frac{x_{2k}\bar{t}_{2k}}{1-x_{2k}})). \end{aligned}$$

$$\frac{x_{2i-1}\bar{t}_{2i-1}}{1-x_{2i-1}} + \frac{x_{2i}\bar{t}_{2i}}{1-x_{2i}} = t_{2i-1}\frac{x_{2i-1}+x_{2i}}{1-x_{2i}} > 0,$$

so that,

$$s_{2k+1} > s_1,$$

$$s_{2k+2} = s_{2k+1} + \frac{x_{2k+1}\bar{t}_{2k+1}}{1-x_{2k+1}} > s_{2k+1}.$$

This leads to

$$s_k > s_1 = s_0.$$

Restrictions on parameters

It has been assumed that there is no new phase boundary initiated. Now we check whether this assumption has been satisfied.

It is obvious that the strains $\bar{\gamma}_k^{\pm}$ in regions $\pm\bar{k}$ and strain $\bar{\gamma}_k$ in region $\bar{k}$ belong to appropriate phases. We check whether $\gamma_k^{\pm}$, γ_k, γ_{Ik} and γ_{Jk} belong to appropriate phases for all k. In the following we show that these strains belong to appropriate phases when the restrictions (5.43),(5.50) and (5.54) are enforced. The proof is by induction.

When $k = 1$, we know that $\gamma_k^{\pm}$, γ_k, γ_{Ik} and γ_{Jk} belong to appropriate phases from Section 5.2.

Assume $\gamma_k^{\pm}$, γ_k, γ_{Ik} and γ_{Jk} belong to appropriate phases when $k = i$.

Since $v_{i+1}^{\pm}$ and $\gamma_{i+1}^{\pm}$ are obtained by solving a Riemann problem with initial data (v_{Ji}, γ_{Ji}) and $(\bar{v}_i^+, \bar{\gamma}_i^+)$, and since γ_{Ji} belongs to the low-strain phase, $\bar{\gamma}_i^+$ belongs to the high-strain phase, then $\gamma_{i+1}^{\pm}$ belong to appropriate phases if (5.43) is satisfied.

From the recursion formulae (5.97) - (5.102) and jump conditions (2.4), (2.5) on shock waves, we find that,

$$\gamma_{Ii+1} = \frac{\gamma_m + \gamma_M}{2} - \frac{\gamma_T}{2(1 + x_{i+1})}. \tag{5.122}$$

If $i+1$ is even, then $\frac{\gamma_T}{2(1+x_{i+1})} > \frac{\gamma_T}{2} > \frac{\gamma_M - \gamma_m}{2}$, so $\gamma_{Ii+1} < \gamma_m$. If $i+1$ is odd, then $-\frac{\gamma_T}{2(1+x_{i-1})} > -\frac{\gamma_T}{2(1+x_{i+1})}$, so $\gamma_{Ii+1} < \gamma_{I1} < \gamma_m$. Thus the strain γ_{Ii+1} belongs to the low-strain phase.

Similarly, we can show that γ_{i+1} is in the low-strain phase.

From the jump conditions on shock waves,

$$\gamma_{Ji+1} = \frac{1}{2}(\bar{\gamma}^-_{i+1} + \gamma_{i+1}). \tag{5.123}$$

As $\bar{\gamma}^-_{i+1} < \gamma_m$ and $\gamma_{i+1} < \gamma_m$, $\gamma_{Ji+1} < \gamma_m$, we conclude that $\gamma^{\pm}_k$, γ_k, γ_{Ik} and γ_{Jk} belong to appropriate phases when $k = i+1$.

We have shown that the assumption holds for all time if restrictions (5.43), (5.50) and (5.54) are satisfied.

Interpretation of the analysis

For a semi-infinite bar initially in a two-phase equilibrium state with a single phase boundary, we see that, due to an impacting square wave, the motion of the phase boundary has the following features:

1. The phase boundary moves forward when the square wave hits it for the first time. The phase boundary moves in the following way:

   forward $\rightarrow$ stationary $\rightarrow$ backward $\rightarrow$ stationary $\rightarrow$ forward....

   The phase boundary moves more slowly when moving backward than it did the last time it moved forward.

2. The phase boundary speed decays exponentially to zero. There is a single effec-

tive material constant that determines the decay of phase boundary propagation speed: it is $a = \frac{2\omega c}{\mu\gamma_T^2} > 0$.

3. The phase boundary position is always to the right of its initial position, and its final position is a finite distance away from its initial position.

5.4 Results for other kinetic relations

An important generalization that may be considered is to replace the kinetic relation $f = \omega\dot{s}$ with the following kinetic relation:

$$\dot{s} = \begin{cases} \frac{1}{\omega}(f - f_*) & , \quad f > f_*, \\ 0 & , \quad -f_* \leq f \leq f_*, \\ \frac{1}{\omega}(f + f_*) & , \quad f < -f_*, \end{cases} \tag{5.124}$$

where f_* and ω are positive materials constants. This kinetic relation is of interest because it involves a barrier against phase boundary motion.

For the kinetic relation (5.124), the initial state given in Section 5.1 need not be a Maxwell state:

$$v(x,0) = 0, \tag{5.125}$$

$$\gamma(x,0) = \gamma_0^- \tag{5.126}$$

for $0 \leq x < s_0$;

$$v(x,0) = 0, \tag{5.127}$$

$$\gamma(x,0) = \gamma_0^+ \tag{5.128}$$

for $s_0 < x < \infty$.

But we require $\sigma(s_0^-, 0) = \sigma(s_0^+, 0)$, i.e. $\gamma_0^+ - \gamma_0^- = \gamma_T$ and $-f_* < f_0 < f_*$, where $f_0 = \frac{\mu\gamma_T}{2}(\gamma_m + \gamma_M - \gamma_0^+ - \gamma_0^-)$

It is clear that we can solve the initial-boundary value problem for the kinetic

relation (5.124), using a procedure which is exactly the same as that explained in Sections 5.2 and 5.3. We will not repeat the procedure. In fact the expressions for particle velocity and strain in this are the same as those given in Sections 5.2 and 5.3; the recursive formula for phase boundary propagation speed is, however, different.

Short time analysis

As there is a barrier against the phase boundary motion, the phase boundary will remain stationary when it interacts with an incident wave, provided that v_0 is small enough. If this is the case (Figure 5.3) from (5.18) – (5.21), we have

$$v_1^- = v_0, \tag{5.129}$$

$$\gamma_1^- = -\frac{v_0}{c} + \gamma_0^-, \tag{5.130}$$

$$v_1^+ = v_0, \tag{5.131}$$

$$\gamma_1^+ = -\frac{v_0}{c} + \gamma_0^+. \tag{5.132}$$

Accordingly, the driving traction on the phase boundary is

$$\begin{aligned} f &= \frac{\mu\gamma_T}{2}(\gamma_m + \gamma M - \gamma_- - \gamma+) \\ &= f_0 + \frac{\mu\gamma_T}{c}v_0 < f_*, \end{aligned} \tag{5.133}$$

i.e. $v_0 \leq \frac{c(f_*-f_0)}{\mu\gamma_T}$.

If $v_0 \leq \frac{c(f_*-f_0)}{\mu\gamma_T}$, then the incident wave is totally transmitted through the phase boundary and the phase boundary remains stationary for $t > 0$.

If $v_0 > \frac{c(f_*-f_0)}{\mu\gamma_T}$, then $\dot{s}_1 \neq 0$. The solution is again given by (5.18) – (5.21), but the phase boundary propagation speed will be determined by $f = f_* + \omega\dot{s}$, i.e.

$$(\frac{1}{1-x_1^2} + a)x_1 = \frac{2}{c\gamma_T}(v_0 - \frac{c(f_* - f_0)}{\mu\gamma_T}). \tag{5.134}$$

The notation here is the same as that in Section 5.2.

As in Section 5.2, we can show that $\dot{s}_2 = 0$, and we can also also derive the restrictions on v_0 and other parameters that assure that there is no new phase boundary nucleated.

Large time analysis

The strain and particle velocity in the bar are given by (5.66) - (5.71) and (5.97) -(5.100); see Figure 5.6. The driving traction on the phase boundary that separates regions $\pm(i+1)$ is

$$f = f_0 - \frac{\mu\gamma_T^2}{2}\left(\frac{x_i}{1+x_i} + \frac{x_{i+1}}{1-x_{i+1}^2}\right). \tag{5.135}$$

We consider x_2 first. From the short time analysis, we know $x_1 \geq 0$. It can be shown that

$$-\left(\frac{x_1}{1+x_1} - \frac{2(f_* + f_0)}{\mu\gamma_T^2}\right) = \left(\frac{1}{1-x_2^2} + a\right)x_2, \tag{5.136}$$

$$\frac{x_1}{1+x_1} < \frac{2(f_* + f_0)}{\mu\gamma_T^2} \rightarrow \dot{s}_2 = 0; \tag{5.137}$$

$$\frac{x_1}{1+x_1} < \frac{2(f_* + f_0)}{\mu\gamma_T^2} \rightarrow \dot{s}_2 < 0. \tag{5.138}$$

Furthermore, by induction we can show that $x_{2i-1} \geq 0$ and $x_{2i} \leq 0$. The recursive formulae for the phase boundary speed are

$$-\left(\frac{x_{2i-1}}{1+x_{2i-1}} - \frac{2(f_* + f_0)}{\mu\gamma_T^2}\right) = \left(\frac{1}{1-x_{2i}^2} + a\right)x_{2i}, \tag{5.139}$$

$$-\left(\frac{x_{2i}}{1+x_{2i}} + \frac{2(f_* - f_0)}{\mu\gamma_T^2}\right) = \left(\frac{1}{1-x_{2i+1}^2} + a\right)x_{2i+1}. \tag{5.140}$$

According to the kinetic relation (5.124),

$$\frac{x_{2i-1}}{1+x_{2i-1}} < \frac{2(f_* + f_0)}{\mu\gamma_T^2} \rightarrow \dot{s}_{2i} = 0; \tag{5.141}$$

$$\frac{x_{2i}}{1+x_{2i}} > -\frac{2(f_* - f_0)}{\mu\gamma_T^2} \rightarrow \dot{s}_{2i+1} = 0. \tag{5.142}$$

We can show that x_{2i-1} and $-x_{2i}$ decay exponentially as i $\rightarrow \infty$. Let $\bar{x}_i$ be the solution to (5.140) and (5.141) when $f_0 = 0$; then we know that $\bar{x}_{2i-1}$ and $-\bar{x}_{2i}$ decay exponentially. For a given v_0, it is easy to show that $\bar{x}_1 > x_1 \geq 0$.

If $x_2 < 0$, then from,

$$-\frac{\bar{x}_1}{1+\bar{x}_1} = (\frac{1}{1-\bar{x}_2^2} + a)\bar{x}_2, \tag{5.143}$$

$$-\frac{x_1}{1+x_1} = (\frac{1}{1-\hat{x}_2^2} + a)\hat{x}_2, \tag{5.144}$$

$$-(\frac{x_1}{1+x_1} - \frac{2(f_* + f_0)}{\mu\gamma_T^2}) = (\frac{1}{1-x_2^2} + a)x_2. \tag{5.145}$$

One can show that $0 \geq x_2 > \hat{x}_2 > \bar{x}_2$. By induction, we can further show that $\bar{x}_{2i-1} > x_{2i-1} \geq 0$ and $-\bar{x}_{2i} > x_{2i} \geq 0$. So x_{2i-1} and $-x_{2i}$ decay exponentially. Thus if $x_1 \neq 0$, it only takes finite time for x_i to reach zero; see (5.141) or (5.142).

We can replace the kinetic relation in the initial-boundary value problem formulated in Section 5.1 by a monotonically increasing continuous kinetic function $\phi(\dot{s})$. If we require that

$$\frac{d\phi}{d\dot{s}} \geq 0, \tag{5.146}$$

$$|\phi(\dot{s})| > \phi'(0)\dot{s}, \tag{5.147}$$

$$\phi'(0) > 0, \tag{5.148}$$

$$\phi(\dot{s}) = -\phi(-\dot{s}), \tag{5.149}$$

then we can obtain similar results on phase boundary motion similar to those in Sections 5.2 or 5.3. Similarly, if $\phi(\dot{s})$ is a monotonically increasing function with a discontinuity at $\dot{s} = 0$, then we can obtain results similar to those for kinetic relation (5.124).

For the special trilinear material considered here, and for a large class of kinetic relation, we have shown the phase boundary will return to an equilibrium state after a long time.

5.5 A numerical calculation

To gain an impression of the analytical results we have obtained so far, a numerical calculation based upon the recursive formula is carried out. As the purpose of the calculation is to visualize the analytical results, the parameters chosen are not real physical data and the their units are not specified. The parameters used are as follows:

1. $\mu = 1, \rho = 1$
2. $\gamma_T = 1.5, \gamma_M = 2, \gamma_m = 1$
3. $c = \sqrt{\frac{\mu}{\rho}} = 1$
4. $\gamma_0^- = \frac{1}{2}(\gamma_M + \gamma_m - \gamma_T) = 0.75$
5. $\gamma_0^+ = \frac{1}{2}(\gamma_M + \gamma_m + \gamma_T) = 2.25$
6. $v_0 = 0.25, s_0 = 1, t^* = 1, \omega = 0.5$

It is easy to check that this set of parameters satisfies (5.43), (5.50) and (5.54). The numerical results are listed in Figures 5.8-5.12 to show the large time behavior of the phase boundary.

From Figure 5.8 we see that the phase boundary propagation speed oscillates as time increases and it decays very fast even with $a < 1$. After only about ten interactions of the phase boundary and the reflected wave, the phase boundary propagation speed is too small to observe. So are the variations of particle velocity and strain; see Figures 5.9 and 5.10. From the numerical results we see that $s_0 < s_\infty < s_2$; see Figure 5.11. The bar is not strictly in an equilibrium state when time approaches infinity; see Figure 5.12. This is due to the fact that the waves transmitted through the phase boundary propagate in a non-dissipative medium to infinity.

5.6 Remarks

The approach used here cannot be applied successfully to an arbitrary initial-boundary value problem, such as the finite bar problem considered by Lin and Pence [55], [56].

Even for the problem formulated in Section 5.1, if the material of the bar is characterized by a nontrilinear but non-monotonic stress-strain relation, we cannot solve the problem analytically. A numerical method must be used.

But for the first time, to the best of our knowledge, we have provided an exact solution to a nontrivial initial-boundary value problem in a nonlinear elastodynamic theory of solid-solid phase transformations. Using this solution, we have shown that a phase boundary will reach an equilibrium state at a large time.

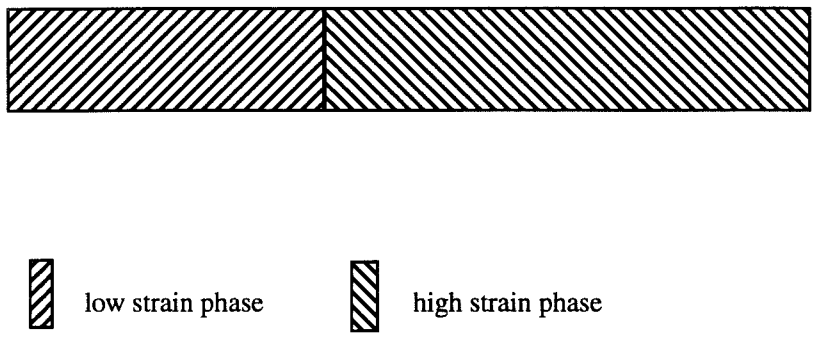

Figure 5.1: The initial state

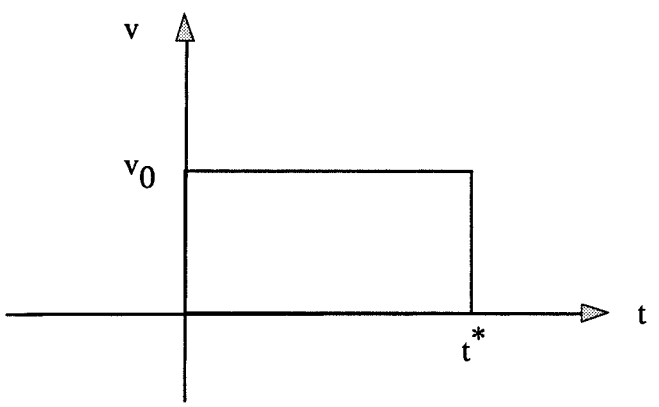

Figure 5.2: The incident square wave

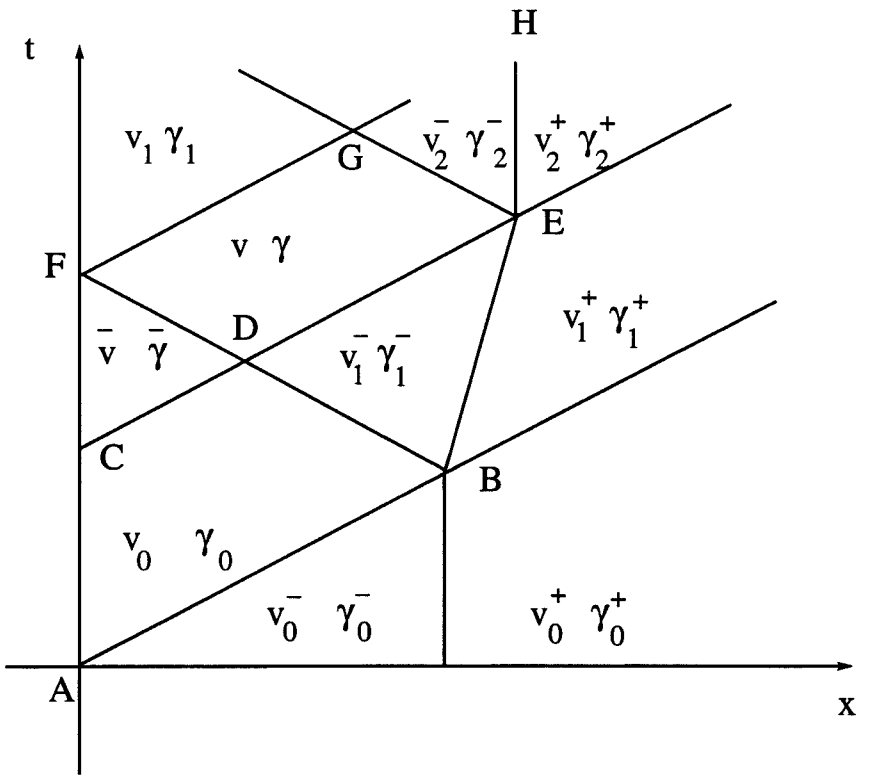

Figure 5.3: A schematic figure for the short time analysis

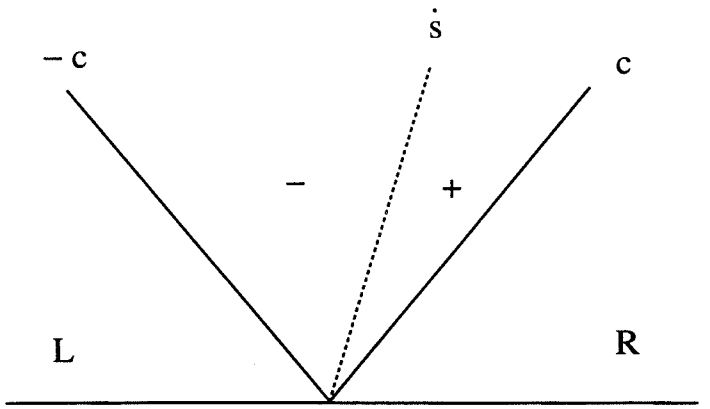

Figure 5.4: Form of solution to a Riemann problem with initial data in different phases

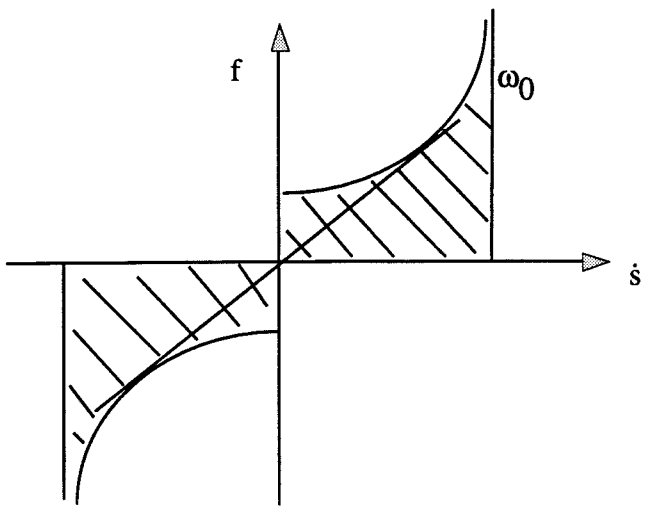

Figure 5.5: Admissible region for the kinetic relation

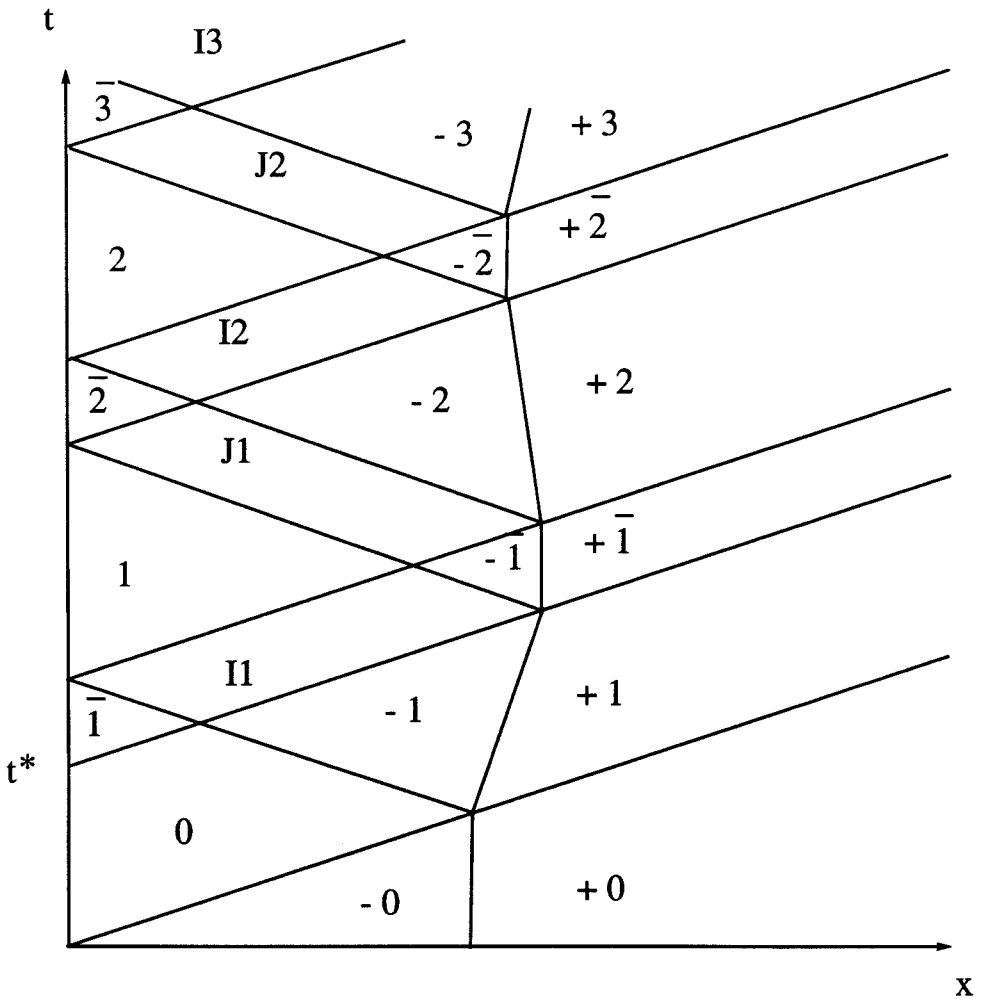

Figure 5.6: A schematic x-t plot

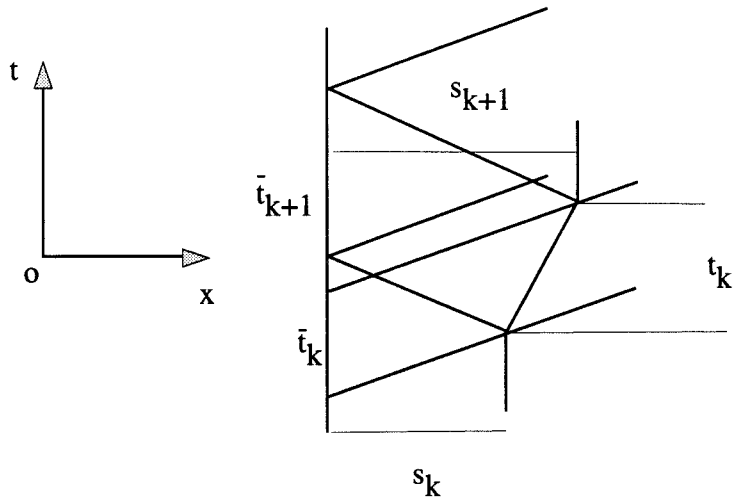

Figure 5.7: Definitions of $s_k, t_k, \bar{t}_k$

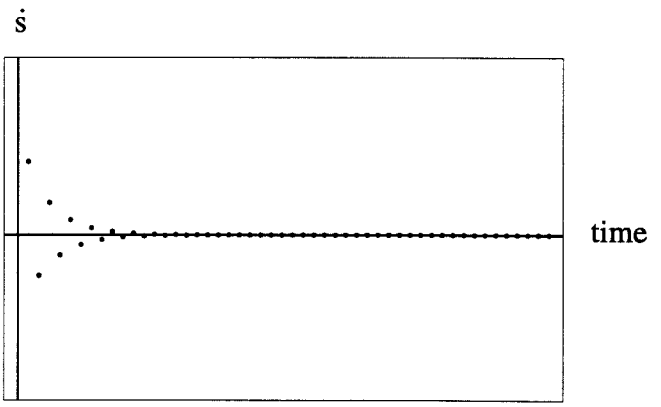

Figure 5.8: Decay of the phase boundary propagation speed

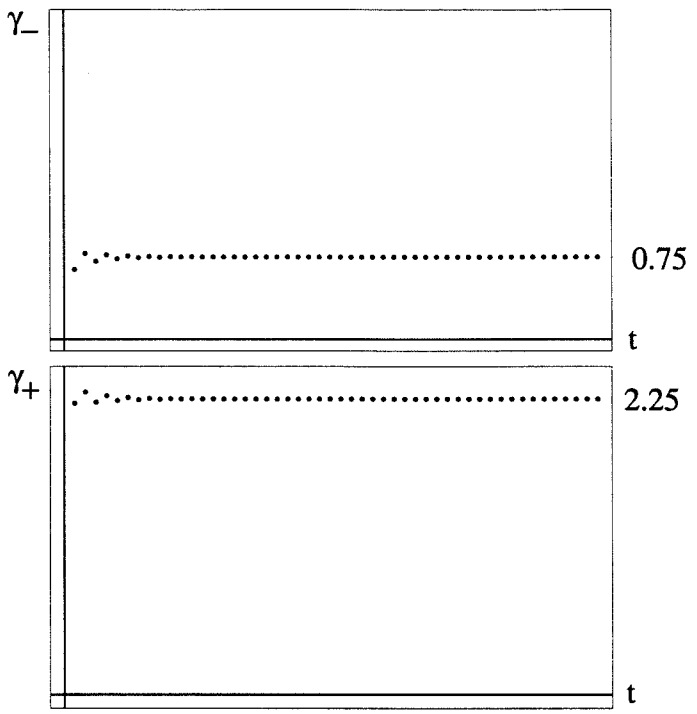

Figure 5.9: Variation of strains on both sides of the phase boundary

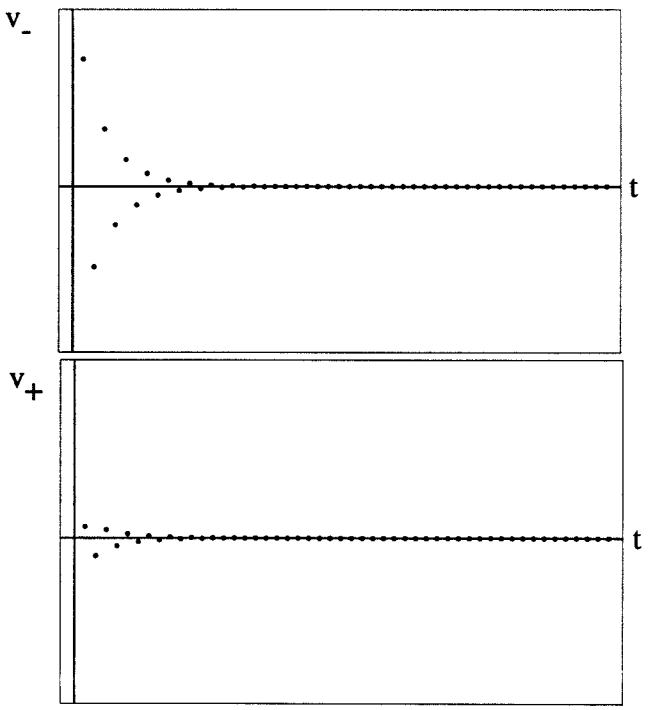

Figure 5.10: Variation of particle velocities on both sides of the phase boundary

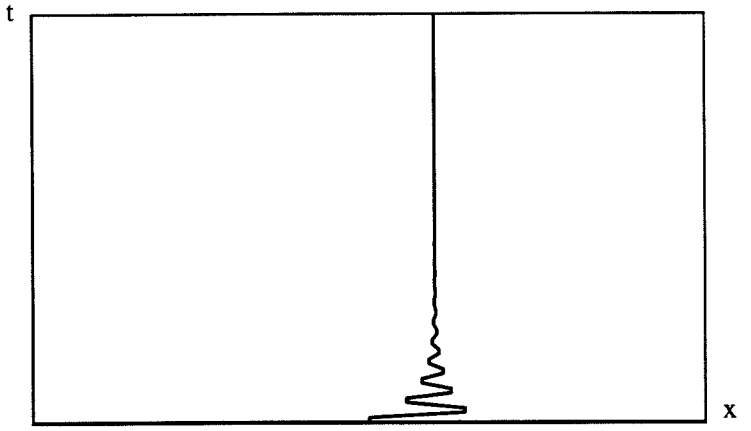

Figure 5.11: Trajectory of the phase boundary

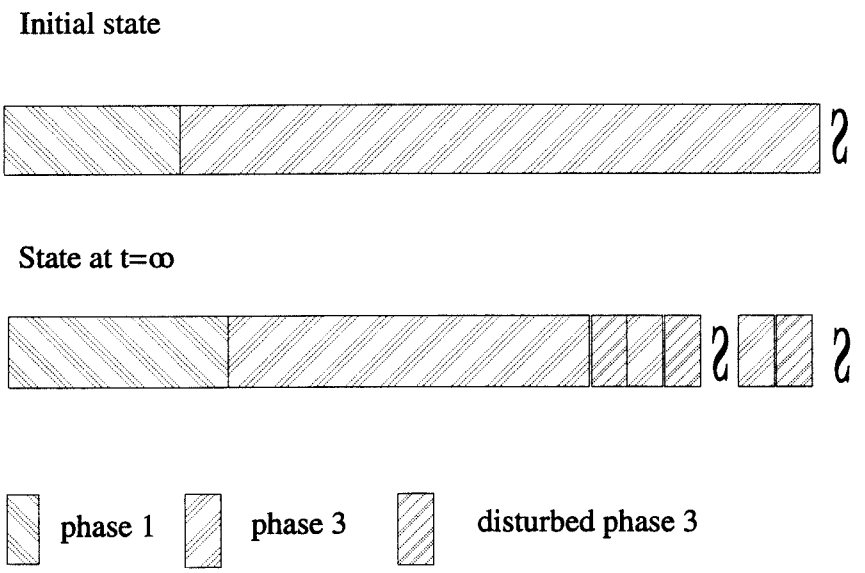

Figure 5.12: The deformation state in the bar at $t = \infty$

Chapter 6 A numerical method of Godunov type

6.1 Introduction

Though there is much work on the computation of phase transformation problems as mentioned in Chapter 1, we are not aware of any work on the computation of the dynamics of phase transformations involving kinetically driven sharp phase boundaries, such as those arising in the A-K model.

Unlike classical shock waves, a phase boundary should not be viewed as a consequence of overlapping characteristics. The emergence of a new phase boundary is a consequence of the local instability of a deformation. So numerical methods developed in the last ten years for classical shock waves in computational fluid dynamics (CFD) cannot be applied directly to phase boundary propagation problems. However we are able to build upon techniques developed in CFD and develop a numerical method capable of computing dynamical phase transition problems. Classical methods for shock wave computation include the following:

(i) *Front tracking schemes.* For recent activity on the subject, we refer to Glimm et al. [33, 34], Hyman [43], Moretti [63], and Oran & Boris [67]. An advantage of front tracking methods lies in the fact that the shock front is sharply computed without any numerical dissipation. However the implementation of such a method is more difficult if complex flow features such as shock wave interactions must be taken into account.

(ii) *The shock capturing schemes,.* These represent a more standard methodology. In particular the first-order accurate Godunov method [35] and its higher order extensions have received much attention in recent years. This research culminated with works by van Leer [88], Colella & Woodward [23], Harten, Osher et al. [41], and others. The implementation of shock capturing methods is generally straightforward. Shock fronts are not sharply computed, but usually spread out over a few mesh cells

only; this is satisfactory for most applications. Several methods that further sharpen numerical shock fronts have been developed: see Harten & Hyman [38] for a self-adjusting grid method, and Harten [40] for the technique of subcell resolution applied to ENO schemes. To combine the advantages of tracking and capturing methods, it may be advantageous to hybridize the two techniques: tracking strong shock waves but capturing those with weak strength [21], [77].

As our first attempt to develop a numerical method for the Abeyaratne-Knowles model, we develop a method of Godunov type for a one-dimensional setting. In this method, a phase boundary is tracked while a shock wave is captured. By doing this we avoid mathematical complexity at a phase boundary or at a nucleation site arising from supplementary constitutive relations. In the following, we develop an algorithm for the cases involving trilinear materials, then we extend it to nontrilinear materials.

6.2 The general approach

We note that the equation of motion and the compatibility equation (2.2), (2.3) can be written in the form of 2×2 conservation laws:

$$U_t + f(U)_x = 0, \tag{6.1}$$

where

$$U = \left\{ \begin{array}{c} v \\ \gamma \end{array} \right\}, f(U) = \left\{ \begin{array}{c} -\sigma(\gamma)/\rho \\ -\gamma \end{array} \right\}$$

and

$$f(U)_x = \left(\begin{array}{cc} 0 & -\frac{\sigma'(\gamma)}{\rho} \\ -1 & 0 \end{array} \right) \left\{ \begin{array}{c} v_x \\ \gamma_x \end{array} \right\}.$$

As the solutions of the Riemann problem for (6.1) involving trilinear materials are known explicitly, it is natural to develop a method of Godunov type. The standard Godunov method could be applied in principle; however it does not produce the correct solution. We observe that a phase boundary is rather different from a

conventional shock wave, and numerical methods for shock waves cannot be applied directly. Our objective is to design a method that does not introduce numerical values in the unstable region, i.e. strains in the interval (γ_m, γ_M), of system (6.1).

We first sketch Godunov's method, and then we explain how it has to be modified to meet present needs. We use the following notation. As variable meshes will be used, we denote by $x^n_{j+\frac{1}{2}}$ the spatial grid points at time t_n. Subsequently $[x^n_{j-\frac{1}{2}}, x^n_{j+\frac{1}{2}}]$ represents a computational cell, x^n_j is the center of the cell, and $h^n_j = x^n_{j-\frac{1}{2}} - x^n_{j+\frac{1}{2}}$ is the cell width at time t_n. We denote by k_n the n-th time step, and we set: $t_n = \sum_{m=1}^{n-1} k_m, t_0 = 0$. If $U(t,x)$ is given, the cell average of U in the cell j and at time t_n is defined as:

$$U^n_j = \frac{1}{h^n_j} \int_{x^n_{j-\frac{1}{2}}}^{x^n_{j+\frac{1}{2}}} U(t_n, x)\, dx. \tag{6.2}$$

Given the approximate solution $\{U^n_j\}$ at time t_n, the Godunov scheme consists of two main steps:

(i) Solve a Riemann problem at each cell interface $x^n_{j-\frac{1}{2}}$ with the initial data (U^n_{j-1}, U^n_j) (j= ..., -1, 0, 1, ...). The solution at the time $t = t_{n+1}$ is known on the whole space interval and at least in the time interval $[t_n, t_{n+1}]$.

(ii) Compute the cell averages at time t_{n+1} in each computational cell and obtain $\{U^{n+1}_j\}$.

Step (i) can be performed for a phase boundary problem in the same way it is done for a problem admitting conventional shock waves only. The Riemann solution, including the effect of the kinetic relation and the nucleation criterion, is known explicitly. Step (ii), however, should not be carried out when a cell contains the two possible phases because from a physical standpoint, it is meaningless to compute an average over quantities in different phases. As a matter of fact, if we do compute averages over quantities in different phases, we may obtain a value for the strain falling in the unstable phase — unstable phases do not arise in the physical model if initial data are metastable. Moreover such values may lead to instability in the computation. To avoid computing averages over a phase mixture, we must know the position of a phase boundary exactly so that we can confine averaging to a single

phase. When we are away from phase boundaries, we want to take the advantage of shock capturing schemes. So our strategy is to develop a front tracking/capturing method that tracks the phase boundaries and captures the standard shock waves.

The method is as follows: first the space is discretized in such a way that a phase boundary is at a grid point (a cell interface). If at time t_n a phase boundary is located at one grid point, the computation will proceed as follows:

(i) Compute all quantities at time t_{n+1} from the approximation at the time t_n, including the phase boundary propagation speed determined by the kinetic relation and the location of the phase boundary at t_{n+1}.

(ii) Shift the grid mesh according to the movement of the phase boundary so that the phase boundary is still a grid point.

This approach is typical of the so-called Largrangian algorithms. To implement the idea, a moving mesh has to be used. The method will be presented in three steps: first an algorithm for an initial value problem with a single phase boundary will be described. In a second stage it will be extended to the initial-boundary value problem. Then the algorithm will be further modified to include the nucleation of new phase boundaries at the boundary of, or inside, the computational domain, and the possible collision of two phase boundaries. For definiteness, we shall restrict the presentation of the method to the case in which Riemann solutions only involve initial data in different phases, i.e. γ_L in the low-strain phase, γ_R in the high-strain phase. Assume that at time t_n an approximation of the solution is known, and the phase boundary occupies a grid point. The speed of the phase boundary at the time t_n will be denoted by V^n. As seen in Section 2.2, it is determined from the kinetic relation by solving a Riemann problem. As a consequence, the location of the phase boundary is known. At the time t_{n+1}, the mesh is shifted uniformly according to: $x_{j+\frac{1}{2}}^{n+1} = x_{j+\frac{1}{2}}^{n} + V^n k_n$. An explicit formula for the scheme can be derived in the following way.

Consider an element T (abcd) about the cell j in (t, x) plane (Figure 6.1). Integrate the conservation laws (6.1) over the element T:

$$\int\int_T (U_t + f(U)_x) dx dt = 0.$$

From Green's Theorem, we have

$$\int_T f(U)dt - Udx = 0, \tag{6.3}$$

which leads to the following cell-averaged form of the conservation laws:

$$\begin{aligned} U_j^{n+1} &= U_j^n - \frac{1}{h_j^n}[\int_{t_n}^{t_{n+1}} (f(U^*(U_{j+1}^n, U_j^n)) - V^n U^*(U_{j+1}^n, U_j^n))dt \\ &- \int_{t_n}^{t_{n+1}} (f(U^*(U_j^n, U_{j-1}^n)) - V^n U^*(U_j^n, U_{j-1}^n))dt. \end{aligned} \tag{6.4}$$

Here $U^*(U_L, U_R)$ is the constant value along cd or ab of the Riemann solution with initial data (U_L, U_R). If we introduce the notation:

$$\tilde{f}^n(U) = f(U) - V^n U,$$

then (6.4) takes the following form:

$$U_j^{n+1} = U_j^n - \frac{k_n}{h_j^n}(\tilde{f}^n(U^*(U_{j+1}^n, U_j^n)) - \tilde{f}^n(U^*(U_j^n, U_{j-1}^n)). \tag{6.5}$$

One has to be careful when a phase boundary is being dealt with. Suppose $x_{j_0+\frac{1}{2}}$ is a phase boundary. Then the Riemann solution at $x_{j_0+\frac{1}{2}}$ in the cell j_0 is:

$$U^*(U_{j_0+1}^n, U_{j_0}^n) = U^-(U_{j_0+1}^n, U_{j_0}^n),$$

and the Riemann solution at $j_0 + \frac{1}{2}$ in cell $j_0 + 1$ is:

$$U^*(U_{j_0+1}^n, U_{j_0}^n) = U^+(U_{j_0+1}^n, U_{j_0}^n),$$

where U^+ and U^- are quantities in the front of the phase boundary and behind it respectively. So

$$U_{j_0}^{n+1} = U_{j_0}^n - \frac{k_n}{h_{j_0}^n}(\tilde{f}^n(U^-(U_{j_0+1}^n, U_{j_0}^n)) - \tilde{f}^n(U^*(U_{j_0}^n, U_{j_0-1}^n)), \tag{6.6}$$

$$U_{j_0+1}^{n+1} = U_{j_0+1}^n - \frac{k_n}{h_{j_0+1}^n}(\tilde{f}^n(U^*(U_{j_0+2}^n, U_{j_0+1}^n)) - \tilde{f}^n(U^+(U_{j_0+1}^n, U_{j_0}^n)). \qquad (6.7)$$

We summarize the algorithm as follows:

1. Compute the speed of propagation of the phase boundary from kinetic relation (3.19).
2. Shift grid points according to: $x_{j+\frac{1}{2}}^{n+1} = x_{j+\frac{1}{2}}^n + V^n k_n$.
3. Compute U_j^{n+1} from (6.5).
4. Repeat steps (1)–(3).

This algorithm differs from a shock capturing scheme in that it involves a moving grid and it utilizes a special solution to the Riemann problem when the moving discontinuity is a phase boundary. This special solution makes use of the kinetic relation.

When $V^n = 0$, this algorithm reduces to the Godunov method. When applied to conventional shock wave problems, the above algorithm is a standard Largrangian method combining shock tracking and shock capturing. Several methods of Godunov type can be used to implement the above idea, such as Godunov, MUSCL, PPM, or ENO schemes. Not every variant in each class of schemes can be used in a straightforward way, however. The scheme needs be "tested" on a cell containing a phase boundary: cell averaging across the phase boundary must be avoided. If this is not possible, the scheme should not be used for phase boundary problems. For instance, several schemes are based on analytically solving a linear advection equation, and extrapolating the result to a general scheme for nonlinear equations: this in general would not produce the desirable property we require here–no numerical interior points to describe a sharp phase boundary. We observe that one can use a scheme in cells (I) which do not contain any phase boundary, and another scheme in cells (II) where a phase boundary is located. Such hybridization should be done carefully however in order to keep the same accuracy in both regions I and II.

Schemes that can be applied include: the first-order Godunov method , a variant of the MUSCL scheme [68] (a second order method), and some even higher order

schemes. In fact any scheme whose numerical flux is constructed through solutions based on solving Riemann problems at cell interfaces can be used. In the numerical experiments we present in Section 6.5, we implement the Godunov method and a slope-limiter scheme.

6.3 Propagation, initiation and interaction

In any computational cell, we distinguish three cases:

(i) propagation of a phase boundary,

(ii) nucleation of a phase boundary at a boundary point, or nucleation of two phase boundaries in the interior of the domain,

(iii) interaction of two phase boundaries.

The interaction between a shock wave and a phase boundary is taken care of automatically since shock waves are captured. In this section, we present details about the algorithm for the computation of the propagation of a single phase boundary. With some modification, the algorithm allows us to treat the nucleation and the interaction of phase boundaries.

6.3.1 Propagation of a phase boundary

One obvious shortcoming of the algorithm described in Section 6.2 is that the grid points are shifted uniformly: it cannot be applied to an initial value problem with multiple phase boundaries or to an initial-boundary value problem. For example, if we have two phase boundaries moving at different speeds, then it is impossible to shift mesh uniformly to make the two phase boundaries locate at grid points at the same time. We therefore need to shift grid points locally. As a consequence we will have a locally nonuniform mesh due to two cells moving with the phase boundary in a certain way. Assume at time t_n, $x_{j_0+\frac{1}{2}}$ represents a position of the phase boundary. At time t_{n+1}, $j_0+\frac{1}{2}$ moves to a new position. Instead of letting all grid points move with the phase boundary, we move only the point $x_{j_0+\frac{1}{2}}$. But subsequently the locations of j_0, j_0+1 are changed (Figure 6.2).

By doing this, the size of cells j_0 and j_0+1 will change as time goes on: one cell will shrink, the other will be enlarged. When one cell is too small, we adjust the location of one grid point.

The modified algorithm then is as follows:

1. Compute U_j^{n+1} from (6.5) with $V^n = 0$ for all of the jth cell not containing the phase boundary.

2. Compute the phase boundary propagation speed V^n from the kinetic relation for the jth cell containing the phase boundary.

3. Shift grid points locally by distinguishing two cases:

   If $V^n < 0$:

   - If $|x^n_{j_0-\frac{1}{2}} - x^n_{j_0+\frac{1}{2}}| > \frac{h}{2}$, then shift the point $j_0+\frac{1}{2}$ and compute the cell averages in the cells j_0 and j_0+1 from the formulas:

$$U^{n+1}_{j_0} = \frac{h^n_{j_0}}{h^{n+1}_{j_0}} U^n_{j_0} - \frac{k^n}{h^{n+1}_{j_0}} (\tilde{f}^n(U^-(U^n_{j_0+1}, U^n_{j_0})) - \tilde{f}^n(U^*(U^n_{j_0}, U^n_{j_0-1})),$$

     and

$$U^{n+1}_{j_0+1} = \frac{h^n_{j_0}}{h^{n+1}_{j_0+1}} U^n_{j_0+1} - \frac{k^n}{h^{n+1}_{j_0+1}} (\tilde{f}^n(U^*(U^n_{j_0+2}, U^n_{j_0+1})) - \tilde{f}^n(U^+(U^n_{j_0+1}, U^n_{j_0})).$$

   - Otherwise adjust the location of the grid point $j_0 - \frac{1}{2}$ in the following way:
     - Move the point $j_0 - \frac{1}{2}$ to the right side of the phase boundary, and re-label it $j_0 + \frac{1}{2}$, so that the cell $[x_{j_0+\frac{1}{2}}, x_{j_0+\frac{3}{2}}]$ keeps a "regular" size. Re-label the phase boundary $j_0 - \frac{1}{2}$.
     - $j_0 - 1, j_0, j_0 + 1$ are changed accordingly for the three adjusted cells.

   Then recompute the cell averages associated with the modified cells. The formulas are similar to those used in the last step, see Figure 6.4.

   If $V^n > 0$, the procedure is similar to that for the case $V^n < 0$:

- If $|x^n_{j_0+\frac{1}{2}} - x^n_{j_0+\frac{3}{2}}| > \frac{h}{2}$, then shift the point $x_{j_0+\frac{1}{2}}$ only, and compute the cell averages in the cells j_0 and j_0+1.
- Otherwise modify the location of the grid point $j_0+\frac{3}{2}$, and compute the cell averages for the adjusted cells.

4. Repeat (1)–(3).

It should be noted that the restriction $|\frac{ck}{h}| < \frac{1}{2}$ is necessary in our algorithm for the stability of numerical computation. This is due to the fact that computational cells can shrink as time evolves. Also a shrunk cell must be large enough compared with normal cell size in order to avoid local time-marching.

6.3.2 Initiation and interaction

Though the above algorithm is presented for the case of a single phase boundary, it can treat multiple phase boundaries and the interaction of phase boundaries as well. When phase boundaries are separated by at least one grid point (i.e. two cells), the algorithm in Section 6.3.1 can be used without modification. When two phase boundaries are sufficiently close to each other, i.e. typically when there is no grid point separating the two phase boundaries, some modification is necessary. This is the subject of this subsection.

Since a phase boundary has to be a grid point when a new phase nucleates, the cells near the new phase boundary will be very small at the initial stage. In the meantime, the large difference in cell sizes may lead to computational instability. Therefore local time-marching and local mesh regridding and refinement are necessary in general. Here we emphasize that:

(1) a phase boundary has to be at a grid point;

(2) conservation of physical quantities has to be preserved when local mesh regridding or local mesh refinement is carried out;

(3) local time marching has to be ended at a regular time step.

The collision of two phase boundaries can be treated as in the method of Shyue [77] for the collision of two strong shocks. After the collision of two phase boundaries,

two possible situations arise:

(a) no phase boundary comes out of the collision;

(b) two phase boundaries nucleate at the position of collision.

Case (a) is a conventional shock wave issue, and Case (b) involves a nucleation problem. Both cases can be treated. The nucleation criterion presented in Section 2.2 is used for Case (b).

6.4 Consistency and entropy condition

It would be interesting to investigate the mathematical properties of the front tracking/capturing method presented in this paper. Questions to be addressed would include consistency, stability, the entropy condition, and strong convergence. The numerical analysis of the method is complicated by the fact that a locally non-uniform mesh is used. The main difficulty concerning convergence is proving that the kinetic relation and nucleation criterion are satisfied by the scheme in the limit as the mesh sizes go to zero. This section is devoted to some preliminary investigation of the properties of our algorithm.

From Section 6.2, the numerical flux in the method is

$$F(U_{j+1}^n, U_j^n) = f(U_*(U_{j+1}^n, U_j^n)) - V^n U^*(U_{j+1}^n, U_j^n),$$

and, in general,

$$F(U, U) = f(U) - VU \neq f(U).$$

It might seem that the algorithm is not in conservative form, and so might be not consistent with the conservation laws (6.1). In fact, let us recall that the mesh is being shifted as time goes on. Therefore let us rewrite the conservation laws (6.1) in a moving coordinates. Let x_0 be a point in the moving coordinates, the the coordinate of the point in the fixed coordinates is $x_0 + Vt$. For the purpose of the algorithm, we write

$$\frac{DU}{Dt} \equiv \frac{dU}{dt}|_{x=x_0+Vt} = V\frac{\partial U}{\partial x} + \frac{\partial U}{\partial t},$$

so that from (6.1), we obtain the following equation:

$$\frac{DU}{Dt} + \frac{\partial}{\partial x}(f(U) - VU) = 0. \tag{6.8}$$

Thus the algorithm is in fact a conservative scheme for the Equations (6.8), and, in view of (6.8), it is not hard to check that it is consistent: assuming that the scheme converges in norm, the limit must be a solution to the conservation laws (6.1).

Observe that because the algorithm is a Godunov-type scheme, analytical solutions to the Riemann problems are used. Those solutions satisfy the entropy criterion (2.10). The projection step in the Godunov scheme preserves the entropy criterion as well. Therefore the entropy condition is satisfied in a discrete sense, and therefore in the limit if the scheme is convergent. So the algorithm is a consistent, conservative, and entropically admissible method. The Lax-Wendroff Theorem can be applied to show that the approximate solutions provided by the algorithm will converge to a weak solution to the conservation laws (6.1) as the mesh size approaches zero. This analysis however does not apply to the initiation criterion or the kinetic relation. In Section 6.5, we demonstrate the convergence of the algorithm numerically.

6.5 Extension to more general materials

Our front tracking/capturing method in principle can be applied to any material although we so far only present the method for trilinear materials. And it is of both theoretical and practical interest to apply the method to more general two-phase materials, such as those defined in Section 3.2. We observe that explicit analytical Riemann solutions for a general two-phase elastic material capable of phase transitions are not easily available. Solving Riemann problems is done numerically by an iterative method for nonlinear algebraic equations. In practice, this is time-consuming, and the convergence of the iteration method cannot be always guaranteed because we cannot always have good initial guess of solutions.

One way to proceed is to use the approximate Riemann solver proposed in Section

3.2. The approximate Riemann solver can be applied to our front tracking/capturing method. As in Section 3.2, for the conservation law (6.1), we approximate

$$f(U)_x = \begin{pmatrix} 0 & -\frac{\sigma'(\gamma)}{\rho} \\ -1 & 0 \end{pmatrix} \begin{Bmatrix} v_x \\ \gamma_x \end{Bmatrix} \approx \begin{pmatrix} 0 & -c^2 \\ -1 & 0 \end{pmatrix} \begin{Bmatrix} v_x \\ \gamma_x \end{Bmatrix} = AU_x.$$

Here c is a constant. The original conservation law is approximated by

$$U_t + AU_x = 0. \tag{6.9}$$

Construction of numerical flux for an approximate Riemann Solver. Consider a Riemann problem with U_L and U_R as initial data that involves no phase boundary or phase change. Let $F(U_L, U_R)$ be the numerical flux at $x = 0$ and $U^*(\frac{x}{t})$ be the solution to (6.9) for the initial data. For M sufficiently large, according to (6.3), we have

$$\int_0^M U dx = MU_R + F(U_L, U_R) - f(U_R) \tag{6.10}$$

for conservation law (6.1);

$$\int_0^M \hat{U}^* dx = MU_R + A\hat{U}^*(0) - AU_R \tag{6.11}$$

for conservation law (6.9).

To preserve the conservation property, we require that

$$\int_0^M U dx = \int_0^M \hat{U} dx.$$

Thus we obtain from (6.10) and (6.11) that

$$F(U_L, U_R) = A\hat{U}^*(0) + f(U_R) - AU_R. \tag{6.12}$$

Approximate Riemann solution in this case can be computed by the Roe's approximate Riemann solver [71].

Following the procedure in Section 6.2, and the idea above, we obtain the following approximate flux at a phase boundary that is propagating with the speed V:

$$\tilde{f}(U_l, U_r) = A\hat{U}^* - V\hat{U}^* + f(U_r) - AU_r, \tag{6.13}$$

where $\hat{U}^*$ is the approximate Riemann solution at the phase boundary. We emphasize that the conservation of U is guaranteed by the approach used here. On the other hand the propagation of a phase boundary is determined by simply using the above flux into the algorithm in Section 3.2. Using an approximate Riemann solver, we can compute propagation of phase boundaries associated with general two-phase elastic materials.

6.6 Numerical results

We implement our numerical method by using Godunov scheme and a slope-limiter scheme, which is equivalent to a variant of the MUSCL scheme [68]. It should be pointed out that the slope-limiter in the MUSCL scheme, based on the so-called min-mod limiter in our code, is determined unilaterally instead of bilaterally by minmod when a phase boundary is present in a cell. In test 1, we apply our method to a Riemann problem whose solutions take values in a single phase at all times, i.e. there is no phase boundary. The results of the test show that the front tracking method is equivalent to the standard shock capturing approaches for shock wave problems.

In Tests 2-6, the material is the trilinear material defined in Section 2. The kinetic relation is given by $f = \omega\dot{s}$. The material constants are: $\mu = 1, \rho = 1, \omega = 0.35, \gamma_m = 0.5, \gamma_M = 1.0, \gamma_T = 0.75$. $\gamma_{cr} = 0.5, \gamma_{cr}^* = 1.0$. In the computations, time step k is 0.001 (time unit), mesh size h is 0.01 (length unit), if not otherwise specified. In applicable diagrams, the analytical solutions are represented by solid lines, numerical solution by dashed lines or dots.

In the following, we use CFL to represent (wave speed)(time step)/(mesh size).

We measure global error by the discrete l_1-norm defined by

$$||U^n|| = \sum_j |U_j^n| h_j \tag{6.14}$$

for discrete grid function U^n.

6.6.1 Test 1: A conventional Riemann problem.

Initial data $v_L = 0.2, \gamma_L = 0.3, v_R = 0.4, \gamma_R = 0.1$ are used in the computation. Here γ_L and γ_R belong to the low-strain phase and there is no new phase initiated. We use the usual shock capturing schemes Godunov method and MUSCL to calculate the problem. We also use our method to calculate the problem. Our method delivered identical results to those delivered by the usual shock capturing schemes.

6.6.2 Test 2: A single phase boundary.

The initial data are $v_L = 0.7, \gamma_L = 0.3, v_R = 0.1, \gamma_R = 1.2$. The strain γ_L belongs to the low-strain phase, the strain γ_R belongs to the high-strain phase. Therefore we have a single phase boundary. We compute the propagation of the phase boundary by our tracking/capturing method. The numerical results are compared with the exact solution that is known from Section 3.2; see Figure 6.5, 6.6. The convergence of the front tracking/capturing method is demonstrated in the following table, where the error is measured by the l_1-norm for particle velocity or strain.

mesh size	e (Godunov scheme)	e' (slope-limiter scheme)
$2h$	1.6210^{-2}	7.7310^{-3}
h	1.1510^{-2}	4.9110^{-3}
$h/2$	8.1510^{-3}	3.1510^{-3}

where $h = 0.01$, $CFL = 0.1$(fixed), time $t = 0.2$. In this particular test, the errors for particle velocity and strain are about the same, so in the above table, we list only one error for each scheme.

The results suggest: the method converges to the exact solution when the mesh size reduces to zero and it tracks the location of the phase boundary accurately; the fronts of sound waves are somewhat smeared out in the results.

6.6.3 Test 3: Nucleation of a phase boundary at an end point

Nucleation of a phase boundary at the boundary of a bar is quite common in bar impact experiments [36]. In this test we only consider a very simple situation: a semi-infinite bar, which is in an initially undeformed state, is impacted at the end $x = 0$ at time $t = 0$. The boundary condition here can be described by $v(0,t) = v_b$, where v_b is a constant. The initial state of the bar is: $v(x,0) = 0, \gamma(x,0) = 0$. In order to initiate a phase boundary at the boundary of the bar, the magnitude of v_b has to be large enough, $|v_b| > c\gamma_{cr}$. In this calculation, we take $v_b = -0.6$ so that we can have a nucleation at the end point. In the real computation, at the first several time steps, the nucleated phase boundary is very close to the end of the bar, so local time marching is necessary. After the first time step we relocate the first grid point to the phase boundary. We do local time marching in the two cells that contain the phase boundary until it is $1\frac{1}{2}$ cells away from the end of the bar. We continue the computation by the algorithm in Section 6.3.1. It should be noted that time step in local time marching is adjusted according to the size of the first cell. The smallest time step in the local time marching is about 1/12 of a normal time step, and local time marching lasts 10 normal time steps. Numerical results are in good agreement with the exact solution; see Figure 6.7 and 6.8.

6.6.4 Test 4: Nucleation of two phase boundaries

Due to interactions of shock waves, a new phase may be initiated in the interior of the domain, so that two phase boundary will be generated from a single grid point. For the regridding of cells around the new phase, we can proceed as in test 3, then proceed by local time marching until the distance between the two new phase boundaries is

no less than twice the regular cell size. However this mesh technique does not work sometimes because the big difference of mesh sizes may produce errors that lead to numerical instability. This suggests that local mesh refinement is necessary.

We consider the nucleation of two phase boundaries in a Riemann problem that involves only the low-strain phase initial data. The initial data is taken to be: $v_L = -0.1, \gamma_L = 0.2, v_R = 0.5, \gamma_R = 0.4$. In the computation the mesh size in the refined region is $1/10$ of regular size, the smallest time step in local time marching is $1/10$ of regular time step. The numerical results are compared with analytical results in Figure 6.9 and 6.10.

6.6.5 Test 5: Collision of two phase boundaries

We construct special initial data which give rise to two phase boundaries colliding at some finite time. The initial data are piecewise constant in three regions that we refer to as L, C, and R. We choose: $v_L = 0.789, \gamma_L = -0.4, v_C = 0., \gamma_C = 1.125, v_R = 0., \gamma_R = 0.375$.

When two phase boundaries are so close to each other that there are no grid points in between, we treat the three cells which contain the phase boundaries as a group with no further regridding in these cells. After the interaction, the whole domain under consideration is in phase 1. Comparison between the numerical results and analytical results are given in Figure 6.11 – 6.13.

6.6.6 Test 6: Impact on a semi-infinite bar with an initially stationary phase boundary

In this example, we consider the effect of the impact on a semi-infinite bar initially in two phase equilibrium state with a single phase boundary. We compare the computed phase boundary position to that of the exact solution obtained in Chapter 5.

A semi-infinite bar is located in $[0, \infty)$ in the reference state, and a phase boundary is initially located at $x = 1.995$ in equilibrium state. The strains in the bar are $\gamma = 0.375, v = 0$ for x in $[0, 1.995)$, and $\gamma = 1.125, v = 0$ for x in $(1.995, \infty)$. At

the time $t = 0$, the bar is loaded by a velocity whose time-history is a given square wave. The duration of the square wave is 0.5 (time unit), the amplitude of the square wave is 0.15 (length unit/time unit). The numerical results are shown in Figures 6.4 – 6.16. When compared with the exact solution, the numerical prediction of the position of the phase boundary is accurate. For fixed CFL, we check the convergence by changing the mesh size and the time step with $h = 0.01$, $CFL = 0.1$ and S is the distance that the phase boundary has moved from its original position at time $t = 3$:

mesh size	$\lvert(S_{exact} - S_{Numerical})/S_{exact}\rvert$
$2h$	2.45%
h	1.58%
$h/2$	0.84%

These results suggest that the numerical solution converges to the exact solution as mesh size goes to zero. Roughly speaking, the accuracy of the method is of order $O(h^2 + k)$ when a slope-limiter scheme is implemented. Improvement of the accuracy in space can be easily implemented, but the improvement of accuracy in time integration requires substantial change of the formulation of the algorithm, (6.4).

As before, the fronts of sound waves are smeared out slightly. This contributes to the error in the calculation of phase boundary propagation speed, and thus the position of the phase boundary. In the computation, the boundary values are carefully chosen so that there is no other phase boundary nucleated at any time in the bar.

6.6.7 Test 7: An example for general two-phase materials

We use our numerical method and the proposed approximate Riemann solver to compute the problem involved in Test 1 and Test 2 of Section 3.2.

A first-order Godunov scheme is used in the implementation. The results for the two tests show that our front tracking method works well when an approximate Riemann solver is used. Here we only present the results for test 1 of Section 3.2.2, see Figures 6.19, 6.20. The error in the computed phase boundary position is 3.81%. For

fixed mesh size, the error decreases slowly with the decrease of the time step, 3.80% for time step 0.001/2, 3.79% for time step 0.001/4. For fixed CFL, the decrease in mesh size does not improve the accuracy of computation. This "locking" of accuracy is due to the inherent error of the approximate Riemann solver. To remedy the deficiency, we propose the following procedure: use Riemann solutions from the approximate Riemann solver as initial guesses for the exact Riemann solver; use the Riemann solutions of the exact Riemann solver to construct numerical flux. It only takes one or two iterations for the exact Riemann solver to converge when the solution from the approximate Riemann solver is taken as initial guess. Using this procedure, we have the following results:

mesh size	$\lvert(S_{exact} - S_{Numerical})/S_{exact}\rvert$
$2h$	0.753%
h	0.479%
$h/2$	0.283%

mesh size	e1 (velocity)	e2(strain)
$2h$	2.72×10^{-2}	1.816×10^{-2}
h	1.712×10^{-2}	1.157×10^{-3}
$h/2$	1.014×10^{-2}	6.724×10^{-3}
$h/4$	5.652×10^{-3}	3.748×10^{-3}

where $h = 0.01$, $CFL = 0.1$(fixed) and $x = S$ is the position of the phase boundary at time $t = 0.2$. Here $e1$ and $e2$ are errors of the particle velocity and strain measured by the l_1-norm. If we compare these results with those obtained from the Godunov scheme in Test 2, we can see that the results obtained here converges at a higher order.

6.7 Discussions

Our tests demonstrate that our tracking/capturing method can treat initial-boundary value problems in the modeling of solid-solid phase transformations. The method is shown to be consistent, entropically admissible and convergent. Though the fronts of sound waves are smeared out slightly in the method, phase boundaries are still accurately tracked. It should be noted that for a real shock (Test 7), even a first-order method can give a relatively sharp shock front. With the methods investigated here, we are capable of applying the Abeyaratne-Knowles model to initial-boundary value problems of practical interest.

Numerically, a locally nonuniform mesh, which changes with time, is used in the tracking/capturing method. The mesh technique is straightforward and easy to implement in simple problems but it seems that the technique is more troublesome to implement in more complicated situations. A limitation of the proposed method is that a phase boundary should be a grid point. A systematic mesh technique should be developed. There is an extensive literature on adaptive mesh refinement techniques, for example, Berger & Colella [15]. The smearing of the fronts of sound waves can be prevented by applying an "artificial compression technique"; see for example [40].

In order to compute propagating phase boundaries for general two-phase elastic materials, we have to use an approximate Riemann solver for the case with nucleation. There are some subtle issues related to this case. On the other hand, we cannot tell how well the solution of the approximate Riemann solver proposed here approximates the exact solution in general at current stage. However it has been shown that we can avoid the disadvantages of the "exact" Riemann solver (time consuming, may not converge) and approximate Riemann solver (relatively poor accuracy), by using the Riemann solutions from the approximate Riemann solver as initial guess of exact Riemann solver.

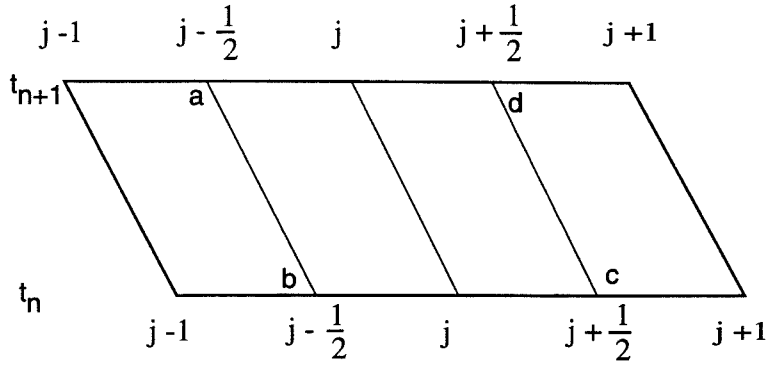

Figure 6.1: A mesh in (x, t) plane

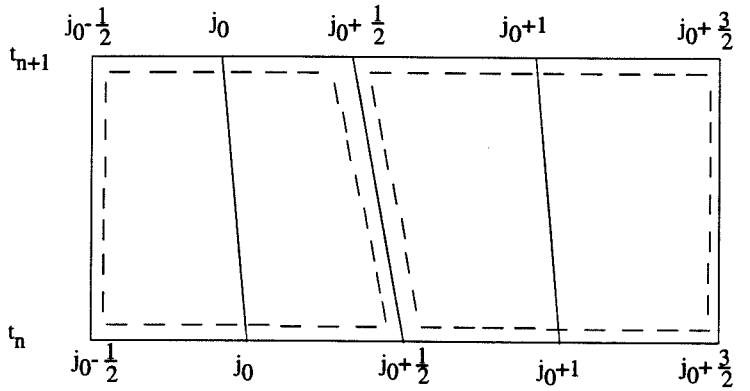

Figure 6.2: Local shifting of a grid point

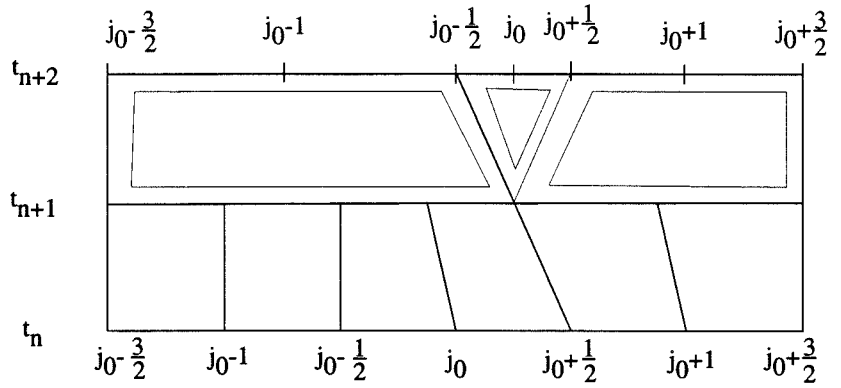

Figure 6.3: Calculation of cell averages for the modified cells

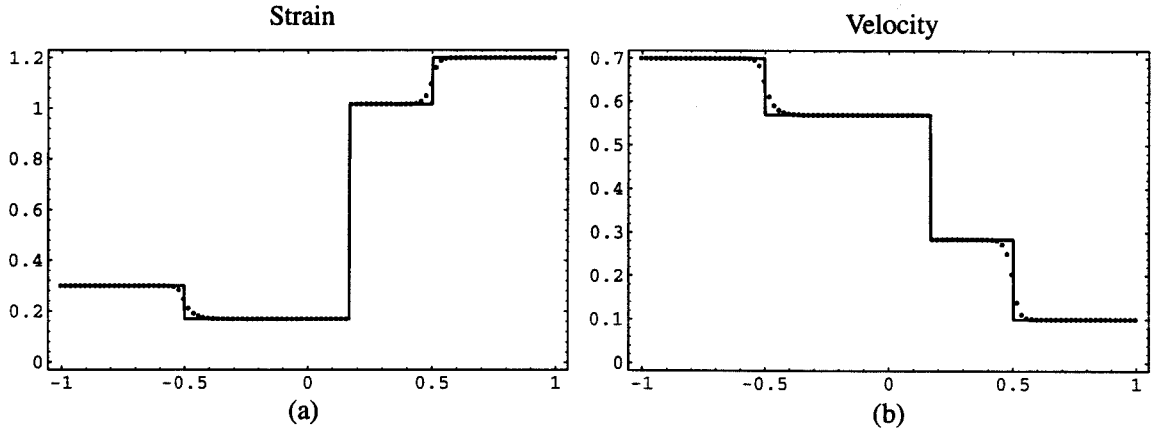

Figure 6.4: Solutions to Riemann problem with initial data in the low-strain phase and high-strain phase at t=0.5 by front tracking: (a) the strain distribution; (b) the velocity distribution

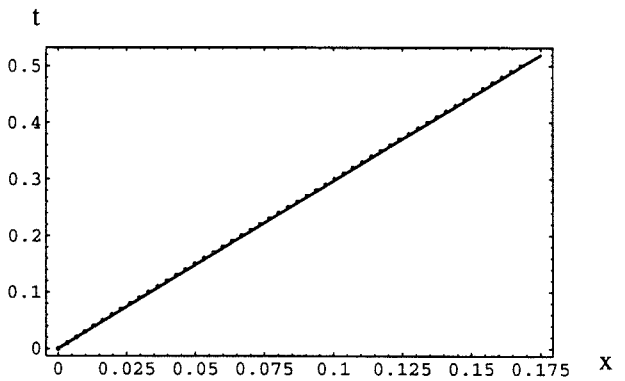

Figure 6.5: Trajectory of the phase boundary determined by front tracking method

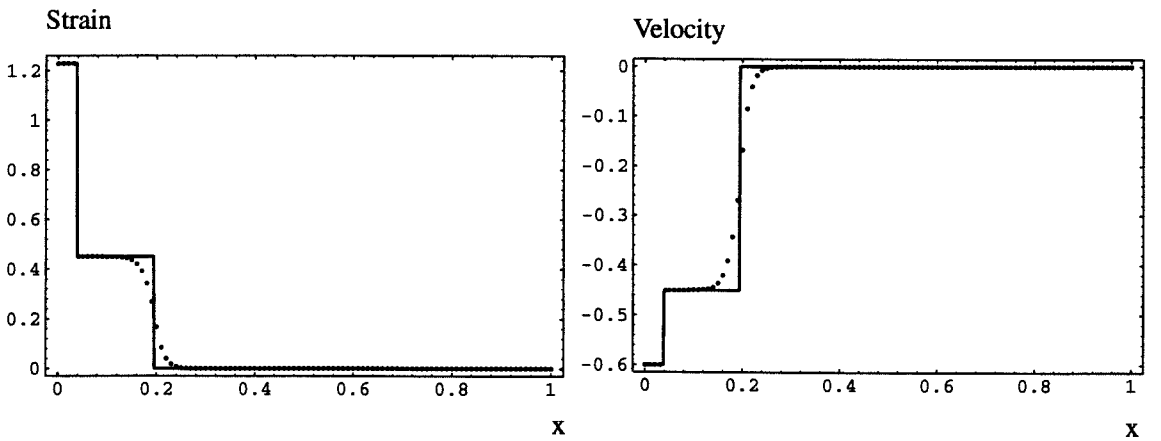

Figure 6.6: Solutions to the problem involving nucleation of a phase boundary by front tracking at t=0.2: a. the strain distribution; b. the particle velocity distribution

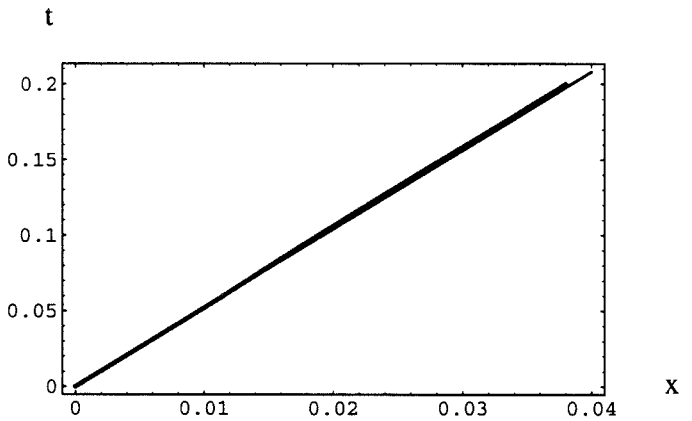

Figure 6.7: Trajectory of the phase boundary

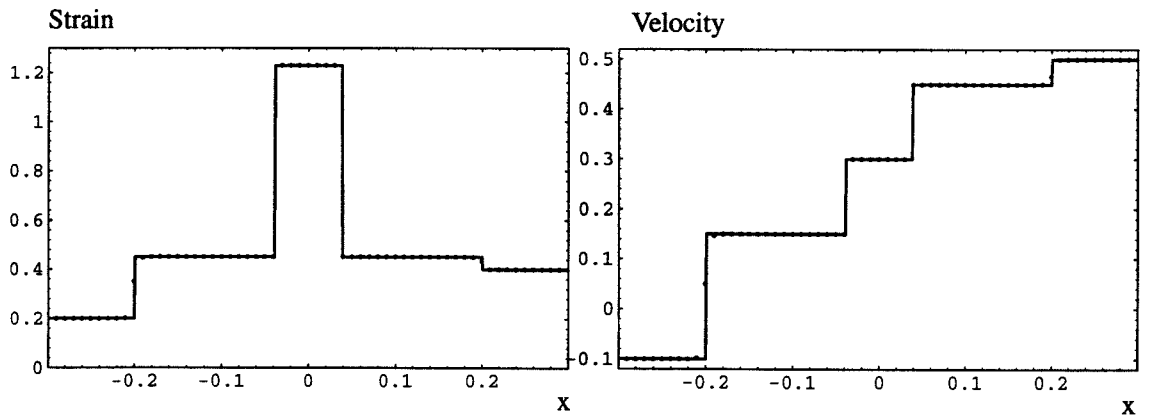

Figure 6.8: Solutions to the problem involving nucleation of two phase boundaries by front tracking at t=0.2: a. the strain distribution; b. the particle velocity distribution

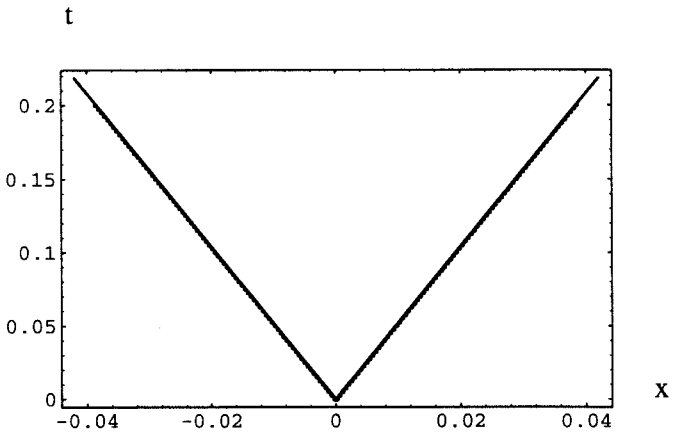

Figure 6.9: Trajectories of phase boundaries

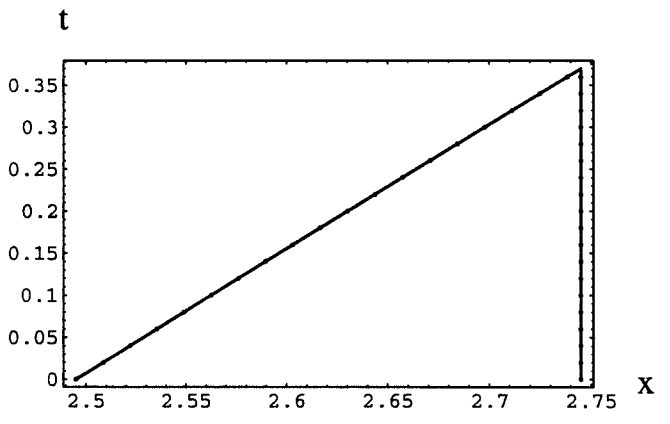

Figure 6.10: Trajectories of phase boundaries for the problem involving collision of phase boundaries

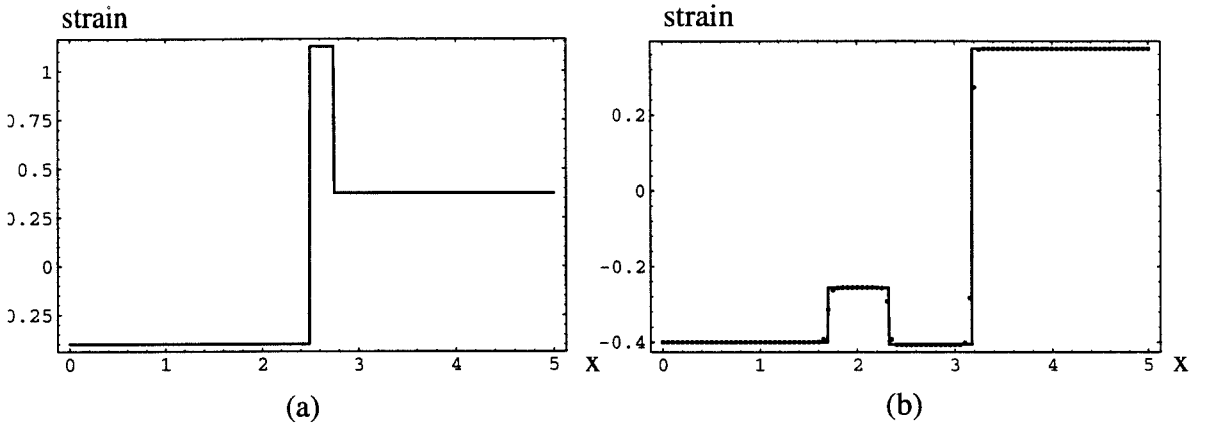

Figure 6.11: The strain distribution : a. initial strain; b. strain after collision, t=0.8

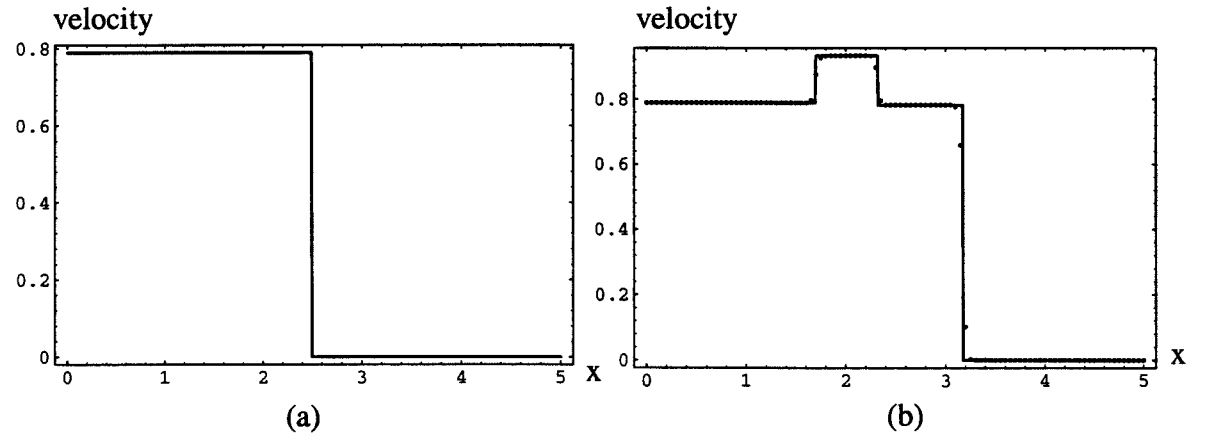

Figure 6.12: The particle velocity distribution : a. initial state; b. velocity after collision, t=0.8

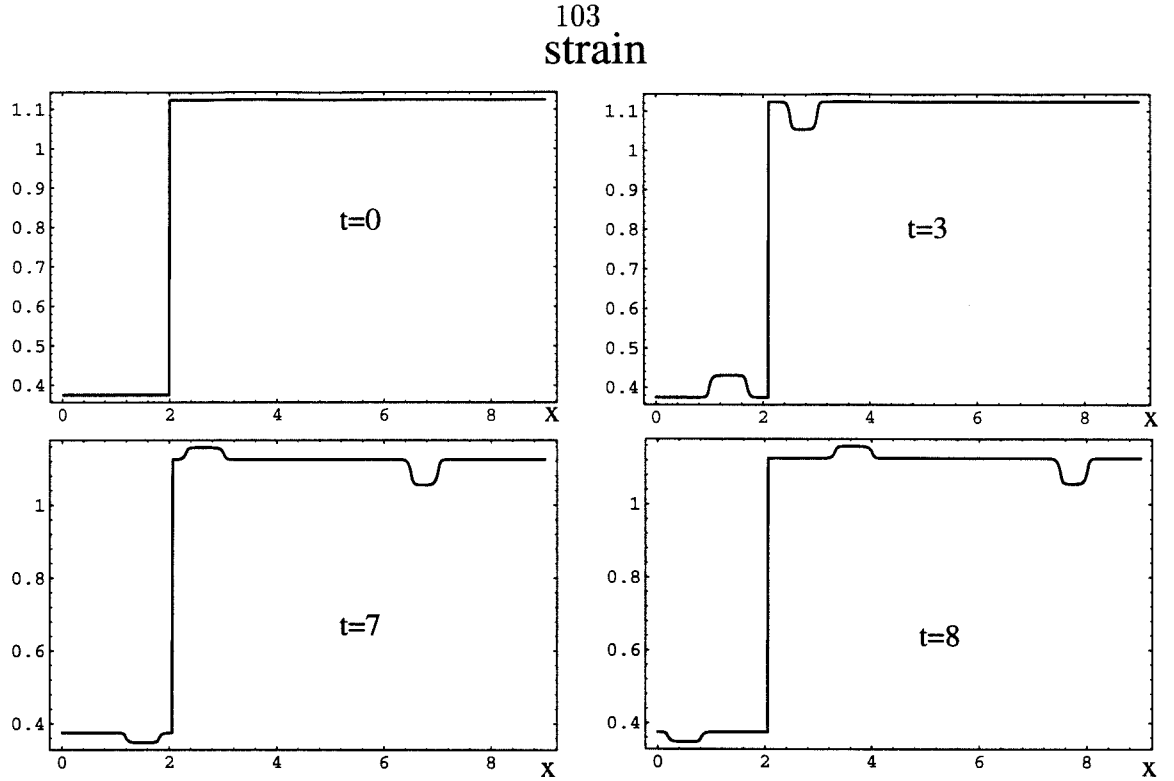

Figure 6.13: The strain distribution in a semi-infinite bar at different times

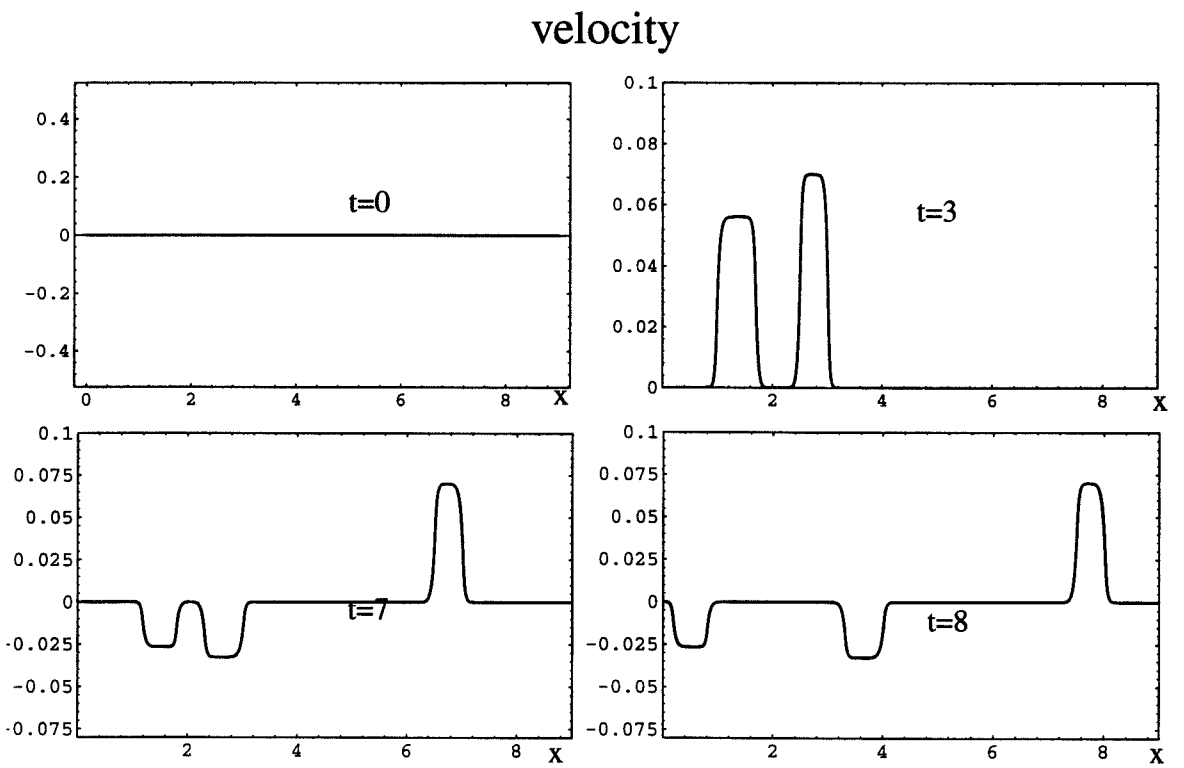

Figure 6.14: The particle velocity distribution in semi-infinite bar at different times

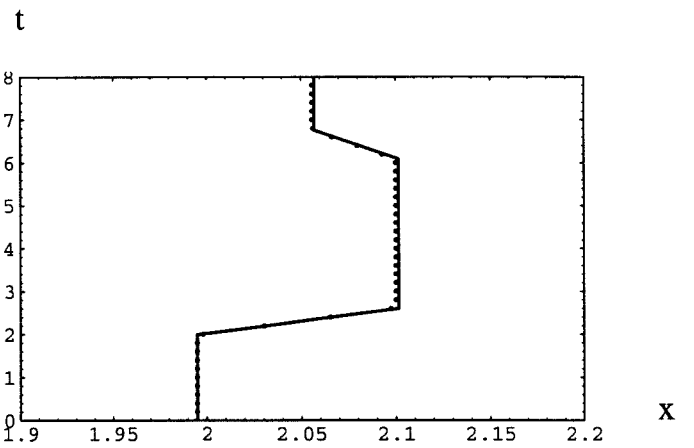

Figure 6.15: Trajectory of the phase boundary determined by front tracking

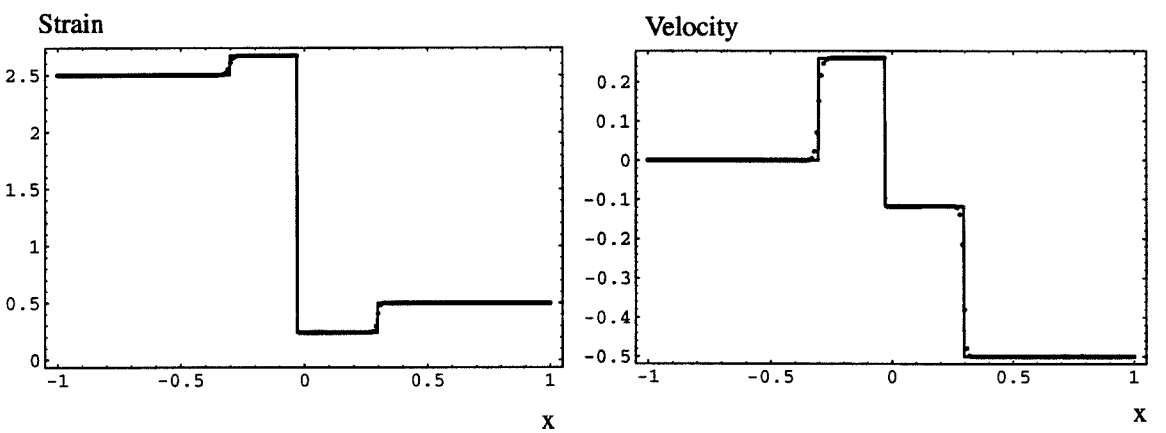

Figure 6.16: Solutions to a Riemann problem with initial data in high-strain/low-strain phases: a. the strain distribution; b. the particle velocity distribution

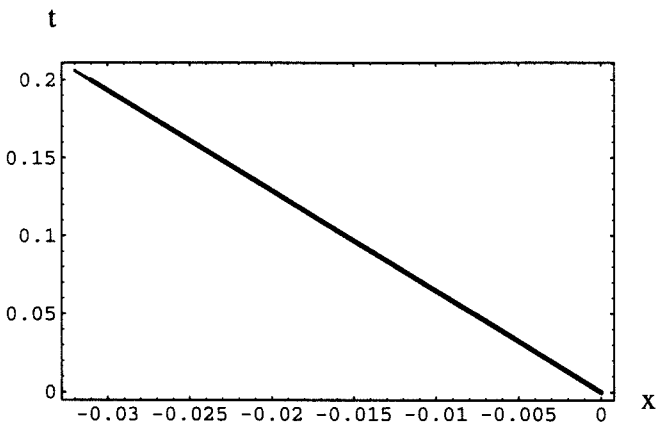

Figure 6.17: Trajectory of the phase boundary

Chapter 7 Large time dynamical behavior of a phase boundary: Numerical computation

In Chapter 5, an exact solution was obtained for a semi-infinite bar initially in an equilibrium state with a single phase boundary subject to an incoming pulse. This solution shows that the bar ultimately returns to an equilibrium state.

It is interesting to check whether or not a dynamic solution converges to an equilibrium state predicted by a static theory. A finite bar problem is considered. Lin and Pence [55], [56] solved the finite bar problem approximately using an energy approach in which the interaction of reflected waves is ignored. Because the implications of this approximate assumption are not clear, it is desirable to investigate this problem further.

The numerical method developed in Chapter 6 is used here for this investigation. We can determine the dynamical state of the bar as well as the dissipation and the total energy of the bar at any time. The numerical method can also be used to analyze this problem for nontrilinear materials.

The initial-boundary value problem to be solved is formulated in Section 7.1. We present a brief analysis of energy and dissipation in the system under consideration in Section 7.2. A boundary value problem which corresponds to the initial-boundary value problem formulated in Section 7.1 is formulated in Section 7.3, and a metastable static solution to the boundary value problem is presented. In Section 7.4, the numerical solution is presented for the special trilinear material defined in Section 2.3, as well as for the nontrilinear material given by (3.32). The results include the strain and particle velocity distribution in the bar at various times, the dissipation due to the moving phase boundary and the total energy of the bar. The prediction of the numerical solution for large time is compared to corresponding static solution mentioned above.

7.1 Formulation of an initial-boundary value problem

A finite bar occupies the interval $0 \leq x \leq L$ in its undeformed reference configuration. The bar is assumed to be made of a two-phase elastic material, either the special trilinear material defined in Section 2.3 or the two-phase material defined by (3.32). The kinetic response function is assumed to be $\phi(\dot{s}) = \omega\dot{s}$ and the nucleation criterion is taken to be the one given in Section 2.2. It is assumed that, at $t = 0$, the bar has a single stationary phase boundary located at $x = s_0$. The portion of the bar in $[0, s_0)$ is in the low-strain phase, while the remainder of the bar is in the high-strain phase. Because of the kinetic relation assumed, the bar must necessarily be in the Maxwell state of stress initially. The bar is assumed to be fixed at $x = L$, and it is impacted at the end $x = 0$ at time $t = 0$. Thus the initial conditions and boundary conditions can be expressed as follows.

Initial conditions:

$$\left.\begin{aligned} v(x,0) &= 0, \\ \gamma(x,0) &= \gamma_0^- \end{aligned}\right\} 0 \leq x < s_0;$$

$$\left.\begin{aligned} v(x,0) &= 0, \\ \gamma(x,0) &= \gamma_0^+ \end{aligned}\right\} s_0 < x \leq L.$$

Here γ_0^+ and γ_0^- are strains in the high-strain and low-strain phases, respectively, that correspond to the Maxwell stress; for the trilinear material, $\gamma_0^- = \frac{1}{2}(\gamma_m + \gamma_M - \gamma_T)$ and $\gamma_0^+ = \frac{1}{2}(\gamma_m + \gamma_M + \gamma_T)$.

The boundary conditions are

$$v(0,t) = \begin{cases} v_0, 0 \leq t < t^*, \\ 0, \quad t > t^* \end{cases} \tag{7.1}$$

and

$$v(L,t) = 0. \tag{7.2}$$

For the formulation given here, according to the initial conditions, the bar is initially stretched.

7.2 Energy and dissipation

As shown in Chapter 2, the total accumulated dissipation at a phase boundary at time t is

$$D(t) = \int_0^t f(t')\dot{s}(t')dt', \tag{7.3}$$

where $f(t)$ is the driving traction at the phase boundary at time t and $\dot{s}$ is the phase boundary propagation velocity.

The total energy in the bar at time t is

$$E(t) = \int_0^L (W(\gamma(x,t)) + \frac{1}{2}\rho v^2(x,t))dx \tag{7.4}$$

where W is the strain energy per unit undeformed volume, $W(\gamma) = \int_0^\gamma \sigma(\gamma')d\gamma'$.

In our analysis, we assume that v_0 is small enough to assure that only one phase boundary is present for all times; thus no new phase boundary is nucleated by the impact.

Two-phase materials

For *general* nontrilinear two-phase elastic materials, the shock waves as well as phase boundaries are dissipative. If the rate of work done on the bar by the impact is denoted by $\dot{w}(t)$, and the rate of dissipation at all shock waves is $\dot{D}_{shock}(t)$, in a procedure that is similar to that lead to (2.8), we have (over the whole bar):

$$\dot{w}(t) - \dot{E}(t) = \dot{D}(t) + \dot{D}_{shock}(t), \qquad t \leq t^*; \tag{7.5}$$

$$-\dot{E}(t) = \dot{D}(t) + \dot{D}_{shock}(t), \qquad t > t^*. \tag{7.6}$$

Trilinear materials

For trilinear materials, the shock waves are dissipation free, so that phase boundaries are the only source of dissipation. For the particular boundary condition given

in Section 7.1, the rate of work done on the bar by the impact is

$$\dot{w}(t) = \mu(\frac{v_0}{c} - \gamma_0^-)v_0 \tag{7.7}$$

and the energy identity (2.8), for $x_1 = 0$, $x_2 = L$, reduces to

$$\mu v_0(\frac{v_0}{c} - \gamma_0^-) - \dot{E}(t) = \dot{D}(t), \qquad t \leq t^*; \tag{7.8}$$

$$-\dot{E}(t) = \dot{D}(t), \qquad t > t^*. \tag{7.9}$$

From (7.9), we see that the total energy of the bar will decrease after time t^*, in fact we can integrate (7.9) from t^* to $t > t^*$to obtain

$$\begin{aligned} E(t) &= E(0) + \mu(\frac{v_0}{c} - \gamma_0^-)v_0 t^* + D(t) \\ &= D(t) + \frac{1}{2}\mu(\gamma_0^-)^2 s_0 + (\frac{1}{2}\mu\gamma_m^2 + \frac{1}{2}\mu(\gamma_m + \gamma_M - \gamma_T)(\gamma_M - \gamma_m) \\ &+ \frac{1}{2}\mu(\gamma_0^+ + \gamma_M - 2\gamma_T)(\gamma_0^+ - \gamma_M))(L - s_0) + \mu(\frac{v_0}{c} - \gamma_0^-)v_0 t^* \end{aligned} \tag{7.10}$$

From (7.6) or (7.9), we expect that the total energy of the bar will decrease until the bar reaches a new equilibrium state.

7.3 Equilibrium state of the phase boundary

It is interesting to check whether the equilibrium state determined by the dynamical model is identical to the equilibrium state determined by a static theory. For a given boundary condition, no matter whether our material is a trilinear or nontrilinear two-phase material, the equilibrium state of the bar must be a Maxwell state. There are infinitely many solutions that can satisfy the given boundary condition.

In the following numerical analysis, the v_0 is assumed to be small enough to assure that only one phase boundary is present for all times; thus no new phase boundary is nucleated by the impact. The purpose here is to compare the numerical solution to a corresponding static solution. We seek a static solution with single phase boundary

for the bar for a given displacement boundary condition. Then there is only one static solution.

For the static problem, we have the following boundary conditions:

$$u(0) = -(s_0\gamma_0^- + (L - s_0)\gamma_0^+) + v_0 t^* \tag{7.11}$$

$$u(L) = 0. \tag{7.12}$$

As the bar must be in a Maxwell state in equilibrium state, the stress in the bar is uniform, namely, the Maxwell stress. Thus the equilibrium equation for the bar is satisfied automatically. Assume the phase boundary is located at s, then

$$-(s\gamma_0^- + (L - s)\gamma_0^+) = u(0),$$

i.e.

$$s = \frac{L\gamma_0^+ + u(0)}{\gamma_0^+ - \gamma_0^-}. \tag{7.13}$$

The total energy in the bar, corresponding to the intial condition in Section 7.1, is

$$\hat{E}_0 = s_0 \int_0^{\gamma_0^-} \sigma(\gamma')d\gamma' + (L - s_0)\int_0^{\gamma_0^+} \sigma(\gamma')d\gamma'. \tag{7.14}$$

The total energy of the equilibrium state in the bar, when (7.11) and (7.12) is imposed, is

$$\hat{E} = s \int_0^{\gamma_0^-} \sigma(\gamma')d\gamma' + (L - s)\int_0^{\gamma_0^+} \sigma(\gamma')d\gamma'. \tag{7.15}$$

Then the change of the total energy of the bar in the above two states, according to the static theory, will be

$$\begin{aligned} \Delta E &= (s - s_0)\int_{\gamma_0^-}^{\gamma_0^+} \sigma(\gamma')d\gamma' \\ &= (s - s_0)(\gamma_0^+ - \gamma_0^-)\sigma_0, \end{aligned} \tag{7.16}$$

where σ_0 is the Maxwell stress: $\sigma_0 = \sigma(\gamma_0^+) = \sigma(\gamma_0^+)$.

7.4 Numerical solutions

Trilinear materials. In the following computation, all the material parameters are the same as those used in Section 5.5. We consider the initial-boundary value problem formulated in Section 7.1.

Example 1. Let $L = 4$, $s_0 = 1.995$. Thus initially the portion of the bar in $[0, 1.995)$ is in the low-strain phase with $\gamma = 0.375, v = 0$, while the remaining part is in the high-strain phase with $\gamma = 1.125, v = 0$. The imposed particle velocity v_0 at $x = 0$ is 0.15, the duration of the impact t^* is 0.5. The results are shown in Figures 7.1-7.5.

Figures 7.1, 7.2 show the distribution of strain and particle velocity in the bar at different times. The evolution of the dynamical state is illustrated by these figures: the particle velocity approaches zero for large time, and the strain approaches the strains that correspond to the Maxwell stress in the two phases.

We can see more clearly that the bar approaches equilibrium state kinematically and energetically. The trajectory of the phase boundary shown in Figure 7.3 is different from that in a semi-infinite bar due to the reflection of waves at both ends of the finite bar, but the phase boundary is evidently approaching an equilibrium position. At $t = 20$, the phase boundary is at $x = 2.0948$, which is quite close to the equilibrium position $x = 2.095$ according to the static solution (7.10).

From Figure 7.4, we see that the total energy of the bar monotonically decreases and asymptotically approaches a constant value – the energy of a new equilibrium state. At t=20, the total energy of the bar is 0.818. The total energy of the new equilibrium state is 0.817 according to the static solution (7.12). From Figure 7.5, we see that the dissipation due to the phase boundary increases monotonically and approaches a constant value.

The phase boundary is still oscillating around its ultimate equilibrium position at $t = 20$ as shown in Figure 7.3. Besides, the negative of the work W done by the impact is 0.017, the energy dissipated is $D(20) = 0.008$, so the energy $E(20)$ should be 0.820, which equals to $E(0) - W - D(20)$. But the computed energy, which was

computed from (7.2), rather than (7.7), is 0.0818. The discrepancy is due to numerical dissipation. The bar has not reached its equilibrium state yet, but is quite close to it. The computed energy of equilibrium state is expected to be slightly smaller than that determined by static solution.

It should be noted that, due to the reflections from both ends and from the phase boundary, there should be many sharp wave fronts moving back and forth in the bar. But there are only two bumps in Figure 7.1, 7.2. We give two explanations for this numerical phenomenon. Firstly, as the phase boundary is initially near the center of the bar, the waves reflected and transmitted at the phase boundary overlapped into two groups of waves. On the other hand, shock wave fronts are smeared out in the computation. So when the wave fronts forms two groups, we see only two bumps.

Example 2. In this example we set $s_0 = 0.995$, which means the phase boundary is initially near one end. All the other parameters are the same as those used in example 1. The results are shown in Figure 7.6-7.10. We see more clearly the interactions among shock waves in Figures 7.6 and 7.7. Before the reflected shock waves from $x = 4$ hit the phase boundary, the phase boundary behaves as if it is in a semi-infinite bar. A dramatic change in the trajectory of the phase boundary is observed in Figure 7.8, when compared with that in a semi-infinite bar. At time t=20, the phase boundary is located at $x = 1.098$, energy dissipated in the bar is 0.009. The total energy of the bar is 1.099. From the static solution, the total energy of the new equilibrium state is 1.098, and the equilibrium position of the phase boundary is 1.095. The bar has not reached equilibrium state yet, but is quite close to it.

Example 3. Large time dynamical solution. As in the situation for semi-infinite bar, it takes an infinitely long time for the phase boundary to settle down in its equilibrium state. So in the real computation it will take a very long time for the numerical approximation to approach equilibrium solution. In order to see this, we recalculate Example 1 with $v_0 = 0.01$ and $t^* = 0.01$. From the computation we get $s = 1.99513$ at t=49.999 (50,000th time step). From static solution we have $s = 1.99513$. The computed result is numerically the same as that given by the static solution.

It is interesting to compare the large time dynamical behavior of a phase boundary in a semi-infinite bar and in a finite bar. There are two major differences between the phase boundaries in the two bars: The phase boundary in the semi-infinite bar reaches its equilibrium state much faster than does the phase boundary in a finite bar at a comparable situation. The absolute distance moved by the phase boundary in the semi-infinite bar is less than that predicted by static theory, while the phase boundary in the finite bar moves exactly the same amount as predicted by static theory. Compared with the finite bar, in a semi-infinite bar, a large portion of the energy is transported to infinity, and thus there is much less energy for the phase boundary to dissipate.

For a material with a general up-down-up stress-strain relation such as that considered by Lin [57], we expect the phase boundary will reach its equilibrium faster than it does for trilinear materials. This is due to the fact that shock waves for the nontrilinear material are dissipative.

Nontrilinear two-phase material. Here we consider the nontrilinear material defined by (3.32). For this material, the Maxwell stress is $\sigma_0 = 1.0234$, the Maxwell strains in the low and high-strain phases are $\gamma_0^l = 0.261121$ and $\gamma_0^h = 2.67221$ respectively.

Example 4. Let $L = 4$, $s_0 = 2.005$. The material of the bar is assumed to be the one defined by (3.32). Thus initially the left portion of the bar is in the high-strain phase with $\gamma = 2.67221$ and $v = 0$, while the remainder is in the low-strain phase with $\gamma = 0.261121$ and $v = 0$. The imposed particle velocity at $x = 0$ v_0 is 0.15, the duration of impact t^* is 0.5. The results are shown in figures 7.11- 7.15.

The overall behavior of the solution obtained for the nontrilinear material is quite similar to that for a trilinear material obtained Example 2. At $t = 20$, the phase boundary is at $x = 1.97033$, the total energy in the bar is 5.43039. According to the static solution, the equilibrium position of the phase boundary is at $x = 1.97389$, the total strain energy in the bar is 5.4266. But we do observe some differences: there are sharp wave fronts as well as rarefaction waves in Figures 7.11 or 7.12, especially at $t = 0.55$, but as in Example 2, when t becomes large, we do not see any shock waves,

but only two bumps in strain or velocity profile. The total energy of the bar decreases continuously though the phase boundary moves and stops alternatively as in the case of the trilinear materials; this is because the shock waves in the nontrilinear material are dissipative.

Thus we have shown numerically that, for the initial-boundary value problem formulated in Section 7.1, the finite bar with a single phase boundary will return to an equilibrium state after a disturbance of finite duration, whether the two-phase material of the bar is trilinear or not.

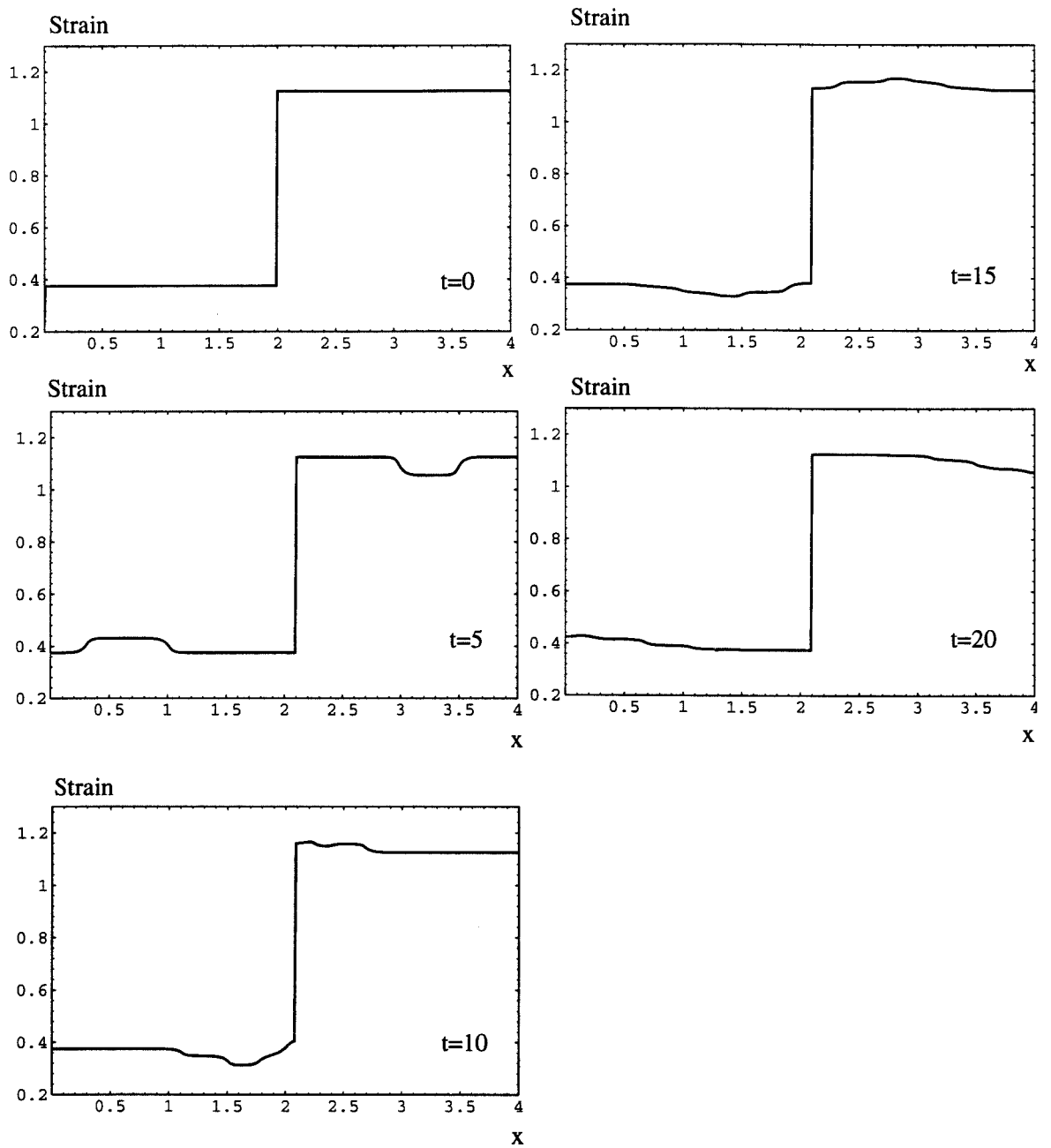

Figure 7.1: The strain distribution in a finite bar

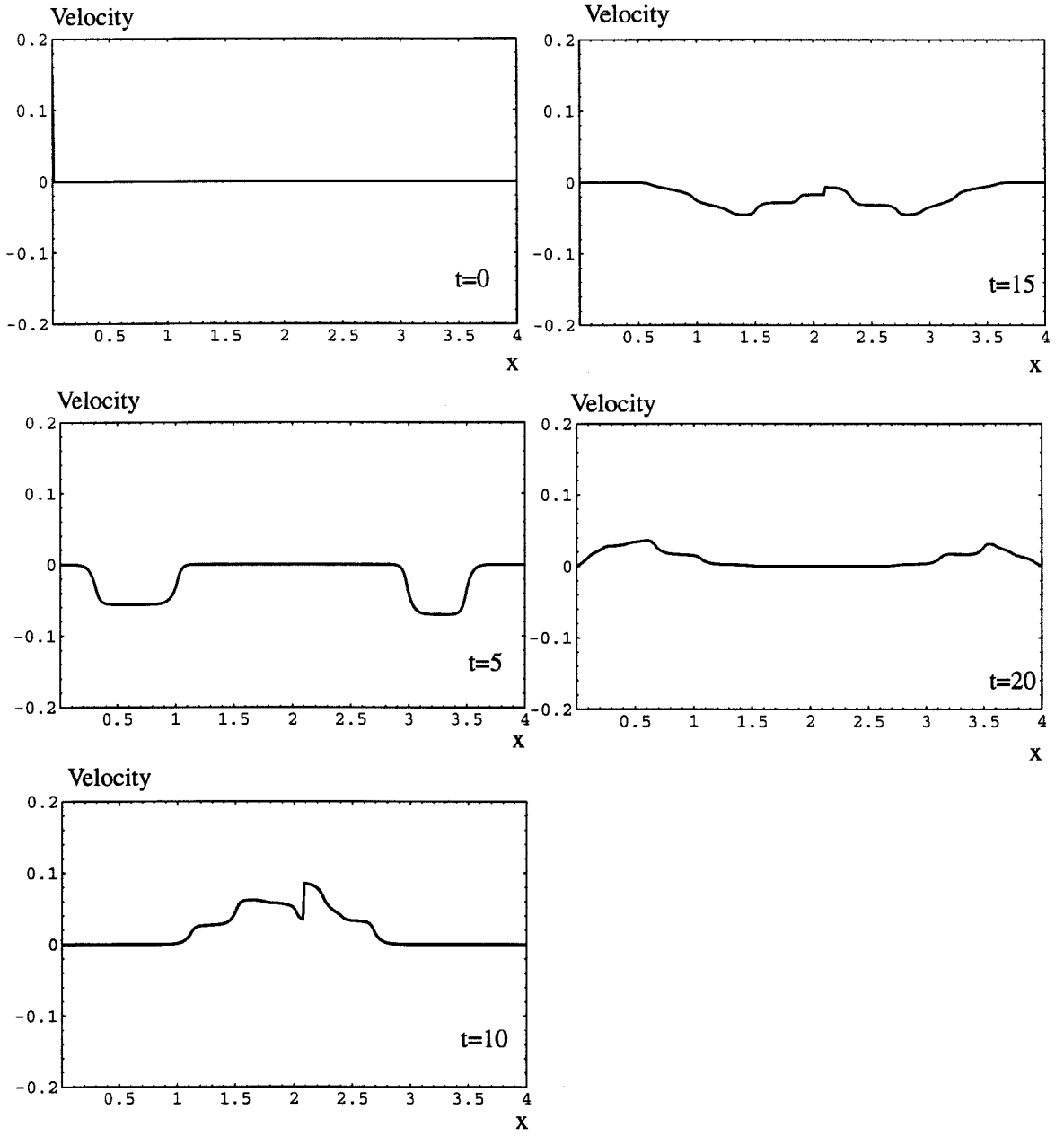

Figure 7.2: The particle velocity distribution in a finite bar

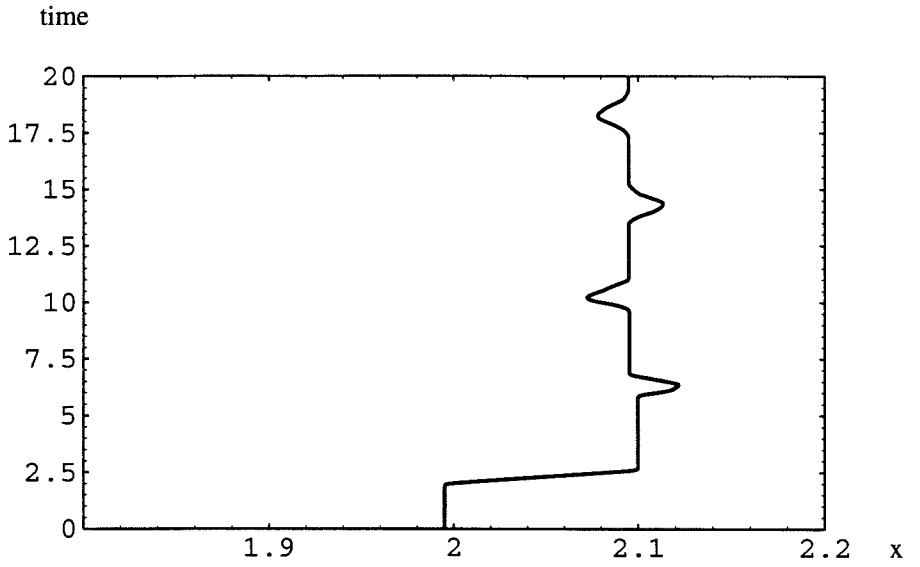

Figure 7.3: Trajectory of a phase boundary

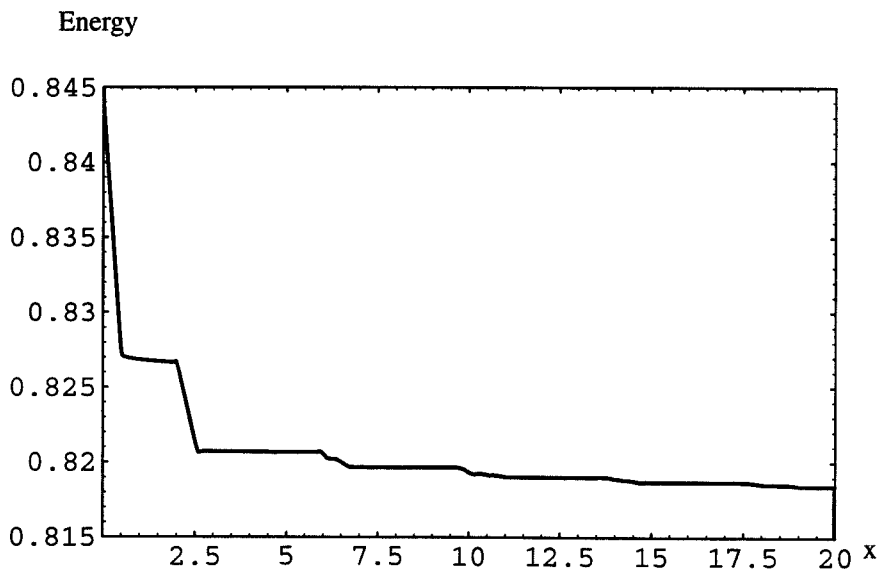

Figure 7.4: Total energy of the finite bar vs. time

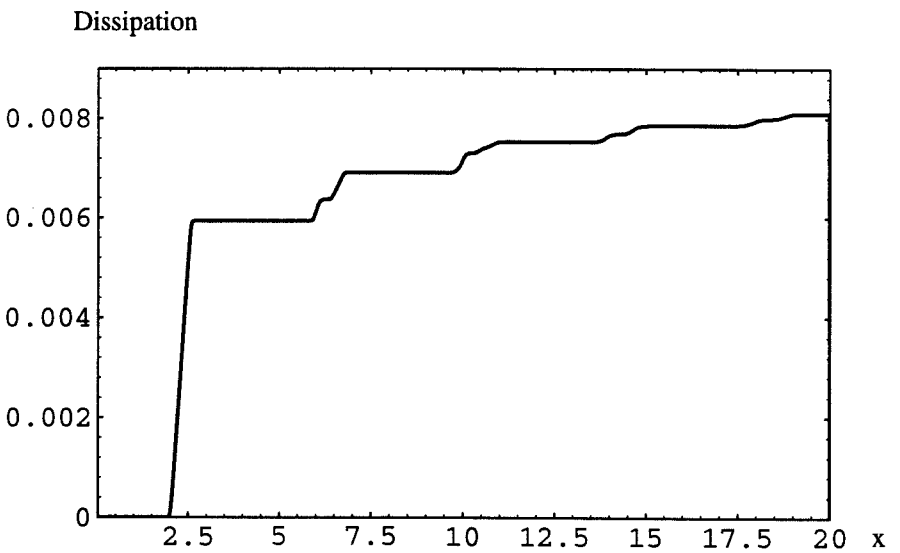

Figure 7.5: Dissipation in the finite bar vs. time

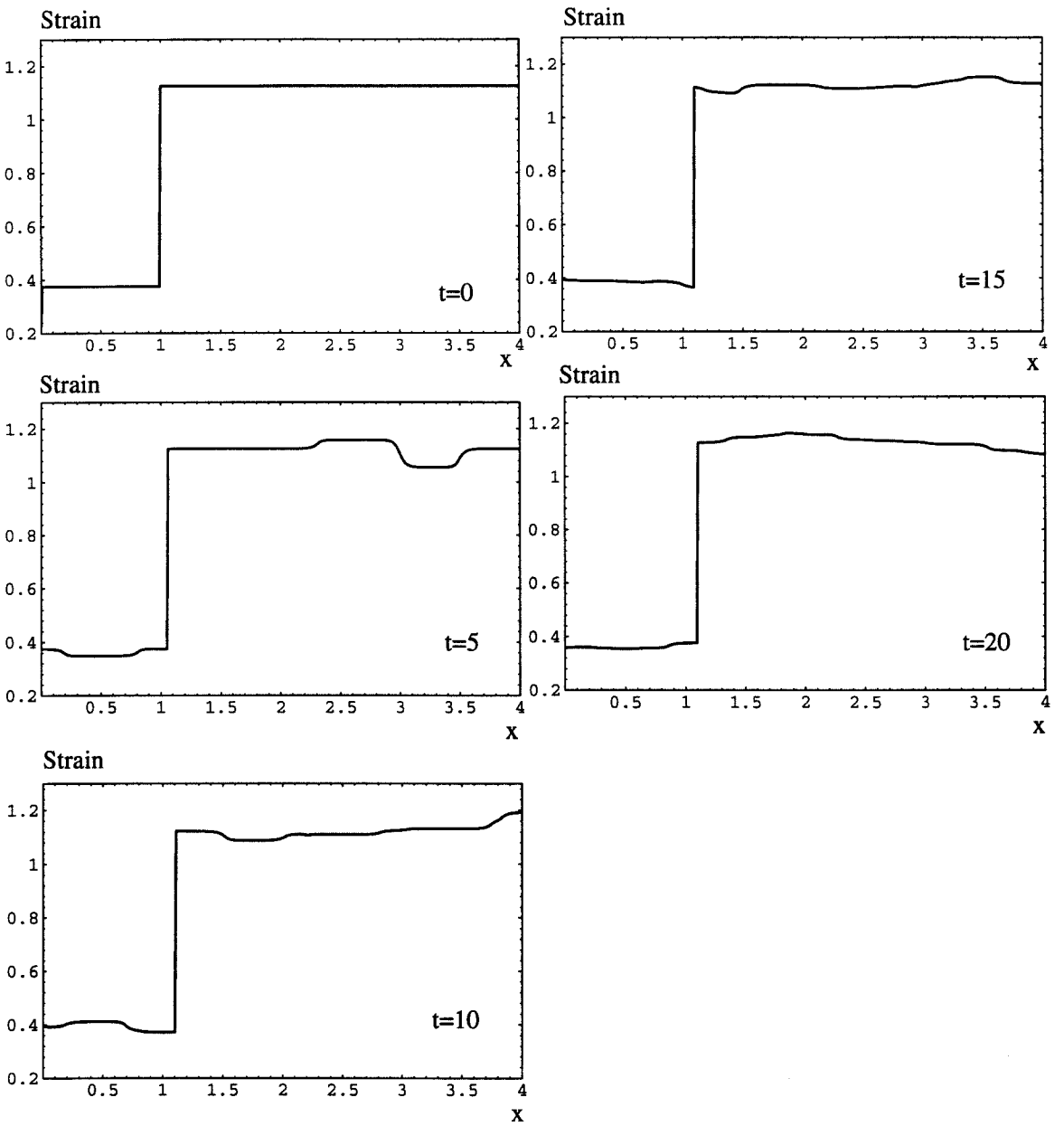

Figure 7.6: The strain distribution in a finite bar

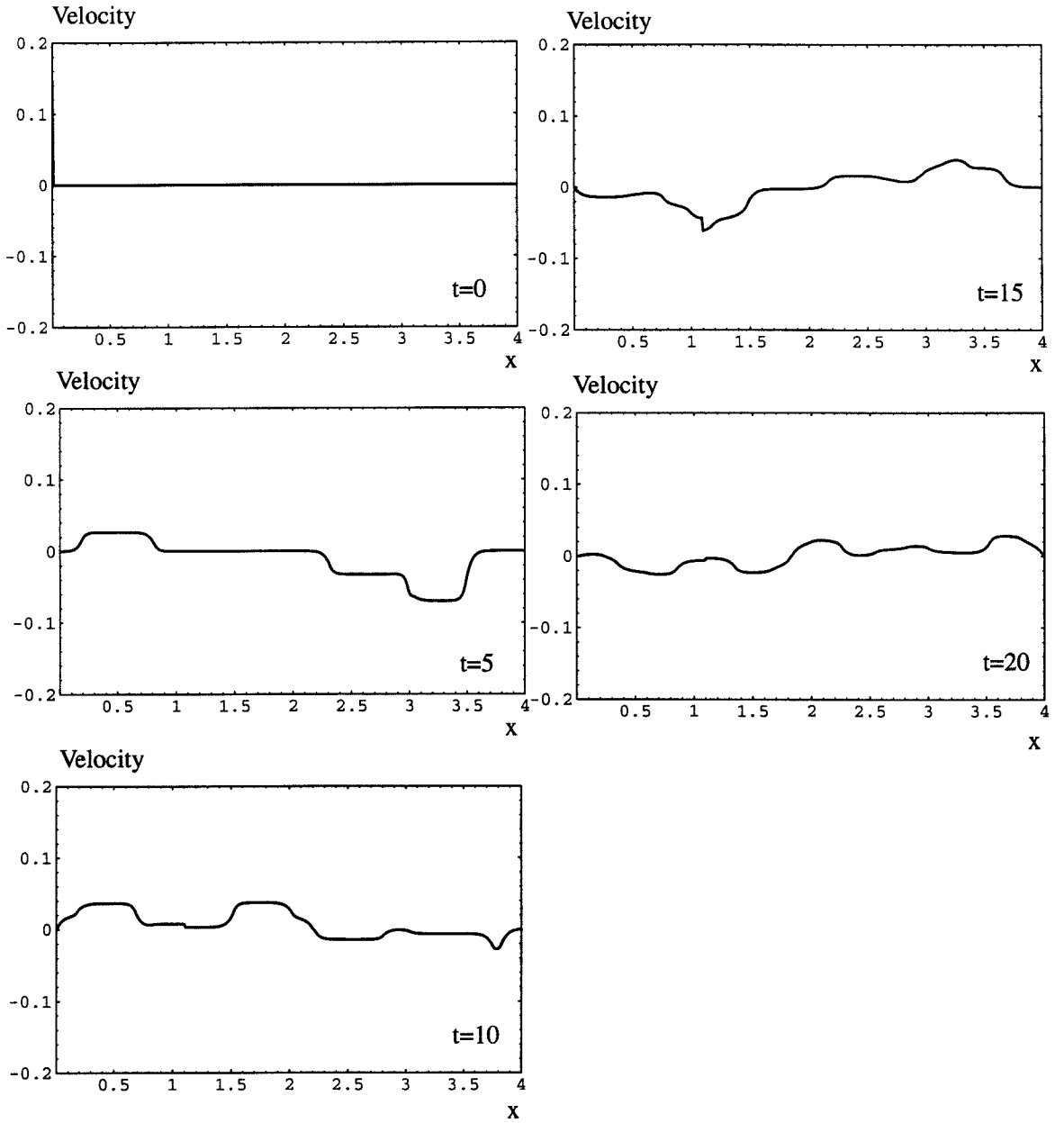

Figure 7.7: The particle velocity distribution in a finite bar

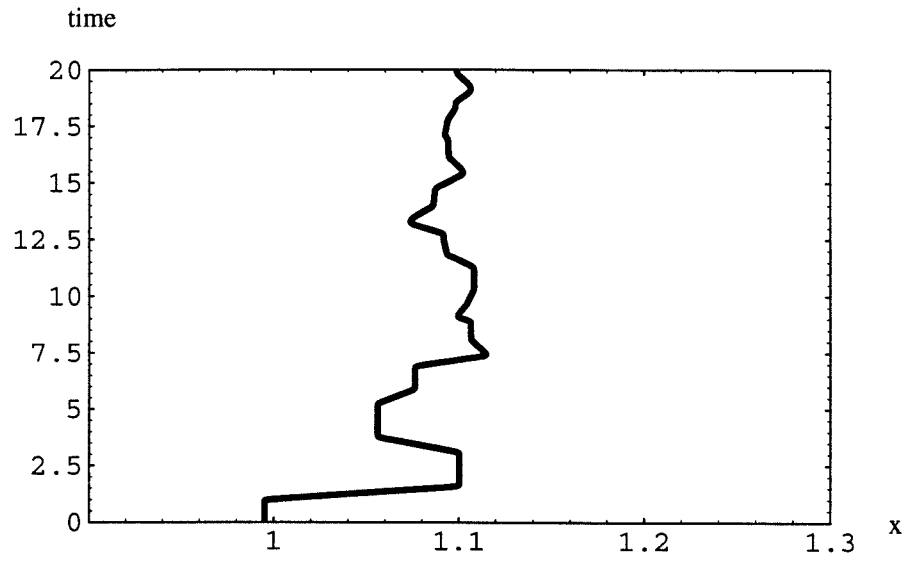

Figure 7.8: Trajectory of a phase boundary

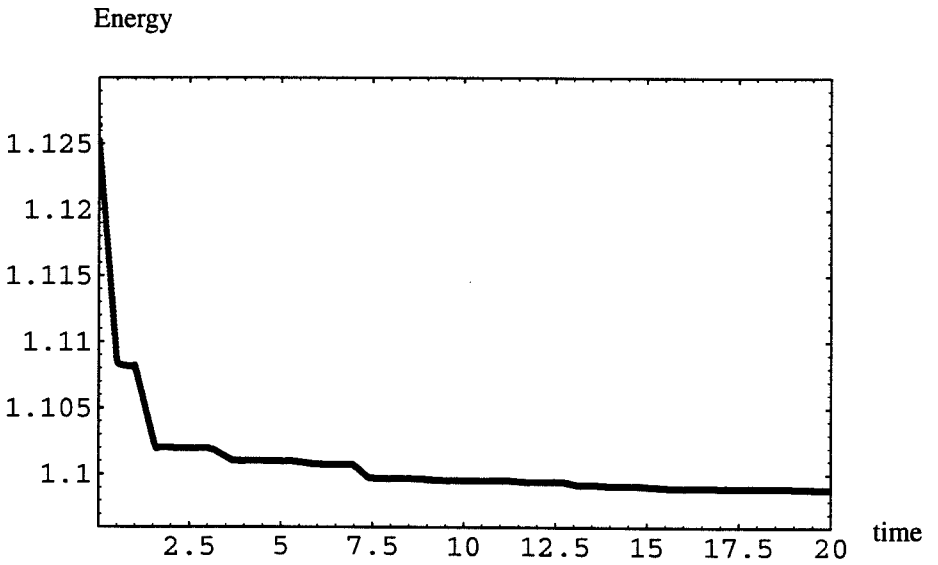

Figure 7.9: Total energy of the finite bar vs. time

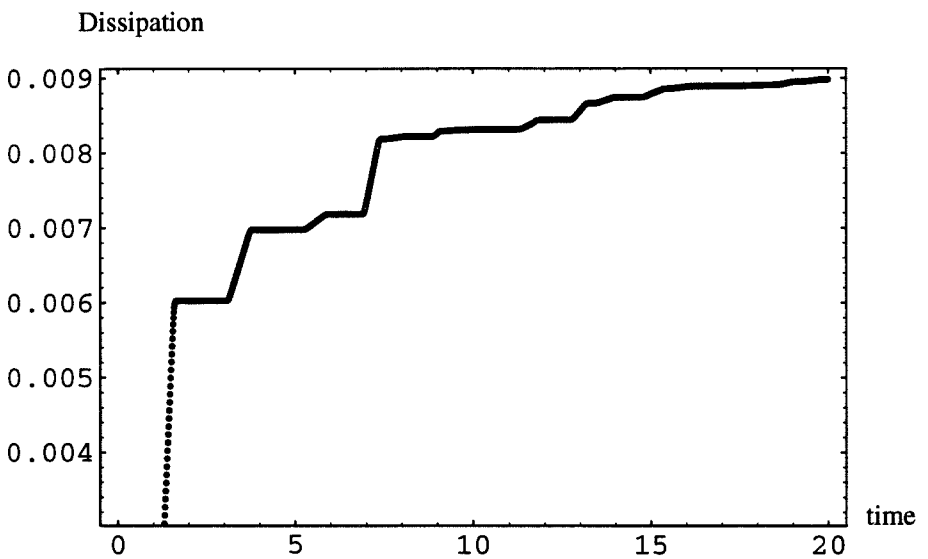

Figure 7.10: Dissipation in the finite bar vs. time

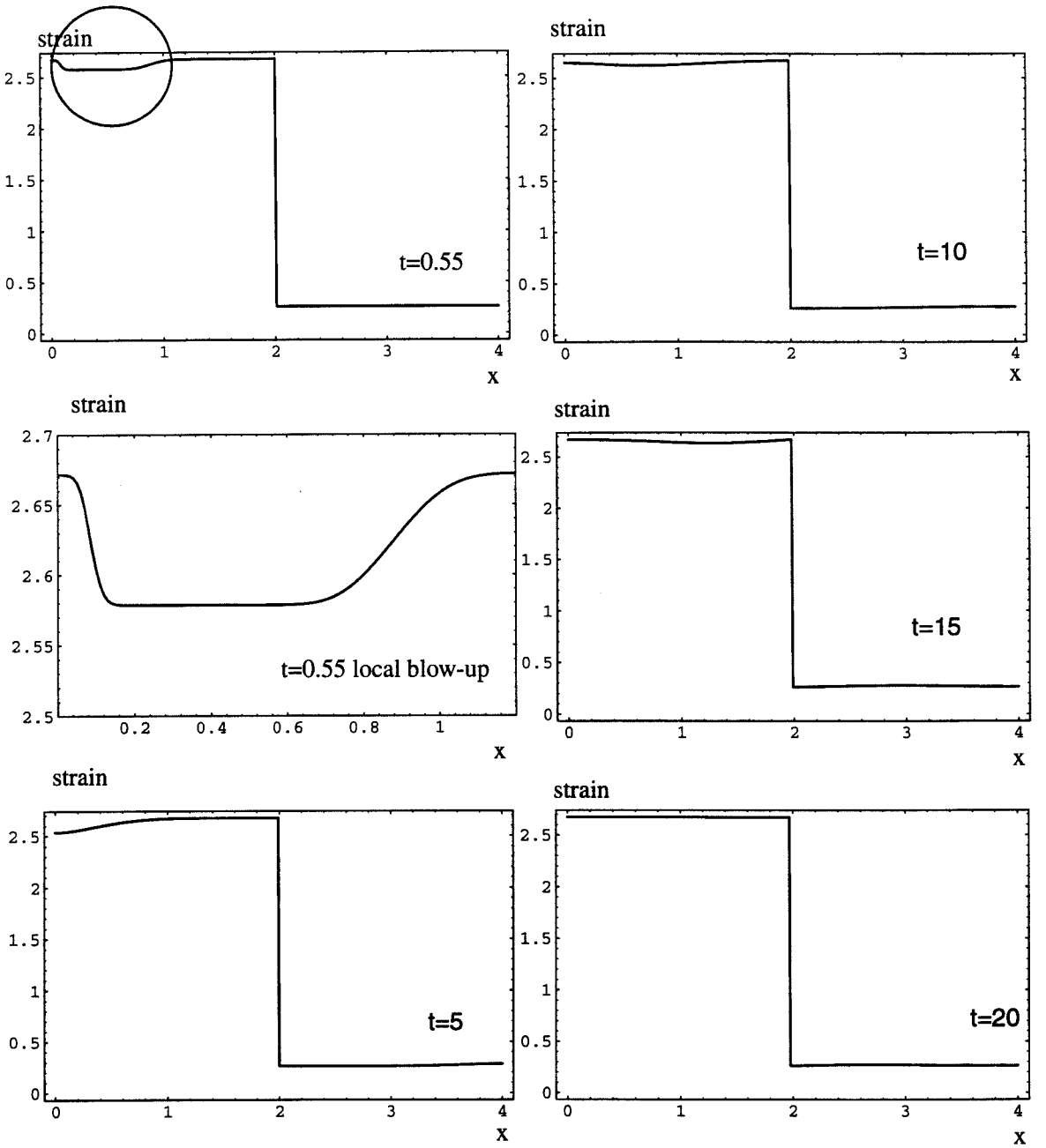

Figure 7.11: The strain distribution in a finite bar for a nontrilinear two-phase elastic material

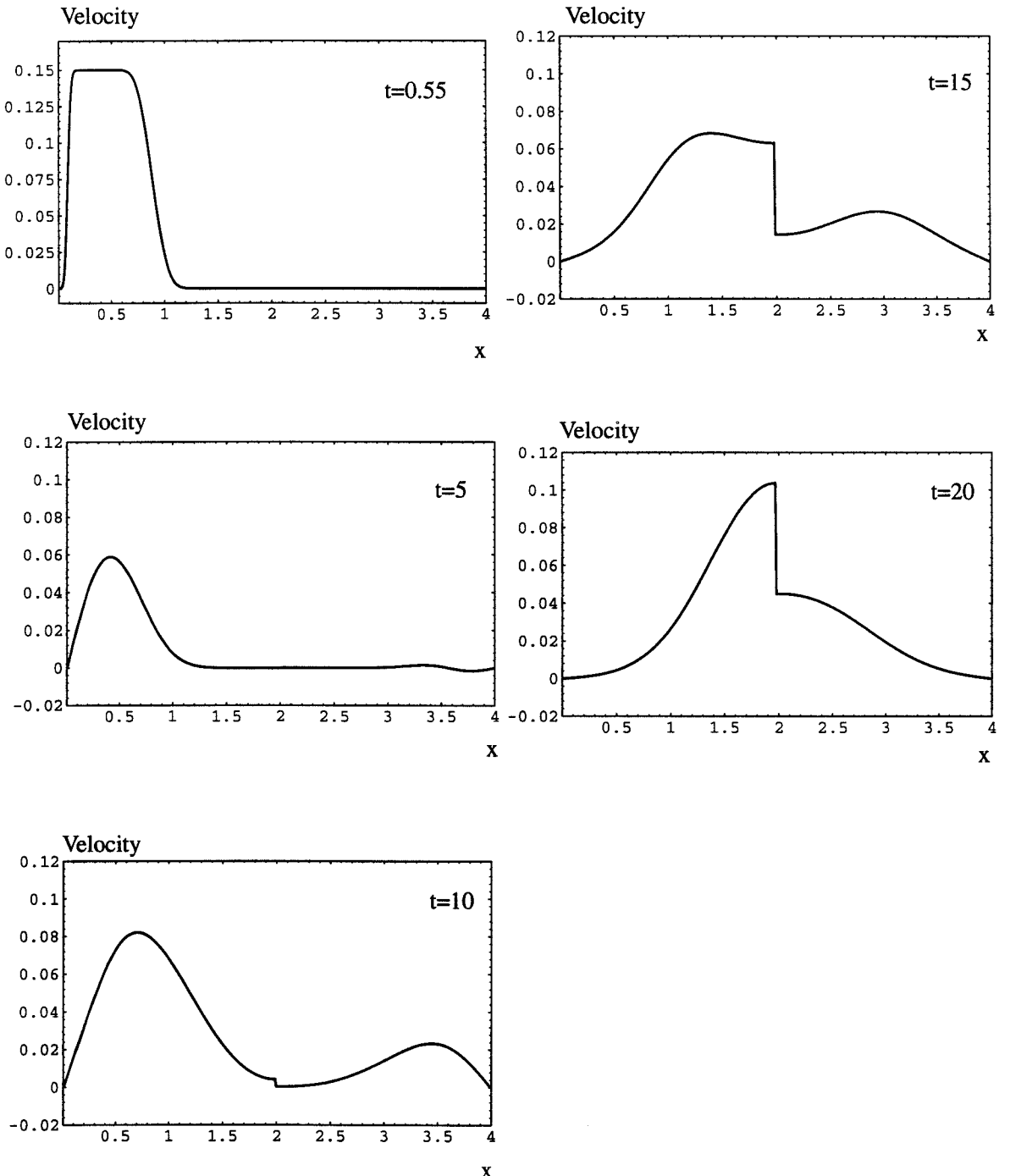

Figure 7.12: The particle velocity distribution in a finite bar for a nontrilinear two-phase elastic material

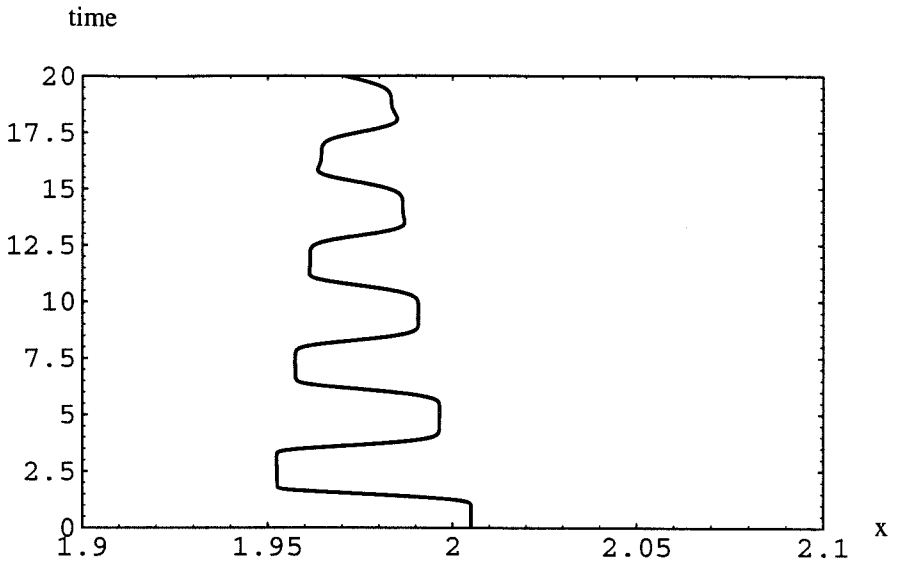

Figure 7.13: Trajectory of a phase boundary for the case of a nontrilinear material

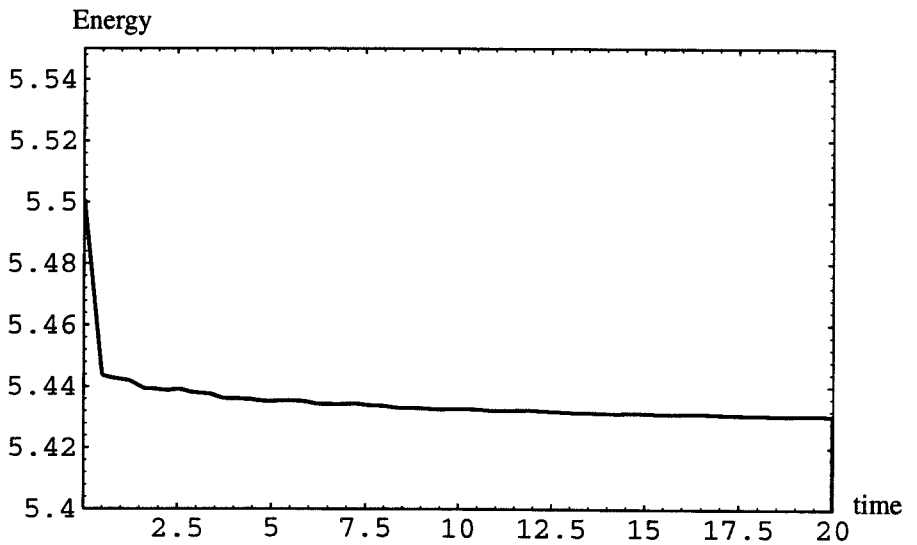

Figure 7.14: Total energy of the finite bar vs. time for the case of a nontrilinear material

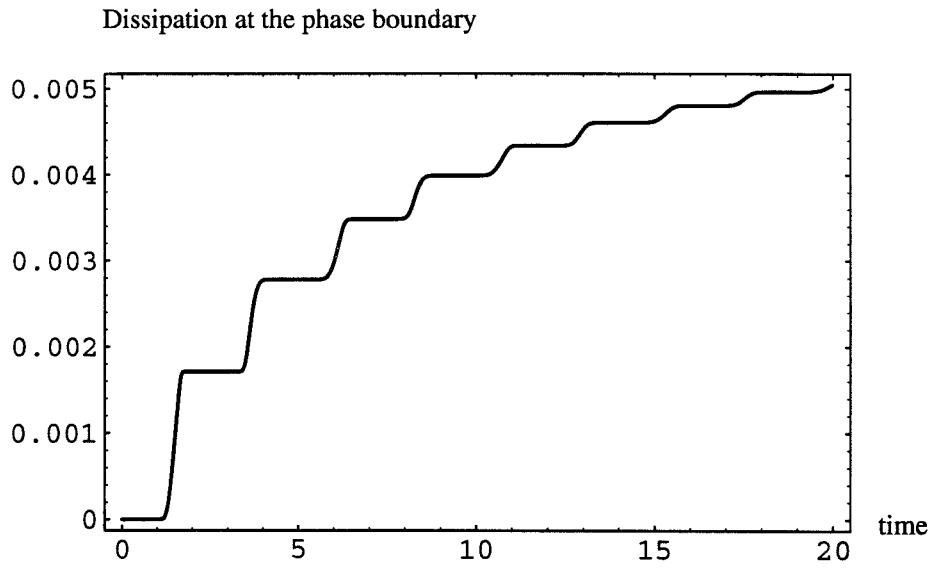

Figure 7.15: Dissipation at the phase boundary vs. time for the case of a nontrilinear material

Bibliography

[1] Abeyaratne, R. Discontinuous deformation gradients in plane elastostatics of incompressible materials, *J. Elasticity*, 10, 255-293 (1980).

[2] Abeyaratne, R. & J.K.Knowles, On the dissipative response due to discontinuous strains in bar of unstable elastic material, *International Journal of Solids and Structure*, 24, 1021-1044 (1988).

[3] Abeyaratne, R. & J.K.Knowles, Equilibrium shocks in plane deformations of incompressible elastic materials, *J. Elasticity*, 22, 63-80 (1989).

[4] Abeyaratne, R. & J.K.Knowles, On the driving traction acting on a surface of a discontinuity in a continuum, *Journal of Mechanics and Physics of Solids*, 38, 345-360 (1990).

[5] Abeyaratne, R. & J.K.Knowles, Kinetic relations and the propagation of phase boundaries in solids, *Arch. Rational Mech. Anal.*, 114, 119-154 (1990).

[6] Abeyaratne, R. & J.K.Knowles, Implication of viscosity and strain-gradient effects for the kinetics of propagating phase boundaries in solids, *SIAM J. Appl. Math.*, 51(5), 1205-1221 (1991).

[7] Abeyaratne, R. & J.K.Knowles, A continuum model of a thermoelastic solid capable of undergoing phase transitions, *Journal of Mechanics and Physics of Solids*, 41, 541-571 (1993).

[8] Abeyaratne, R. & J.K.Knowles, Dynamics of propagating phase boundaries: thermoelastic solids with heat conduction. *Arch. Rational Mech. Anal.*, 126, 203-230 (1994).

[9] Abeyaratne, R. & J.K.Knowles, Dynamics of propagating phase boundaries: Adiabatic theory for thermoelastic solids. *Physica D*, 79, 269-288 (1994).

[10] Abeyaratne, R., S-J Kim and J.K.Knowles, A one-dimensional continuum model for shape memory alloys, *Int. J Solids & Structure*, 31(16), 2229-2249 (1994).

[11] Afouf, M. & R. Caflisch, A numerical study of Riemann problem solutions and stability for a system of viscous conservation laws of mixed type, *SIAM J. Appl. Math.*, 51, 605-634 (1991).

[12] Amengual,A., F.C. Lovey and V. Torra, Problems associated to nucleation and growth in the Cu-Zn-Al SMA, *Journal de Physique IV*, 1(NC4), 379-384 (1991).

[13] Ball,J.M., P.J. Holmes, R.D. James, R.L. Pego and P.J. Swart, On the dynamics of fine structure, *Journal of Nonlinear Science*,1, 17-70 (1991).

[14] Ball, J. & R.D.James, Fine phase mixtures as minimizers of energy, *Arch. Rational Mech. Anal.*, 100, 13-52 (1986).

[15] Berger, M.J. & P. Colella, Local adaptive mesh refinement for shock hydrodynamics, *J. Comp. Phys.*, 82, 64-84 (1989).

[16] Berveiller, M. & E. Pattor, M. Buisson, Thermomechanical constitutive equations for shape memory alloys, *Journal de Physique IV*, 1(NC4), 387-396 (1991).

[17] Bhattacharya, K., Wedge-like microstructures in martensite, *Acta. Metall.*, 39, 2431-2444 (1991).

[18] Bhattacharya, K., Comparison of the geometrically nonlinear and linear theories of martensitic transformation, *Continuum Mechanics and Thermodynamics*, 5(3), 205-242 (1993).

[19] Budiansky,B., J.W. Hutchinson and J.C. Lambropoulos, Continuum theory of dilatant transformation toughening ceramics, *Int. J. Solids & Structure*, 19(4), 337-355 (1983).

[20] Christian,J.W., *The theory of transformations in metals and alloys* (2nd edition), Pergamon Press, 1981.

[21] Chern, I-L & P. Colella, A conservative front tracking method for hyperbolic systems of conservation laws, UCRL-97200, Lawrence Livermore National Laborotories, 1987.

[22] Chu,C-W, Ph.D. Thesis, University of Minnesota, 1993.

[23] Colella, P. & P.R. Woodward, The piecewise parabolic method(PPM) for gas dynamical simulations, *J. Comp. Phy.*, 54, 174-201 (1984).

[24] Collins, C. & M. Luskin, The computation of the austenite-martensite phase transitions, *Lecture Notes in Physics* (ed. M. Rascle, D. Serre and M. Slemrod), 344, 34-50 (1989).

[25] Dafermos, C. M., The entropy rate admissibility criterion for solutions of hyperbolic conservation laws, *J. Diff. Eq.*, 14, 202-212 (1973).

[26] Delaey, L., R.V. Krishan, H. Tas and H. Warlimont, Thermoelasticitiy, pseudoelasticity and the memory effects associated with the martensitic transformations (Part 1,2 & 3), *Journal of Materials Science*, 9, 1521-1555 (1979).

[27] Ericksen, J.L., Equilibrium of bars, *J. Elast.*, 5, 191-201 (1975).

[28] Evans, A.G. & A.H.Heuer, Transformation toughening in ceramics:martensitic transformation near a crack tip stress field, *J. Am. Ceramics Soc.*, 63, 241-248 (1980).

[29] Fisher,F.D. & M. Berveiller, K. Tanaka, Continuum mechanical aspects of phase transformations in solids, *Ingenieur Archiv*, 64(2), 54-85 (1994).

[30] Fried, E., Ph.D. Thesis, Caltech, 1991.

[31] Fried, E. & M.E. Gurtin, Dynamic solid-solid phase transitions with phase characterized by an order parameter, *Physica D*, 72, 287-308 (1994).

[32] Gangchoffer, J.F & K. Simonsson, S. Denis, E. Gautier et al., Martensitic-transformation plasticity simulations by finite elements., *Journal de Physique IV*, 4(NC3), 215-230 (1994).

[33] Glimm, J., E. Isaacso, D. Marchensin and O.A.McBryn, Front tracking for hyperbolic systems, *Adv. in Appl. Math.*, 2, 91-119 (1981).

[34] Glimm, J., C. Klingenber, O. McBryan,B.Plohr and D. Sharp, Front tracking and two-dimensional Riemann problems, *Adv. Appl. Math.*, 6(3), 259-290 (1985).

[35] Godunov, S.K., A finite difference method for the numerical computation of discontinuous solutions of the equations of fluid mechanics, *Mat. Sb.*, 47, 271-290 (1959).

[36] Grady, D.E., Compression wave studies in Oakhall limestone, *Sandia Report*, 1983.

[37] Gurtin, M.E. & A. Struthers, Multi-phase thermomechanics and interfacial structure 3. Evolving phase boundaries in the presence of bulk deformation, *Arch. Rat. Mech. Anal.*, 112, 97-160 (1990).

[38] Harten,A. & J.M. Hyman, Self adjusting grid methods for one-dimensional hyperbolic conservation laws, *J. Comput. Phys.*, 50, 235-269 (1983).

[39] Harten,A., High resolution schemes for hyperbolic conservation laws, *J. Comput. Phys.*, 49, 357-393 (1983).

[40] Harten, A., ENO schemes with subcell resolutions, *J. Comput. Phys.*, 83, 148-184 (1987).

[41] Harten,A. & S.Osher, Uniformly high order accurate nonoscillatory schemes. I, *SIAM J. Num. Anal.*, 24, 279-309 (1987).

[42] Huo,Y. & I. Müller, Nonequilibrium thermodynamics of pseudoelasticity, *Continuum Mechanics and Thermodynamics*, 5(3), 163-204 (1993).

[43] Hyman, J.M., Numerical methods for tracking interfaces. *Physica D*, 12, 396-407 (1984).

[44] James, R.D., The propagation of phase boundaries in elastic bars, *Arch. Rational Mech. Anal.*, 77, 143-176 (1980).

[45] James, R.D., Displacive phase transformations in solids, *Journal of Mechanics and Physics of Solids*, 34(4), 359-394 (1986).

[46] James, R.D. & D. Kinderlehrer, Theory of magnetomstriction with application to $Tb_xDy_{1-x}Fe_2$, *Philosophical Magazine B*, 68(2), 237-274 (1993).

[47] Jiang, Q., On the modeling of thermoelastic phase-transformation in solids, *J. Elasticity*, 32(10), 61-91 (1993).

[48] Jiang, Q., Macroscopic behavior of a bar undergoing the paraelactric - ferroelectric phase transformations, *Journal of Mechanics and Physics of Solids*, 41(10), 1599-1635 (1993).

[49] Khachaturyan, A.G., *Theory of structural transformation in solids*, John Wiely and Sons, 1983.

[50] Kloueck, P. & M. Luskin, Computational modelling of the martensitc transformation with surface energy, *Continuum Mech. and Thermodynamics*, 6, 209-240 (1994).

[51] Kohn, R.V. & S. Muller, Branching of twins near an austenite twined - martensite interface, *Philosophical Magazine A*, 66(5), 697-715 (1992).

[52] Knowles,J.K., On the dissipation associated with equilibrium shocks in finite elasticity, *Journal of Elasticity*, 9, 131-158 (1979).

[53] LeVeque, R.J., *Numerical methods for conservation laws* (2nd edition). Birkhauser Verlag (1992)

[54] Liang, C. & C.A. Rogger, A multidimensional constitutive model for shape memory alloys, *Journal of Engineering Mathematics*, 26(3), 429-443 (1992).

[55] Lin,J. & T.J.Pence, On the dissipation due to wave ringing in non- elliptic elastic materials, *Journal of Nonlinear Science*, 3, 269-305 (1993).

[56] Lin,J. & T.J.Pence, *Kinetically driven elastic phase boundary motion activated by concurrent dynamic pulse*, ARO report 93 -1, 10th Army conference on applied mathematics and computing (1993).

[57] Lin, Y., *A Riemann problem for an elastic bar that changes phase*, Technical report No. 10, ONR Grant 00014-90-J-1871, 1992.

[58] Lin, Y., Ph.D. Thesis, MIT, 1993.

[59] Lusk, M.T., Ph.D. Thesis, Caltech, 1992.

[60] Mamiya, E. N. & J. C. Simo, Numerical simulation of equilibrium shocks in maximally dissipative elastic systems. Part I. The one-dimensional case, *J. Elasticity*, 35, 175-211 (1994).

[61] Meyers, M.A.& J.R.C. Guimaraes, Shock-induced martensite formation in Fe-31%Ni-0.1%C alloy, *Materials Science and Engineering*, 24, 289-292 (1976).

[62] Meyers, M.A., An estimation of the nucleation time in the martensitic transformation, *Metallurgical transactions A*, 10, 1723-1727 (1979).

[63] Moretti, G., A technique for integrating two-dimensional Euler equations, *Computer and Fluids*, 15, 59-75 (1987).

[64] National Research Council, *Mathematical science in materials science: opportunities and perspectives*, National Academy Press,1993.

[65] Nicolaides, R.A. & N.J. Walkington, Numerical minimizations of free energy functionals for diffusionless phase transitions, *Recent advances in adaptive and sensory materials and their applications* (ed. C.A. Rogers & R.C. Rogers), 131-141 (1992).

[66] Nishiyama,Z., *Martensitic transformation*, Academic Press, 1978.

[67] Oran, E.S & J.P.Boris, *Numerical simulations of reactive flow*, Elsever, NewYork, 1987.

[68] Osher, S., Convergence of generalized MUSCL schemes, *SIAM J. Num Anal*, 22(5), 947-961 (1985).

[69] Pego,R., Phase transitions in one-dimensional nonlinear viscoelasticity, *Arch. Rat. Mech. Analysis*, 97, 353-394 (1987).

[70] Pence, T.J., On the encounter of an acoustic shear pulse with a phase boundary in an elastic material: reflection and transmission behavior, *J. of Elasticity*, 25, 31-74 (1991).

[71] Roe, P.L., Approximate Riemann solvers, parameter vectors and difference scheme, *J. Comp. Phys.*, 43, 357-372 (1981).

[72] Roitburd, A.L., Martensitic transformation as a typical phase transformation in solids, in *Solid State Physics*, 33, 317-390, Academic Press, 1978

[73] Rosakis, P., Ellipticity and deformation with discontinuous gradients, *Arch. Rat. Mech. Analysis*, 109, 1-37 (1990).

[74] Rosakis, P., Compact zones of shear transformation in an anisotropic solid, *J. Mech. Phys. Solids*, 40(6), 1163-1196 (1992).

[75] Rybka, P., Dynamical modeling of phase transitions by means of viscoelasticity in many dimensions, *Proc. Roy. Soc. Edinburgh*, 121A, 101-139 (1992).

[76] Shaccham, M., Numerical solution of constrained nonlinear algebraic equations, *Int. J.Num. Methods Eng.*, 23, 1455-1481 (1986).

[77] Shyue, K-M, Ph.D. Thesis, University of Washington at Seattle, 1993.

[78] Silling,S.A., Numerical studies of loss of ellipticity near singularities in an elastic material. *J. of Elasticity*, 19, 213-239 (1988).

[79] Silling, S.A., Dynamic growth of martensitic plates in an elastic material., *J. of Elasticity*, 28, 143-164 (1992).

[80] Slemrod, M. Lax-Friedrichs and the viscosity capillarity criterion, *Physical Mathematics and Nonlinear PDEs*, (ed. S.M. Rankin and J.M. Lightbourne) (1985).

[81] Snell, E.O.,J.C. Shyne and A. Goldgerg , Stress-assisted and strain - induced martensite morphologies in an Fe-21 Ni-0.6 C alloy, *Metallography*, 10, 299-314 (1977).

[82] Srinivasan,A.V. & D.G. Cutts, L.M. Schetkey, Thermal and mechanical considerations in using shape memory alloys to control vibrations in flexible structures, *Meturllugical Transaction A*, 22A, 623-627 (1991).

[83] Stringfellow,R.G. & D.M. Parks, G.B. Cohen, A constitutive model for transformation plasticity accompanying strain-induced martensitic transformation in metastable austenitic steels, *Acta Metallurgica et Materialia*, 40(7), 1703-1716 (1992).

[84] Sun, Q.P. & K.Ch. Hwang, S.W. Yu, A micromechanical constitutive model of transformation plasticity with shear and dilatation effect, *Journal of Mechanics and Physics of Solids*, 39, 507-524 (1991).

[85] Swart,P.J. & P. Holmes, Energy minimization and the formation of microstructure in dynamic antiplane shear, *Arch. Rat. Mech. Anal.*, 121(1), 37-85 (1992).

[86] Thadhani,N.N & M.A. Meyers, Kinetics of martensitic transformation induced by a tensile stress pulse, *Acta Metallurgica*, 34, 1625-1641 (1986).

[87] Tsai, H-Y, Ph.D. Thesis, Cornell University, 1994.

[88] van Leer,B., Towards the ultimate conservative difference scheme V. A second order sequel to Godunov's method, *J. Comput. Phys.*, 32, 101-136 (1979).

[89] Weiner J.H., Thermal activation and tunneling phenomena in solids, *Proceedings of the Sixth U.S. National Congress of Applied Mechanics*, ed. G. Carrier, ASME publishers, NY, 62-77, 1970.

[90] Xu,P. & J.W. Morris, Jr., Computer simulation of microstructure development during martensitic transformation, *Metallurgical Transactions A*, 23A, 2999-3012 (1992).